

**WATER SORPTION PROPERTIES OF
SUB-MICRON THIN IONOMER FILMS**

by

Hyun Ki (Key) Shim

A thesis submitted to the Department of Chemical Engineering

In conformity with the requirements for
the degree of Master of Applied Science

Queen's University

Kingston, Ontario, Canada

February, 2016

Copyright © Hyun Ki (Key) Shim, 2016

Abstract

This thesis is focused on the water uptake and swelling properties of sub-micron thin ion-conducting polymer (ionomer) films. One motivation for this work stems from the need to resolve the discrepancy between high water uptake and low proton conductivity properties observed in Nafion[®] thin films on SiO₂ substrate. In addition, the effects of film thickness, substrate, ionomer equivalent weight (EW), and annealing on the intrinsic properties of ionomer thin films were studied. Ionomer thin films were characterized using the quartz crystal microbalance (QCM) and ellipsometry for their density, refractive index (RI), water uptake and swelling properties.

Water uptake studies showed that the effect of substrate on water uptake of Nafion[®] thin films were not as strong as expected. Meanwhile, a thickness-dependent water uptake was observed for Nafion[®] thin films. Similar trends were observed for the two low EW ionomers suggesting similar nano-structure in the thin film form. Interestingly, comparison of water uptake showed that low EW ionomers adsorb comparable or less water than Nafion in the thin film form.

A combined QCM and ellipsometer setup was employed for the first time to simultaneously measure the water uptake and swelling, respectively as a function of humidity. All thin films appear to be affected by confinement effect as evident by the swelling dimension and volume of mixing. Thermally annealed (160 °C) Nafion[®] thin films experienced a significant decrease in water uptake and swelling properties.

Acknowledgements

First and foremost, I would like to thank my supervisor, Prof. Kunal Karan for guiding me through my graduate program. Although my journey consisted of many obstacles, he was always there to support me. The wisdom that I learned from him is not only limited to work, but also in life. I would like to thank my co-supervisor, Prof. Brant Peppley for his presence and support during my stay at Queen's University.

I would like to thank all my peers at both Queen's University and University of Calgary, as well as the PEFC research group at FCRC, Karan group at UofC, and also CaRPE-FC at SFU. Special thanks go to Dr. Devproshad Paul for helping me out since day 1.

I am grateful to my father, mother, and sister for entrusting me with their unconditional love and trust. I would also like to thank my best friends Andrew Cho, Corren Cho, Hojae Cheong, Peter Kim, Thomas Kim, Francis Lim, Peter Lim, Kyel Ok, and Frank Yoo (AKA Sinkle) for our friendship since high school. Here's to a much more exciting adventure and bright future.

Table of Contents

Abstract	ii
Acknowledgements	iii
List of Figures	vii
List of Abbreviations	xi
Chapter 1 Introduction	1
1.1 Motivation.....	3
1.2 Objectives	4
1.3 Approach.....	4
1.4 Thesis Layout.....	5
Chapter 2 Literature Review	8
2.1 Introduction.....	8
2.2 PEFC	8
2.3 Nafion [®] ionomer	12
2.3.1 Nano-structure and morphology	12
2.3.1.1 Nafion [®] as PEM	12
2.3.1.2 Nafion [®] thin film	16
2.3.2 Water uptake and swelling	17
2.3.3 Proton conductivity as a function of water content.....	22
2.3.4 Water transport behavior.....	23
2.4 Summary	28
Chapter 3 Experimental Techniques: Theory and Application.....	29
3.1 Introduction.....	29
3.2 Characterization techniques	29
3.2.1 Quartz Crystal Microbalance (QCM).....	29
3.2.2 Variable Angle Spectroscopic Ellipsometry (VASE)	30
3.2.3 Atomic Force Microscopy (AFM)	33
3.2.4 Goniometer	34
3.2.5 Electrochemical Impedance Spectroscopy (EIS)	36
3.3 Summary	37
Chapter 4 Fabrication and Characterization of Sub-Micron Thin Ionomer Films	38
4.1 Introduction.....	38
4.2 Fabrication of film	38

4.2.1 Substrate cleaning	39
4.2.2 Ionomer dispersion preparation	39
4.2.3 Self-assembly method.....	40
4.2.4 Spin-coating method	41
4.3 Characterization of film	41
4.3.1 QCM measurement for ionomer film mass determination.....	41
4.3.2 Ellipsometry measurement.....	41
4.3.3 AFM measurement.....	42
4.4 Results and Discussions	42
4.4.1 Dry film mass.....	42
4.4.2 Film uniformity: thickness and roughness	46
4.4.2.1 Thickness	46
4.4.2.2 Roughness	51
4.4.3 Thickness-dependent density and refractive index	53
4.4.4 Water contact angle (WCA).....	55
4.5 Conclusions.....	56
Chapter 5 Thickness and Substrate-dependent Water Uptake Properties	58
5.1 Introduction.....	58
5.2 Anomalous water uptake on SiO ₂ substrate	58
5.2.1 Corrected versus non-corrected λ	63
5.2.2 Substrate-effect on water uptake.....	64
5.2.3 Correlating conductivity with water uptake	67
5.3 Equilibrium water uptake on Au substrate.....	68
5.4 Equilibrium water uptake for Nafion films on Pt substrate	72
5.5 Conclusions.....	74
Chapter 6 Effect of Equivalent Weight on Water Uptake Properties	76
6.1 Introduction.....	76
6.2 Film preparation and characterization.....	76
6.3 Water uptake properties	79
6.4 Comparison of Nafion [®] , PFSI710 and PFSI790 thin films.....	82
6.5 Conclusions.....	85
Chapter 7 Combined Water Uptake and Swellability Study of Sub-Micron Thin Ionomer Films and the Effect of Annealing.....	87
7.1 Introduction.....	87

7.2 Experimental setup.....	87
7.3 Water uptake and swelling properties of Nafion® films.....	92
7.4 Water uptake and swelling properties of AFCC ionomer films.....	96
7.5 Effect of aging and thermal annealing on Nafion® films	100
7.6 Conclusions.....	108
Chapter 8 Conclusions and Recommendations.....	110
8.1 Conclusions.....	110
8.2 Recommendations.....	111
Bibliography (or References).....	113

List of Figures

Figure 1.1: (a) MEA (b) Microstructure of CL (c) Transport and Reactions in the CL.....	2
Figure 2.1: Illustration of PEFC. Figure is taken from reference [7].....	9
Figure 2.2: TEM image of Pt/ionomer/C microstructure in the CL. Figure is taken from reference [13]..	11
Figure 2.3: Polarization curve showing the effect of flooding on cell performance. Figure is taken from reference [15].....	12
Figure 2.4: Molecular structure of Nafion [®]	13
Figure 2.5: SAXS experimental data of ionomer membrane. Figure is taken from reference [16].	14
Figure 2.6: Structural models of Nafion [®] ionomer membrane. Figures are taken from references [17-18].	15
Figure 2.7: Proposed nano-structure of ultra-thin and thin Nafion [®] films according to <i>Paul et al.</i> Figure is taken from reference [28].....	17
Figure 2.8: Equilibrium water vapor sorption of Nafion [®] membrane at 30 °C. Figure is taken from reference [29].....	18
Figure 2.9: Linear swelling strain of Nafion membrane. Figure is taken from reference [31].	19
Figure 2.10: Water uptake of Nafion [®] films (300~600 nm) on various substrates compared to bulk membrane (solid line). Figure is taken from reference [34].	20
Figure 2.11: Water sorption of Nafion [®] thin films on SiO ₂ substrates and a function of thickness. Figure is taken from reference [6].....	20
Figure 2.12: Thickness swelling from ellipsometry (left) and water uptake from QCM (right) of spin-cast Nafion thin film on Au substrate as a function of RH. Figure is taken from reference [9]	21
Figure 2.13: Proton conductivity of Nafion [®] membrane and thin films at 25 °C as a function of (a) RH and (b) water uptake. Data is taken from reference [8].	23
Figure 2.14: Diagram of (Left) interfacial and bulk phenomenon expected to be present during water transport and (Right) possible water activity profile during water transport.	24
Figure 2.15: Membrane Mass-Transfer Coefficients at 80 °C Reported by Various Authors taken from reference [33].....	25
Figure 2.16: Water self-diffusion coefficient in Nafion [®] reported by various authors taken from reference [31].....	26
Figure 3.1: Typical ellipsometry configuration. Figure is taken from reference [50].	31
Figure 3.2: Flowchart of ellipsometry data analysis. Figure is taken from reference [51].....	32

Figure 3.3: Force experienced by tip versus distance of tip to surface. Figure is taken from reference [53].	34
Figure 3.4: Instrumentation of goniometer (contact angle measurement).	35
Figure 3.5: Impedance presentation of (a) Equivalent circuit and (b) Nyquist plot.....	36
Figure 4.1: Schematic of front (left) and back (right) design of quartz crystal for QCM measurements. Drawing is not to scale.....	39
Figure 4.2: Self-assembled Nafion® thin film preparation on quartz crystal.	40
Figure 4.3: Experimental setup for QCM measurements.....	43
Figure 4.4: Representative RH and temperature profiles during a QCM experimentation.....	44
Figure 4.5: Frequency and RH stability during a humidity step change.....	44
Figure 4.6: Dry film mass as a function of dispersion wt% of spin-coated films. The error bars indicate system error.....	46
Figure 4.7: Ellipsometry measurement and diagram of corresponding layer for Au (top), Pt (middle), and SiO ₂ (bottom) substrates.	49
Figure 4.8: Thickness measurements performed on self-assembled Nafion film.	50
Figure 4.9: Thickness measurements performed on ~77 nm thick spin-coated Nafion film.	50
Figure 4.10: Film thickness as a function of dispersion wt% of spin-coated films. The error bars indicate spatial variation.....	51
Figure 4.11: AFM image (left) and typical line-analysis (right) for films on (a) Au, (b) Pt, and (c) SiO ₂ . ..	52
Figure 4.12: Thickness-dependent density (□) and refractive index (Δ) of Nafion® films prepared on Au QCs. Error bars indicate system error.	54
Figure 4.13: Thickness-dependent density (□) and refractive index (Δ) of Nafion® films prepared on Pt QCs. Error bars indicate system error.	55
Figure 4.14: Line-analysis of samples blank Pt substrate showing high degree of roughness.	55
Figure 5.1: Water uptake of Nafion® films on 300 nm SiO ₂ substrate (◇). Data reported by Modestino et al ⁶ (X) are also included.....	59
Figure 5.2: Water uptake of Nafion® films on 300 nm SiO ₂ substrate (◇) at 75% RH. Data reported by Modestino et al ⁶ (depicted by symbol X) are also included.....	60
Figure 5.3: Water uptake of films on 100 nm SiO ₂ substrate (□) at 75% RH added to Figure 5.2.....	61
Figure 5.4: Comparison of water uptake of blank substrates. Error bars indicate sample-to-sample variation.	62
Figure 5.5: Uncorrected (open) and corrected (solid) water uptake of 25 nm films on 100 (red ◇) and 300 (blue □) nm SiO ₂ substrate.....	64

Figure 5.6: Water uptake of <math><55\text{ nm}</math> films on Au (\square), Pt (Δ), and SiO ₂ (\diamond) compared to WU of CL (\circ) taken from reference [5]. The uncorrected (open) and corrected (solid) data for film on SiO ₂ substrate are presented.	65
Figure 5.7: Water uptake of $80 \pm 3\text{ nm}$ films on Au (\square), Pt (Δ), and SiO ₂ (\diamond). The uncorrected (open) and corrected (solid) data for film on SiO ₂ substrate are presented.....	66
Figure 5.8: Water uptake of $150 \pm 4\text{ nm}$ films on Au (\square), Pt (Δ), and SiO ₂ (\diamond). The uncorrected (open) and corrected (solid) data for film on SiO ₂ substrate are presented.....	66
Figure 5.9: Conductivity versus λ of thin films on SiO ₂ compared to membrane.	67
Figure 5.10: Thickness-dependent absolute mass water uptake at various RH of Nafion [®] thin films on Au. Error bars indicate sample-to-sample variation.	69
Figure 5.11: Water uptake for Nafion [®] films on Au substrate.	69
Figure 5.12: Proton conductivity of the Nafion [®] thin films of varying thicknesses 4-300 nm as a function of RH at 25 °C. Figure is taken from reference [8]......	71
Figure 5.13: Proton conductivity of 23 and 83 nm Nafion [®] thin films at 25 °C as a function of RH. Data for <math><55, 160\text{ nm}</math>, and membrane was taken from reference [8]......	72
Figure 5.14: Thickness-dependent absolute mass water uptake at various RH for Nafion [®] thin films on Pt.	73
Figure 5.15: Water uptake for Nafion [®] thin films on Pt.	74
Figure 6.1: Thickness-dependent density (\square) and refractive index (Δ) of PFSI710 films prepared on Au QCs. Error bars indicate system error.	78
Figure 6.2: Thickness-dependent density (\square) and refractive index (Δ) of PFSI790 films prepared on Au QCs. Error bars indicate system error.	78
Figure 6.3: Thickness-dependent absolute mass water uptake at various RH for PFSI710 thin films.	79
Figure 6.4: Thickness-dependent absolute mass water uptake at various RH for PFSI790 thin films.	80
Figure 6.5: Water uptake for PFSI710 films on Au.	81
Figure 6.6: Water uptake for PFSI790 films on Au.	81
Figure 6.7: Water uptake of $23.5 \pm 1.5\text{ nm}$ films on Au.	83
Figure 6.8: Water uptake of $50.7 \pm 3.1\text{ nm}$ films of different ionomers on Au.	83
Figure 6.9: Water uptake of $80.5 \pm 1.5\text{ nm}$ films on Au.	84
Figure 6.10: Water uptake of $94.0 \pm 1.0\text{ nm}$ films on Au.	84
Figure 7.1: Combined QCM (water uptake) and ellipsometry (thickness) setup.....	88
Figure 7.2: Sample thickness and humidity profile during a step-change in humidity.....	89
Figure 7.3: Sample thickness and temperature profile during a step-change in humidity.	90

Figure 7.4: Sample frequency versus temperature-corrected frequency profile during a humidity step change.	91
Figure 7.5: Swelling as a function of water content for untreated Nafion [®] films on Au.	92
Figure 7.6 Normalized swelling as a function of water content for untreated Nafion [®] films on Au.	93
Figure 7.7: Swelling dimension (solid □) and volume of mixing (open □) of Nafion [®] thin films on Au. Dashed lines indicate range of volume of mixing for Nafion [®] membranes.	95
Figure 7.8: Swelling as a function of water content for untreated PFSI710 films on Au.	96
Figure 7.9: Swelling as a function of water content for untreated PFSI790 films on Au.	97
Figure 7.10: Swelling dimension (solid ◇) and volume of mixing (open ◇) PFSI710 thin films on Au.	98
Figure 7.11: Swelling dimension (solid Δ) and volume of mixing (open Δ) PFSI790 thin films on Au. ...	98
Figure 7.12: Swelling dimension of Nafion [®] (□), PFSI710 (◇), and PFSI790 (Δ) films on Au.	99
Figure 7.13: Volume of mixing for Nafion [®] (□), PFSI710 (◇), and PFSI790 (Δ) films on Au.	100
Figure 7.14: Effect of aging on water uptake for 150 nm Nafion [®] film on Au.	101
Figure 7.15: Density of Nafion [®] films on Au before and after thermal annealing.	102
Figure 7.16: Water uptake (solid) and swelling (open) data for 25 nm Nafion [®] film on Au.	103
Figure 7.17: Water uptake (solid) and swelling (open) data for 82 nm Nafion [®] film on Au.	104
Figure 7.18: Water uptake (solid) and swelling (open) data for 150 nm Nafion [®] film on Au.	104
Figure 7.19: Swelling as a function of water content for annealed Nafion [®] films on Au.	105
Figure 7.20: Effect of annealing on swelling as a function of water content for 25 nm Nafion [®] film on Au.	106
Figure 7.21: Effect of annealing on swelling as a function of water content for 82 nm Nafion [®] film on Au.	106
Figure 7.22: Effect of annealing on swelling as a function of water content for 150 nm Nafion [®] film on Au.	107
Figure 7.23: Swelling dimension (solid) and volume of mixing (open) of untreated (□) and annealed (Δ) Nafion [®] thin films on Au. Dashed lines indicate range of volume of mixing for Nafion [®] membranes. ...	108

List of Abbreviations

AFM	Atomic force microscopy
AFCC	Automotive fuel cell cooperation
Au	Gold
C	Carbon
CL	Catalyst layer
EIS	Electrochemical impedance spectroscopy
EW	Equivalent weight
GDL	Gas diffusion layer
GISAXS	Grazing-incidence small-angle x-ray scattering
HOR	Hydrogen oxidation reaction
IDA	Interdigitated array
IEC	Ion exchange capacity
IPA	Isopropyl alcohol
ITO	Indium tin oxide
MEA	Membrane electrode assembly
MSE	Mean squared error
NR	Neutron Reflectometry
ORR	Oxygen reduction reaction
PEFC	Polymer electrolyte fuel cell
PEM	Polymer electrolyte membrane
PFSA	Perfluoro-sulfonic acid
Pt	Platinum
PTFE	Polytetrafluoroethylene

QC	Quartz crystal
QCM	Quartz crystal microbalance
RH	Relative humidity
RI	Refractive index
SAXS	Small angle x-ray scattering
SiO ₂	Silicon Dioxide
TEM	Transmission electron microscopy
VASE	Variable angle spectroscopic ellipsometry
WAXS	Wide angle x-ray scattering
WCA	Water contact angle

Chapter 1

Introduction

Demand for clean and sustainable energy systems is increasing in the automotive industry as regulations are being put in place to reduce emission.^{1,2} Polymer electrolyte fuel cell (PEFC) is a promising technology for direct conversion of chemical energy to electricity efficiently. Due to its high efficiency and zero local emission, hydrogen-fueled PEFCs are considered to be cleaner alternative to the internal combustion engines as energy conversion system for transportation application. However, for fuel cells to be fully commercialized the cost must be further reduced while the performance and durability must be increased. For PEFCs, all of these issues are strongly related to the catalyst layer (CL) where the electrochemical reactions take place. The cost is associated with the use of precious Platinum (Pt) catalyst. The performance is dependent on the intrinsic properties as well as the microstructure-dependent effective properties of the material phases of the CL. The durability issues are linked to the loss of Pt catalyst as well as the degradation of its carbon support and the ion-conducting polymer (ionomer).

To introduce these issues, the key components of a PEFC are shown in Figure 1.1. These include the membrane electrode assembly, porous carbon paper or cloth called porous transport layer (PTL), and the gas flow channels. The membrane electrode assembly (MEA) is composed of the anode and cathode CLs separated by a proton-conducting polymer electrolyte membrane (PEM). Currently the industry leading PEM is Nafion[®], a perfluoro-sulfonic acid (PFSA). The ion-conducting polymer (ionomer), which is utilized as the PEM, and also in the CL where it exists as a thin film along with platinum (Pt) and carbon (C) aggregates, is responsible for proton conduction. For fuel cell operations, water-mediated proton transport through the ionomer is

crucial; sufficient hydration of ionomer is required for proton transport. Extensive studies on the Nafion ionomer in its bulk or membrane form, particularly on its proton conductivity and water uptake properties as well as its internal structure, have been reported.³ However, the ionomer in the CL exists as an ultra-thin film (4-10 nm) that is thought to coat the aggregates of Pt/C catalysts. The properties of the ionomer material at such small length scales are not fully understood. It has been hypothesized that the confinement effect of polymers on substrates can result in dramatically different structures and properties than the bulk counterpart. The primary functional property of the ionomer in the CL is proton conduction, which in turn is a function of water content that in turn is dependent on local humidity. In addition, recent experimental studies on low-Pt loading CLs,^{4,5} have alluded that the local transport (Figure 1.1(c)) and the interfacial effects of ionomer films are responsible for higher than known or accountable-for-losses in the CLs.⁶ In order to understand the transport limitations that inhibit fuel cell performance, both the intrinsic and effective properties of the ionomer in the CL is of interest.⁷ Unfortunately, direct investigation of Nafion® in the CL is difficult because of many factors including the composite nature of the CL, the heterogeneity, and challenges in probing within nanometers size pores.

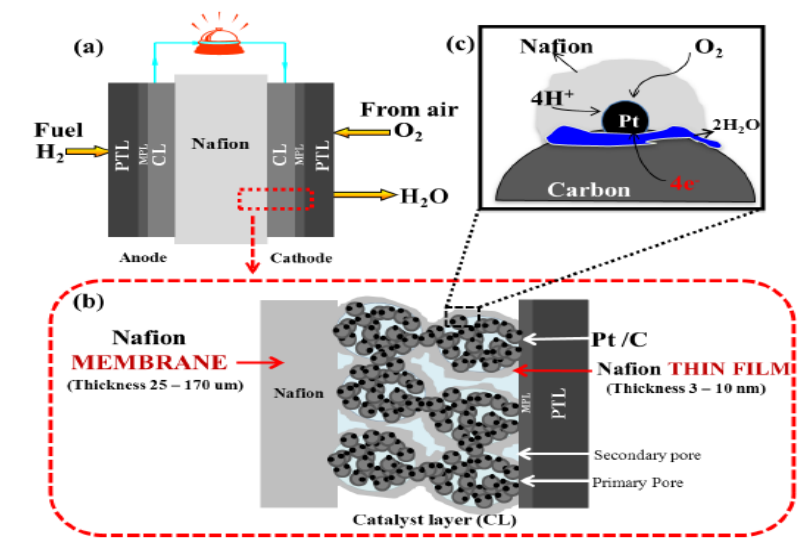


Figure 1.1: (a) MEA (b) Microstructure of CL (c) Transport and Reactions in the CL.

Thus, in order to study the fundamental properties of Nafion[®] in the thin film form, a uniform film cast on a planar well-defined substrate allows for measurements on material of controlled thickness. In fact, a thickness-dependent proton conductivity of Nafion[®] thin films has been observed.⁸ Nafion[®] thin films prepared on silica (SiO₂) substrate exhibited significantly lower proton conductivity compared to the membrane form. The conductivity was found to decrease with thickness. However, when the water uptake of these films was studied, an opposite trend was observed; that is, the thin films were found to absorb significantly more water than the membrane.⁶ Furthermore, thin Nafion films on gold (Au) substrate showed much lower water uptake than the membrane.⁹ Also, thermal annealing was found to result in a decrease in proton conductivity. A more detailed review on ionomer thin films are presented in Chapter 2.

1.1 Motivation

The aforementioned observations on Nafion thin film conductivity and water uptake has prompted several questions:

- Why was a higher water uptake but a lower conductivity for thinner films (<20 nm) observed?
- Is there a possibility of experimental artifact in the prior measurements of water uptake?
- How is the water uptake related to physical dimension change or swelling?
- Upon thermal annealing, do water uptake and swelling exhibit similar relationship as that in unannealed films?

1.2 Objectives

The overall goal of this thesis is to study the behavior of ionomer thin films at varying but controlled conditions of relative humidity. In particular, the focus is to characterize the mass water uptake and swelling of the thin films as a function of ionomer film thickness and substrate. The specific tasks undertaken in this study to meet the aforementioned goal are outlined below:

- To fabricate ultra-thin films of controllable and uniform thickness on planar substrates.
- To characterize the physical properties of the prepared films including uniformity of the films and gravimetric density.
- To develop experimental setup and protocols for measurement of water uptake of thin ionomer films using quartz crystal microbalance (QCM) setup.
- To develop experimental setup and protocols for measurement of swelling behavior of thin ionomer films using ellipsometry.
- To quantify water uptake and swelling property as a function of humidity, thickness, substrate, and equivalent weight.
- To investigate the influence of thermal treatment on the properties of Nafion[®] thin films.

1.3 Approach

In order to answer the above questions in section 1.1, an experimental study in this thesis has been undertaken. A quartz crystal microbalance (QCM) was employed independently to quantify the water uptake of the ionomer thin films. Later, a custom-built cell to accommodate QCM holder in a spectroscopic ellipsometry setup was employed for simultaneous measurement of

mass uptake of water and thickness change of the thin ionomer films. The effects of thickness, substrate type and thermal annealing on water uptake have been systematically investigated.

The discrepancy between proton conductivity and water uptake of Nafion[®] thin films on SiO₂ substrate has been investigated. Finally, in collaboration with Automotive fuel cell cooperation (AFCC) the water uptake properties of two different ionomers has been investigated. A review of literature presented in the next chapter provides the existing knowledge of ionomers in both the membrane and thin film form.

1.4 Thesis Layout

Below is a description of the chapter-wise layout of the thesis including a brief summary of the key content of each chapter.

Chapter 1: Introduction

This chapter introduces the motivation and approach for this thesis. The basic knowledge of fuel cells is provided for readers to understand the objective of this thesis.

Chapter 2: Literature Review

This chapter presents the fundamentals of PEFCs and the role of the ionomer inside the catalyst layer. The knowledge gap existing between ionomers in the membrane form and thin film form in literature has been studied, focusing mainly on Nafion[®]. The structure and properties of Nafion[®] in the membrane form is provided. A thorough literature review on the water uptake property of Nafion[®] and the effect of thickness, substrate, annealing and equivalent weight is also included. Furthermore, a thorough literature review on the kinetics of water sorption has been presented, along with the difficulties that were encountered.

Chapter 3: Experimental Techniques: Theory and Application

In this chapter, the theory and application of the experimental techniques employed in this thesis has been presented. The fundamentals behind the operation of the instruments are presented along with how the raw data can be interpreted to meaning observations.

Chapter 4: Fabrication and Characterization of Sub-Micron Thin Ionomer Films

The fabrication processes of sub-micron thin ionomer films on quartz crystals are presented in this Chapter. Two methods for film fabrication are introduced: self-assembly and spin-coating. The physical and optical characteristics of the films including mass, thickness, roughness, density and refractive index are introduced. Chapters 5 through 7 are restricted to spin-coated films.

Chapter 5: Thickness and Substrate-dependent Water Uptake Properties

This chapter focuses on the water uptake property of Nafion[®] in the thin film form. The anomalous water uptake observed for films prepared on SiO₂ substrates is investigated and resolved. The effect of thickness on water uptake of Nafion[®] thin films are studied and compared to the previously reported proton conductivity.

Chapter 6: Effect of Ionomer Equivalent Weight on Water Uptake Properties

This chapter reports the water uptake property of two new ionomers with differing equivalent weight. The thickness-dependent water uptake of these ionomers is compared to the results observed for Nafion[®].

Chapter 7: Combined Water Uptake and Swellability Study of Sub-Micron Thin Ionomer Films and the Effect of Annealing

This chapter reports the first-ever combined QCM-Ellipsometry system that allows simultaneous monitoring of mass and thickness change in thin films during water sorption and desorption. The water uptake and swellability of ionomer films are studied in conjunction. Furthermore, the effect of thermal annealing on the water uptake and swelling properties in Nafion films[®] is presented.

Chapter 8: Conclusions and Recommendations

A summary of the observations and findings of this thesis is presented in this chapter.

Chapter 2

Literature Review

2.1 Introduction

This chapter provides an overview and the importance of studying supported ionomer thin films. A brief introduction and history of PEFC is described along with its operational characteristics. The structure and properties of ionomers in the membrane form and as thin films are presented and the differences between the two are discussed. The reasoning behind the experiments that were performed will be explained to guide the readers.

2.2 PEFC

While the fundamental idea of fuel cells has been around since the 19th century, PEFCs gained increasing attention mostly due to NASA utilizing it for the Gemini program in the 1960s. However, due to the high cost of PEFCs, the adoption of PEFCs to terrestrial applications was minimal and could only be used in special applications where high funding was available. Interest in PEFCs has skyrocketed in the past two decades mainly due to environmental concerns,¹⁰ coupled with the introduction of the PFSA ionomer membrane Nafion[®] by E.I. Du Pont de Nemours and Company. PEFCs are thought to play a major role as clean and efficient energy conversion technology for stationary and automotive applications.

The basic function of PEFCs is the conversion of chemical energy into electrical energy by electro-oxidation of hydrogen and electro-reduction of oxygen in a single device. The

electrochemical reactions take place in the electrodes, also known as CLs. The CL is a porous composite structure consisting of Platinum (Pt) catalyst on carbon (C) support, and an ion-conducting polymer (ionomer). As shown in Figure 2.1, the two electrodes (the cathode and the anode) are separated from each other by an ionomeric membrane usually known as the polymer electrolyte membrane (PEM). The reacting gases for the anode and the cathode, i.e. hydrogen and oxygen, respectively, are supplied to the cell via the channels in a conducting solid plate, known as the flow-field plate. An electron conducting porous layer, typically made of porous carbon paper, separates the flow-field plate from the CL. This layer commonly known as the gas diffusion layer (GDL) is supposed to distribute the gases uniformly to the CL. In addition, the GDL also transports electrons, heat, and water to/from the CL from/to the flow-field plate.

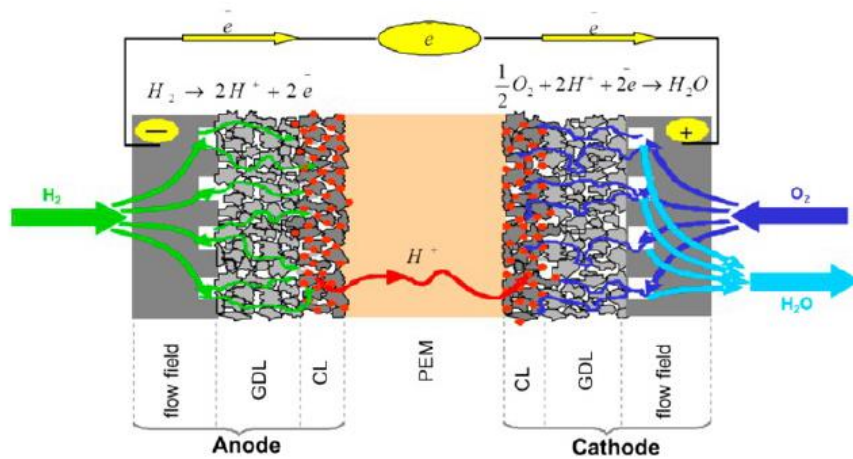
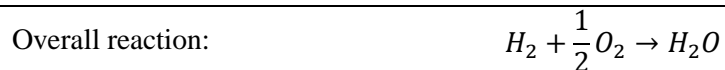
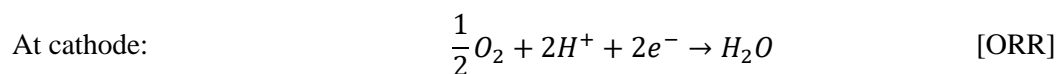
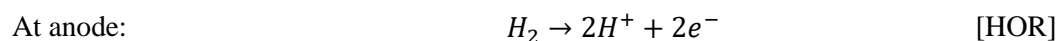


Figure 2.1: Illustration of PEFC. Figure is taken from reference [7].

The overall reaction of hydrogen and oxygen reacting to produce water can be broken down into the following two half-cell reactions; hydrogen oxidation reaction (HOR) and the oxygen reduction reaction (ORR) occur at the anode and cathode respectively:



At the anode, hydrogen is oxidized by catalytic Pt nanoparticles and the reaction byproducts are transported to the cathode via different paths – protons travel internally via the PEM whereas the electrons through the external circuit to the cathode side. At the cathode, oxygen is reduced upon combination with protons and electrons generated on the cathode to produce water as a byproduct. The rate of reaction not only depends on the intrinsic electrocatalytic activity of the catalyst but also on the reactants and byproducts transport, which dictates the local concentration or potential of the pertinent reacting species.^{11,12} The activity of the catalyst is dependent on its size, morphology, and structure. Platinum as a catalyst is very efficient for both the HOR and ORR but it is also very expensive. For maximizing the utilization of catalyst on a mass basis, 2-5 nanometers sized Pt particles dispersed on carbon support is used. In a CL, aggregates of these Pt/C catalysts are held together by a coating of the ionomer. The roles of the carbon support and ionomer are not limited merely to the physical aspect of support and binding. From an electrochemistry point-of-view, it is also the role of the carbon support to provide electronic pathways for electrical current flow to and from reaction sites while the ionomer is responsible for the transport of protons, and the local transport of reactant molecules (O_2 or H_2) and product water to or from the reacting Pt/ionomer interface. The transport of various species is affected by the CL microstructure. Unfortunately, the microstructure of the CL remains debatable due primarily to difficulty in resolving the various material phases – Pt, carbon and ionomer – with sufficient spatial resolution. One of the first images showing a single carbon

particle decorated by Pt particles and covered by a thin film of ionomer was that by *Karen More* from Oak Ridge National Lab.¹³ The now-famous image is reproduced below as Figure 2.2

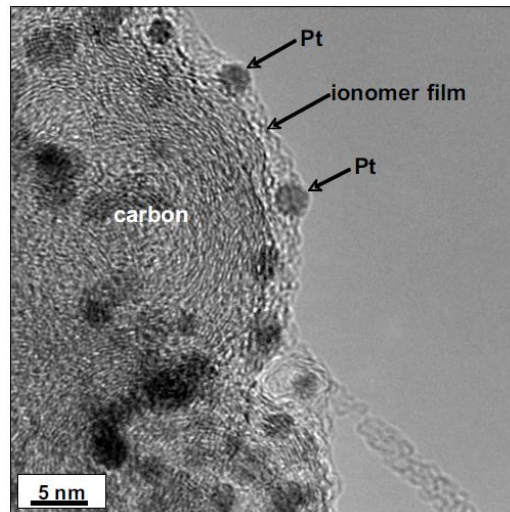


Figure 2.2: TEM image of Pt/ionomer/C microstructure in the CL. Figure is taken from reference [13].

Although the image in Figure 2.2 shows uniformly coated ionomer film, other images in the paper show the ionomer is non-uniformly distributed. While electron conductivity of the carbon is relatively high, significant resistance to gas and proton transport through the ionomer phase are present which can result in poor utilization of Pt. The gas and proton transport are further linked to water management.^{7,11,12,14-16} While it is necessary for the CL to be hydrated enough for facile proton transport, excessive water will flood the cathode and hinder transport of gases leading to decreased performance as evident in Figure 2.3. Thus, understanding both the role played by ionomer on water transport and the influence of water on ionomer properties is important.

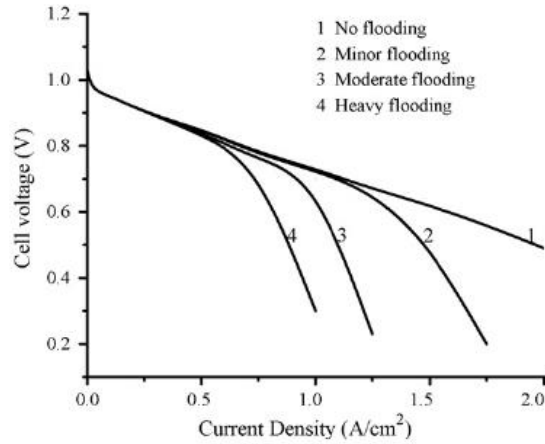


Figure 2.3: Polarization curve showing the effect of flooding on cell performance. Figure is taken from reference [15].

2.3 Nafion[®] ionomer

2.3.1 Nano-structure and morphology

2.3.1.1 Nafion[®] as PEM

Nafion[®], developed by DuPont in the 1960s, is a copolymer of perfluorinated vinyl ether co-monomer and tetrafluoroethylene (Teflon[®]). It is a perfluoro-sulfonic acid with molecular structure as shown in Figure 2.4. The side chain contains sulfonic group, which is hydrophilic while the fluorocarbon monomer backbone is hydrophobic. The most commonly employed Nafion[®] 1100 corresponds to when $x=6$ and $y=1$. 1100 represents the ionomer's equivalent weight (EW) which is grams of dry Nafion[®] per sulfonic acid group when the material is in the acid form. The ion-exchange capacity (IEC), which is widely used for ion exchange resins, is related to the EW by the equation $IEC=1000/EW$.

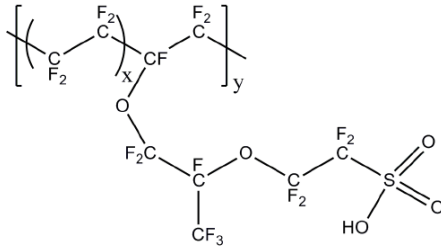


Figure 2.4: Molecular structure of Nafion®.

Nafion® plays an important role in PEFCs because of its chemical stability and hydration properties. While many studies have been conducted on free-standing membrane form,¹ the exact nanostructure of Nafion® is still debated. Using x-ray scattering and diffraction techniques, various models attempt to define the structure.¹⁷⁻²⁰ Unfortunately Nafion® only yields a single peak within the ionic domain (denoted as the ionomer peak) which can be fit to various models depending on the assumptions employed. A typical small angle x-ray scattering (SAXS) data showing the ionomer peak is shown in Figure 2.5. Other techniques such as TEM²¹ or atomic force microscopy²² (AFM) have been employed to provide insight on the structure with limited success.

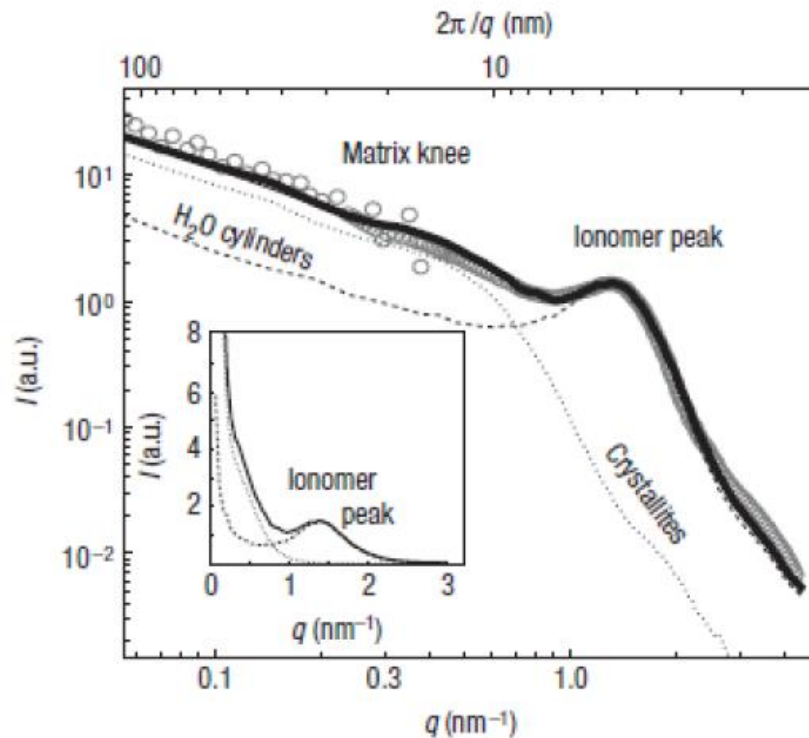
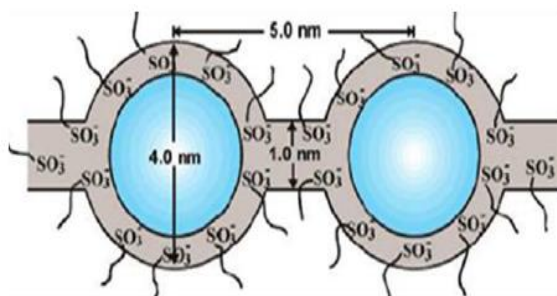
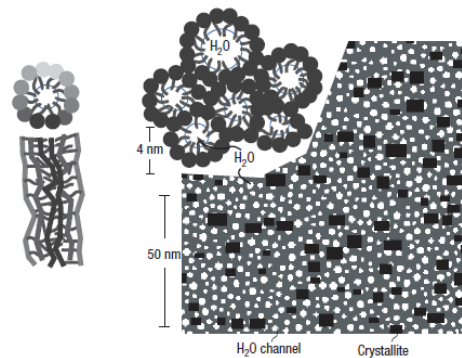


Figure 2.5: SAXS experimental data of ionomer membrane. Figure is taken from reference [16].

One of the earliest proposed structural models for Nafion is the cluster-network model by *Gierke et al*¹⁷. Using SAXS and wide angle x-ray scattering (WAXS) on ionomers with EW ranging from 1100 to 1800, they concluded that the swollen state of Nafion[®] is best described assuming spherical ionic clusters with an inverted micellar structure as shown in Figure 2.6(a). According to them, the cluster diameter, number of sulfonate sites per cluster, and the number of water molecules per cluster could be estimated and was found to increase linearly with increasing water content. They attributed this phenomenon to the expansion in cluster size and redistribution of the sulfonate sites.



(a) Cluster-network model.¹⁷



(b) Water-channel model.¹⁸

Figure 2.6: Structural models of Nafion[®] ionomer membrane. Figures are taken from references [17-18].

While Gierke's cluster-network model¹⁷ is widely popular, many researchers are skeptical about the shape and spatial distribution of the ionic clusters. SAXS studies have been fitted to elongated structures within the ionic domain, which is not explained by Gierke's model. Other models that were proposed include the sandwich model by *Haubold et al*¹⁹ and the fibrillar structure model by *Rubatat et al*²⁰. However, *Schmidtz-Rohr et al*¹⁸ attempted to fit SAXS data available in literature to various proposed models but to no avail. Instead they proposed a water-channel model, which successfully fit all available SAXS data. The model is shown in Figure 2.6(b) and it consists of parallel water channels surrounded by partially hydrophilic side branches.

In addition to the ionomer peak, an additional peak appears at $q = \sim 0.05 \text{ nm}^{-1}$. According to *Gebel et al*²³, this peak is encountered in semi-crystalline polymers such as polyethylene or polytetrafluoroethylene (PTFE). *Mauritz and Moore*³ attributed this peak to the crystalline organization within the fluorocarbon matrix and observed that it disappeared near the melting point of PTFE.

2.3.1.2 Nafion® thin film

As mentioned previously, Nafion® exists as ultra-thin (4-10 nm) film in the CL. Here, it is important to define thin films. In this work, thin films are referred to sub-micron films supported on a substrate. Films of thickness less than 100 nm may be defined as ultra-thin films. Recently, there have been a number of studies on thin and ultra-thin Nafion films, including those from our group, aimed at probing the structure and properties of the films. These studies have shown the properties and structure of the Nafion films are thickness- and substrate-dependent. For supported sub-micron polymer films, interfacial confinement at the polymer-substrate boundary are well known and contributes to thickness-dependent structure and properties.⁷ The interfacial characteristics dominate the observable bulk-like characteristics.

For Nafion, *Dura et al*²⁴ reported that for films (~60 nm) on SiO₂, lamellar structures are formed as confirmed by Neutron reflectometry (NR). However, the same study on Au and Pt surfaces showed no multilayer structure. *Mohamed et al*²⁵ observed SO₃H nano-clusters are oriented differently with different substrate using positron annihilation study and water contact angle. Films of thicknesses >100 nm exhibited a hydrophobic surface similar to that observed in freestanding membranes.^{26,27} While the contact angle of thinner films on Si substrates went as low as 6° indicating hydrophilic surface, the contact angle for films on glassy carbon and Pt/Si only went down to roughly 61°. In our group *Paul et al*²⁸ also proposed the nanostructure of ultra-thin and thin Nafion® films on SiO₂ as shown in Figure 2.7. Ultra-thin films (<55 nm) have a hydrophilic surface while thicker films (>55 nm) have a hydrophobic surface.

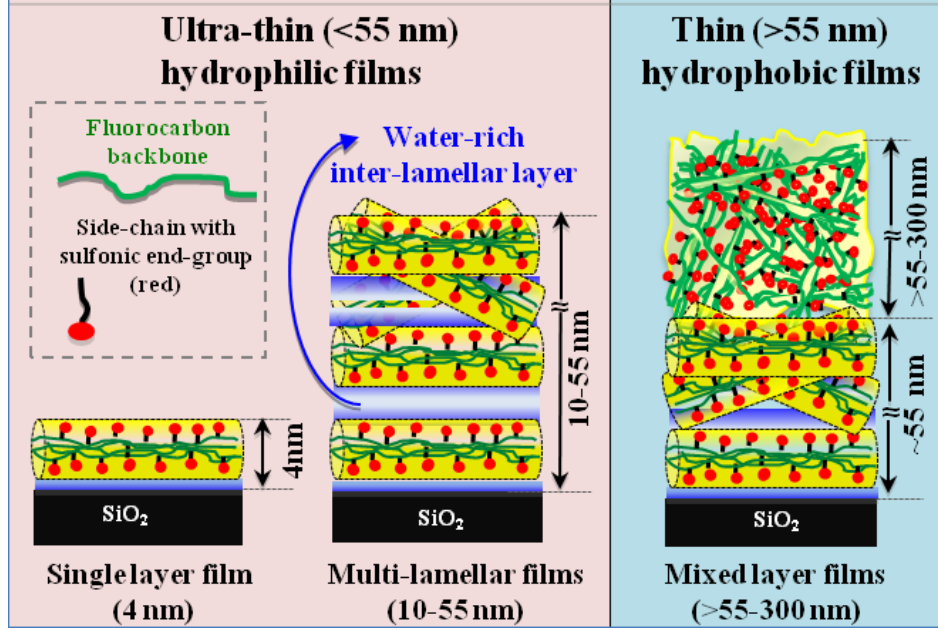


Figure 2.7: Proposed nano-structure of ultra-thin and thin Nafion® films according to Paul *et al.* Figure is taken from reference [28].

2.3.2 Water uptake and swelling

Nafion membrane: Water uptake of Nafion® is expressed in hydration number (λ), number of moles of water per moles of sulfonic acid groups. λ is calculated using the water mass uptake and IEC,

$$\lambda = \left(\frac{m_{RH} - m_0}{M_{H_2O}} \right) \left(\frac{1000}{m_0 \cdot IEC} \right) \quad (2.1)$$

where m_{RH} is the sample mass at a designated relative humidity (RH), m_0 is the dry mass of the film, M_{H_2O} is the molecular mass of water, and IEC is the ion exchange capacity.

For Nafion membrane, the water uptake has been well studied. Water uptake in Nafion[®] membrane can be seen as a two-step process.²⁹ Water molecules in the polymer are strongly attracted to the ionic components and slowly fill the ionic domain while trying to overcome the hydrophobic backbone resistance. Once the resistance is overcome by sufficient chemical potential, the polymer swells allowing more water molecules to be captured by the sulfonate ions. The water vapor sorption isotherm of Nafion[®] membrane can be seen in Figure 2.8. An interesting phenomenon that Nafion[®] membranes experience is the Schroeder's Paradox,³⁰ where Nafion[®] membrane exposed to liquid water exhibits a λ of 22 as opposed to only λ of 14 when exposed to saturated vapor phase. This has been attributed to surface tension at the interface.

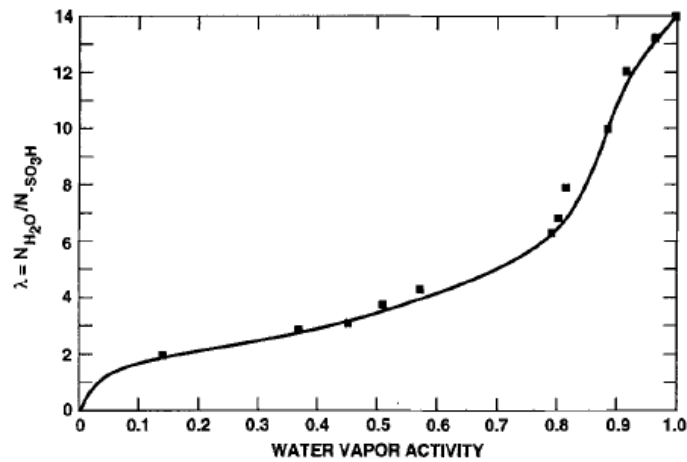


Figure 2.8: Equilibrium water vapor sorption of Nafion[®] membrane at 30 °C. Figure is taken from reference [29].

The same two-step process can be observed in the swelling property of Nafion[®] membranes. Using a creep instrument, *Benziger et al*³¹ studied the swelling strain of at varying temperatures which can be seen in Figure 2.9. The results are similar to that of the water sorption equilibrium, which is an indication that there exists a linear relationship between water uptake and swelling.

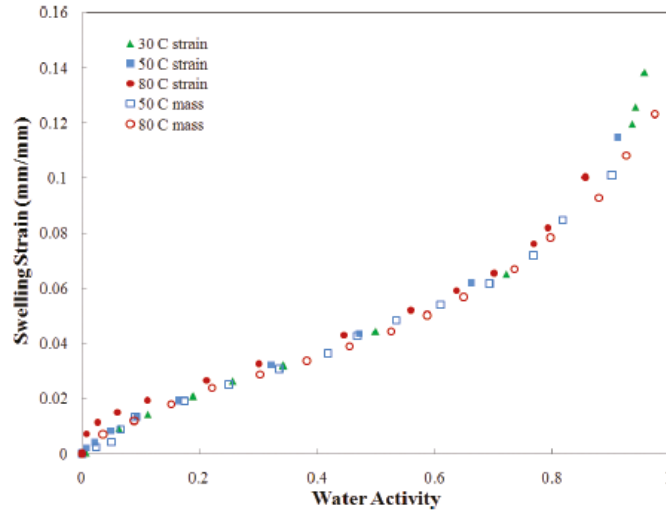


Figure 2.9: Linear swelling strain of Nafion membrane. Figure is taken from reference [31].

Nafion thin films: Water uptake of sub-micron Nafion® films has been studied by various groups using the Quartz Crystal Microbalance (QCM). One of the earliest studies using the QCM was conducted by *Krtil et al.*³² They reported the water uptake of 20 - 80 nm film on silver quartz crystal had similar values to that of bulk membrane. Meanwhile, *Kongkanand*³³ and *Corti et al*³⁴ observed lower water uptake for thinner films. *Kongkanand* studied water uptake of films of thickness ranging from 33 – 3000 nm on Au quartz crystal and observed lower water uptake compared to membrane at all water activities. He also observed that water uptake decreased as thickness decreased. *Corti et al* observed similar trends for films on Au, Si, glass, graphite, and indium tin oxide (ITO) substrates using Environmental ellipsometric porosimetry technique as illustrated in Figure 2.10. They further deduced that films cast on substrates that exhibit hydrophilic properties (Si, glass) absorb higher water content compared to hydrophobic (graphite, Au, ITO) substrates.

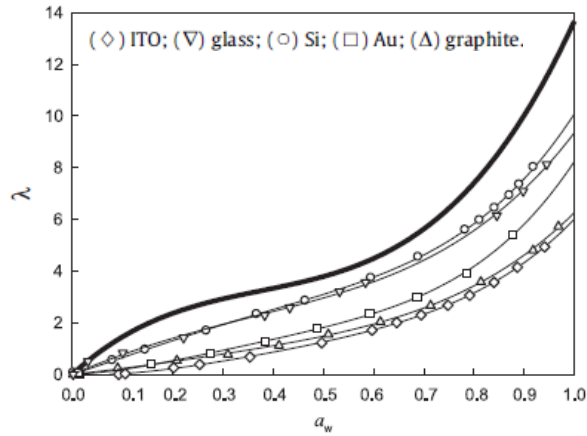


Figure 2.10: Water uptake of Nafion® films (300~600 nm) on various substrates compared to bulk membrane (solid line). Figure is taken from reference [34].

However, a collaborative study by our group found that not all thin films exhibit lower water uptake compared to the bulk membrane.⁶ It was found that while 55 and 160 nm films on SiO₂ showed lower water uptake compared to the bulk membrane, water uptake of 4 and 10 nm films showed significantly higher water uptake. Furthermore, the water uptake was found to increase as thickness decreased. The results can be seen in Figure 2.11.

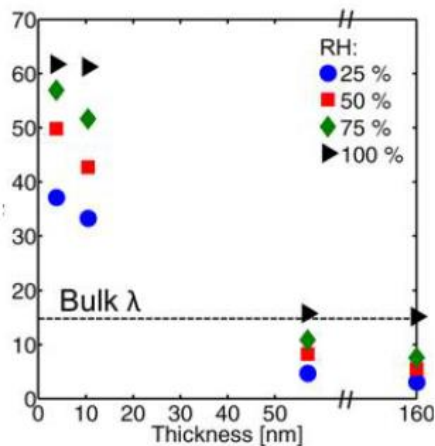


Figure 2.11: Water sorption of Nafion® thin films on SiO₂ substrates and a function of thickness. Figure is taken from reference [6].

Meanwhile in a similar study on Au substrates it was observed that water uptake of Nafion® thin films were insensitive to thickness and absorbed less water than Nafion® membranes. The swelling property observed using Ellipsometry also showed no trend with thickness. This is presented in Figure 2.12.

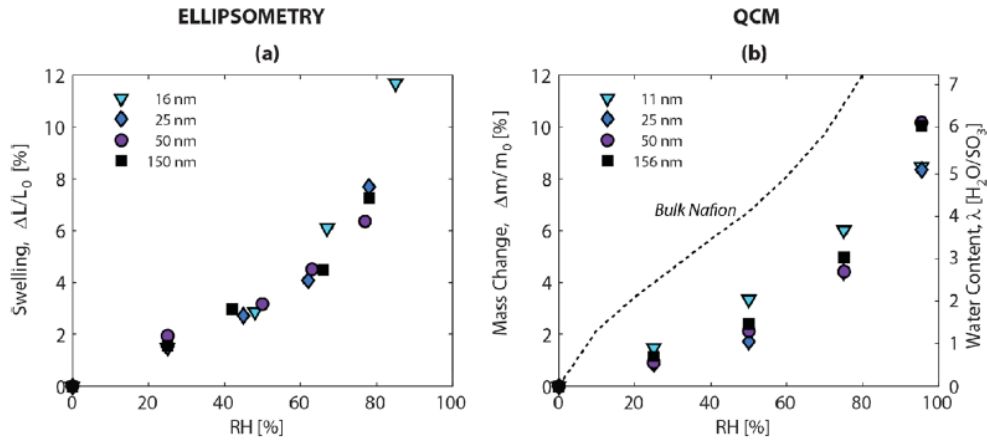


Figure 2.12: Thickness swelling from ellipsometry (left) and water uptake from QCM (right) of spin-cast Nafion thin film on Au substrate as a function of RH. Figure is taken from reference [9]

Effect of thermal annealing: When a polymer is thermally annealed above its glass transition temperature, the morphology restructures as to minimize the surface energy. Annealing improves the mechanical properties of Nafion® membranes but it also affects the water uptake properties.⁹ For Nafion® thin films, in our group *Paul et al*^{9,35} observed a visible decrease in conductivity for sub-micron thin films after thermal annealing as well as decreased water uptake and swelling. *Corti et al*³⁴ investigated the effect of annealing on Nafion® thin films utilizing grazing-incidence small-angle X-ray scattering (GISAXS) and reported a reduction in water uptake due to formation of crystalline domains at the substrate interface. Annealing studies in the membrane form has been reported to seeing similar effects.^{26,36-38}

Effect of EW: Research to develop alternatives to the commercially leading Nafion[®] membranes has been ongoing. PEFCs operate at high temperature and low humidity environment and it is well known that Nafion[®] membranes' performance significantly depreciate at these conditions.^{39,40} In addition, the use of fluorine based technology to produce Nafion[®] membranes are of environmental concern. The cost of production is not cheap as well.^{40,41} Ionomers to replace Nafion[®] and achieve higher performance for PEFC applications is needed.

In order to achieve higher water retention capabilities, many alternatives that have been developed are short-side-chain ionomers; they have lower molecular weight per each sulfonate group. This results in a lower equivalent weight. Some well-known ionomers that has been studied intensively are: Dow ionomer^{42,44} (~840 EW) from Dow Chemical Company, 3M ionomer⁴³ (~800 EW) from 3M, and Hyflon/Aquivion⁴² (~870 EW) from Solvay Specialty Polymers. Water uptake properties of these ionomers have been studied in the membrane form. Several literatures have shown that as the equivalent weight decreases the water uptake properties increase^{42,43} while some reports that water uptake are comparable.⁴⁴ However, no literature has been published on equivalent weight-dependent water uptake or swelling properties of various ionomers in the thin film form.

2.3.3 Proton conductivity as a function of water content

As mentioned several times throughout the thesis, the main role of ionomers in PEFCs is proton conduction, and is directly influenced by water uptake. In our group *Paul et al*⁸ focused on the proton conductivity of Nafion[®] thin films on SiO₂ substrates. The proton conductivity of Nafion[®] thin films compared to membrane is presented in Figure 2.13. It can be seen in Figure

2.13(a) that Nafion membrane shows higher conductivity than thin films at all humidities. Combining the conductivity data and water uptake data reported by *Paul et al*, Figure 2.13(b) shows that while thin films absorb more water than membranes, they exhibit lower conductivity. This discrepancy between high water uptake and low proton conductivity needs to be resolved.

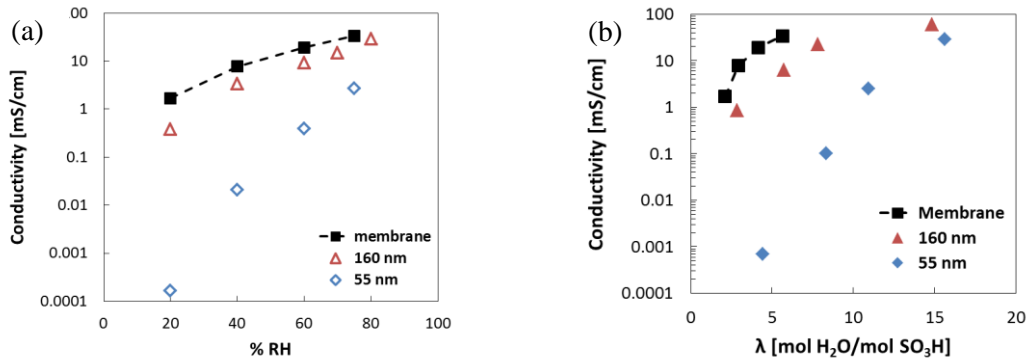


Figure 2.13: Proton conductivity of Nafion® membrane and thin films at 25 °C as a function of (a) RH and (b) water uptake. Data is taken from reference [8].

2.3.4 Water transport behavior

Original aim of this thesis project was to understand the kinetics of water transport through the ionomer. Knowledge of water transport would allow us to gain knowledge on the nanostructure of ionomer thin films, mainly how the water channels are present within the polymer. However, due to lack of the structure of Nafion® thin films, describing water transport is not simple. A lot of assumptions must be made to model the behavior of water transport. Ionomers are amphiphilic; how they orient themselves at the free surface play an important role in water sorption and subsequent transport within the film. Ionomers experience swelling upon sorption of water when exposed to water-containing environment. This swelling phenomenon can

be caused by the expansion of channels or clusters, which will affect the rate of diffusion. As stated earlier, the thickness of the film will also have an effect on swelling. Change in thickness can result in different orientations of the hydrophobic backbone and hydrophilic side chain. Substrates effect also exists as they have their own affinity for water. To accurately model the transport of water through ionomer thin films, there are many factors that must be taken into account.

Water transport through Nafion[®] thin films can be classified into three major phenomena; interfacial transport, diffusion and relaxation. A diagram depicting each phenomenon is shown in Figure 2.14. It is still not known what the rate-limiting step occurs for water transport in the ionomer thin film. There are many different factors that must be taken into account to justify the results obtained through experiment, which also varies to some degree between researchers.^{31,33}

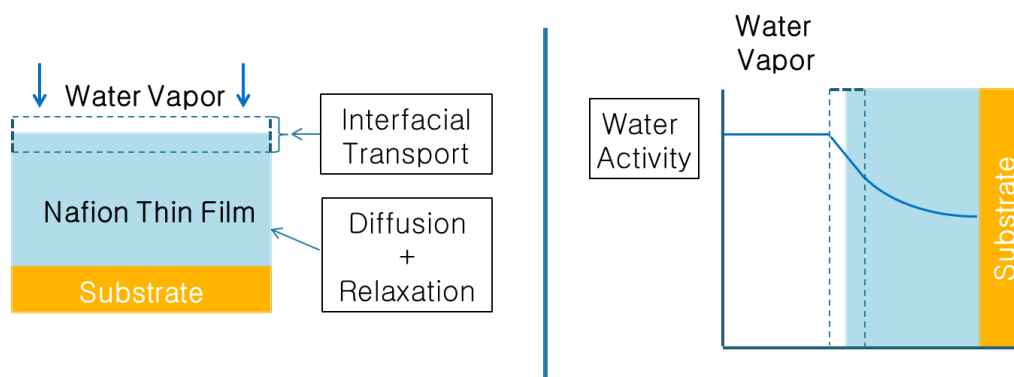


Figure 2.14: Diagram of (Left) interfacial and bulk phenomenon expected to be present during water transport and (Right) possible water activity profile during water transport.

At the vapor-polymer interface, water molecules must transfer from the vapor phase into the polymer, which itself is phase-segregated; this is referred to as interfacial transport.⁴⁵ At the macroscopic level, a chemical potential gradient exists when the un-equilibrated polymer is

brought in contact with water vapour. Sorption of water by the polymer can alter both the interfacial and internal structures of the polymer film. At the microscopic level, water molecules will experience both a repulsive force from the hydrophobic backbone and an attractive force from the hydrophilic SO_3^- group. Interfacial resistance is evident from the time it takes for water content at the membrane/gas diffusion layer (GDL) interface taking time to reach equilibrium as observed by *Hsing et al*⁴⁶ during their adsorption experiment. Regarding interfacial resistance, *Benziger et al*³¹ stated that “*the hydrophobicity of the membrane surface, the change in phase of water at the interface, and a gas-phase boundary layer will contribute to the interfacial resistance*”³¹. *Kongkanand*³³ attributed interfacial resistance to the disordering of water channels at the vapor-polymer interphase and went further to hypothesize that for Nafion[®] thin films, a significant portion of the net water transport would be attributed to interfacial resistance. As the film thickness decreases, the orientation of the ionomer will change and the wetting properties of the substrate will have an effect. A list of mass-transfer coefficient values reported in literature has been present by *Kongkanand*:

authors	mass-transfer coefficient (m/s)	methods
Berg et al. ³²	5.7×10^{-6}	model fit on fuel cell data
Okada et al. ³⁰	1×10^{-6}	model fit on fuel cell data
Futerko and Hsing ³¹	5×10^{-7}	model fit on fuel cell data
Ge et al. ⁴⁴	sorption: $(1-8) \times 10^{-6}$; desorption: $(0.4-3) \times 10^{-5}$	model fit on permeability measurement
Satterfield and Benziger ⁷	$2-4 \times 10^{-6}$	water sorption measurement
Zhao et al. ²⁸	1.2×10^{-5} (70 °C)	permeability measurement
Romero and Mérida ¹⁰	7×10^{-3}	permeability measurement
Adachi et al. ¹¹	4.5×10^{-6} (70 °C)	permeability measurement
Tabuchi et al. ¹²	3×10^{-6} (70 °C)	Raman spectroscopy
this work	sorption: 2×10^{-6} ; desorption: 5.9×10^{-6}	water sorption measurement on thin film

Figure 2.15: Membrane Mass-Transfer Coefficients at 80 °C Reported by Various Authors taken from reference [33].

Inside the polymer, water molecules travel through the hydrophilic channels due to a chemical potential gradient and are attracted to the sulfonic groups. Many assume that they

follow a Fickian diffusion type transport. Using a simple Fickian diffusion with one impermeable layer, *Krtil et al*³² found the diffusion coefficient of water in a 20 nm thin film on silver substrate was 7 orders of magnitude lower than that of the membrane. A list of water diffusion coefficients for Nafion[®] reported in literature has been provided by *Benziger et al*³¹:

researchers	conditions	results
Zawodzinski et al. ¹⁵	$T = 30\text{ }^{\circ}\text{C}$ $\lambda = 2-14$ $\Delta \geq 20\text{ ms}$	$D = (0.6-5.8) \times 10^{-6}\text{ cm}^2/\text{s}$ no change with Δ
Tsushima et al. ¹⁴	T not specified $\lambda = 6-20$ Δ not specified	$D \sim (4-7.5) \times 10^{-6}\text{ cm}^2/\text{s}$
Hensley et al. ⁴⁸	$T = 25, 90\text{ }^{\circ}\text{C}$ RH = 100% $\Delta = 4.2\text{ ms}$	$D \sim 7 \times 10^{-6}\text{ cm}^2/\text{s}$ at $T = 25\text{ }^{\circ}\text{C}$ $D \sim 27 \times 10^{-6}\text{ cm}^2/\text{s}$ at $T = 90\text{ }^{\circ}\text{C}$
Kidena et al. ¹³	$T = 40-80\text{ }^{\circ}\text{C}$ RH = 40-80% $\Delta = 20\text{ ms}$	$D \sim (2-5.5) \times 10^{-6}\text{ cm}^2/\text{s}$ at $T = 40\text{ }^{\circ}\text{C}$ $D \sim (3-7.2) \times 10^{-6}\text{ cm}^2/\text{s}$ at $T = 60\text{ }^{\circ}\text{C}$ $D \sim (3-10) \times 10^{-6}\text{ cm}^2/\text{s}$ at $T = 80\text{ }^{\circ}\text{C}$
Ye et al. ⁴⁹	$T = 22\text{ }^{\circ}\text{C}$ RH = 90% at $50\text{ }^{\circ}\text{C}$ $\Delta = 50-300\text{ ms}$	$D = 4.8 \times 10^{-6}\text{ cm}^2/\text{s}$ no change with Δ
Edmondson et al. ¹²	$T = 25\text{ }^{\circ}\text{C}$ water mass fraction = 0.04-0.2 $\Delta = 10-20\text{ ms}$	$D \sim (1-7) \times 10^{-6}\text{ cm}^2/\text{s}$ no mention of Δ dependence
Gong et al. ⁵⁰	$T = 23-84\text{ }^{\circ}\text{C}$ water mass fraction = 0.03-0.2 $\Delta = 3-600\text{ ms}$	$D \sim 0.2-20 \times 10^{-6}\text{ cm}^2/\text{s}$ no mention of Δ dependence
Ohkubo et al. ²⁵	$T = -40-35\text{ }^{\circ}\text{C}$ $\lambda = 4$ and 15 $\Delta = 1-100\text{ ms}$	D decreases with $\Delta = 1$ to 2 ms and becomes constant beyond that
Roy et al. ⁵¹	$T = 25\text{ }^{\circ}\text{C}$ fully saturated with water $\Delta = 10-80\text{ ms}$	$D \sim (2-3) \times 10^{-6}\text{ cm}^2/\text{s}$ D decreases from $\Delta = 10$ to 20 ms and states constant beyond that

Figure 2.16: Water self-diffusion coefficient in Nafion[®] reported by various authors taken from reference [31].

However, since the diffusion coefficient is a function of water content, a simple Fickian model is inadequate. In particular, the size and connectivity of the hydrophilic pores and water channels change with the water content. The absorption of water also affects the mobility of polymers. Thus, while not the universally accepted terminology, this phenomenon is termed ‘relaxation’ in many models. *Berens and Hopfenberg*⁴⁷, famous for their diffusion-relaxation

model, attributed this term to “(the) redistribution of available free volume through relatively large scale segmental motions in the relaxing polymer”⁴⁵. Similarly, Satterfield and Benziger⁴⁸ utilized this term for the rate of polymer re-arrangement and polymer swelling in their interfacial transport-relaxation model. Furthermore, Krtil *et al*³² added that the transport of water molecules in and out of the ionic clusters, deemed water transfer reaction would play a huge factor in water transport inside Nafion[®]. Interestingly, the two terms relaxation and reaction are interchangeable “because the immobilization can be also thought to be relaxation between the immobilized molecules and the fixing sites”⁴⁷ according to Pantelic. Thus differentiating between the two types of transport will be another task.

By putting all these information together, more complex models are being presented to get a better understanding of water transport through Nafion[®]. A recent paper by Benziger *et al*³¹ studied diffusion and interfacial transport of water in Nafion[®] membranes with a more complicated model. They included terms such as tortuosity and volume of hydrophilic domains in the polymer to obtain effective diffusivity and interfacial transport. The volume of hydrophilic domain was calculated by comparing the actual swelling to ideal swelling. Tortuosity was calculated by swelling strain (creep experiment) and diffusivity (nuclear magnetic resonance).

Studying absorption and desorption kinetics would have been a very interesting topic to investigate. During the early stages of this project, several concerns arose while setting up the experimental apparatus. It was apparent that distinguishing between external changes (RH, temp) to internal water uptake was not possible. Although time-varying data for absorption and desorption were obtained, it was concluded kinetics of external environment equilibration were of time scales compared to that of the kinetics of the water sorption by the film. To further validate this point, no paper that studied kinetics reported their humidity data and assumed the humidity

change was a step change. Even when the same setup reported in literature were used, it was not possible to make the humidity change be a 'step-change'. There was always a delay, which took several minutes for the humidity change to reach equilibrium. This is likely comparable to the time constants for one or more of the steps in water transport in ionomer films. Further, the slow response observed could have been an issue with the sensor itself, as the sensing probe also incorporates an unspecified polymer, this could not be verified. For a membrane, a diffusivity of $10^8 \text{ cm}^2/\text{s}$ was observed from a water vapor sorption experiments.⁴⁵ Assuming then that a 100 nm film has a diffusivity value 3-order of magnitude lower, the response time, τ , will be only 100 seconds. For a 10 nm film assuming 4 orders of magnitude lower diffusivity values, the response time will be 10 seconds. With these assumptions, it is obvious that a humidity step change that takes a few minutes will be impossible to show the accurate diffusion phenomena for the ionomer.

2.4 Summary

In summary, the functional properties of thin ionomer films are not fully known. Hydration number of thin ionomer films has been reported. However, significant differences in hydration of films on SiO_2 and other substrates remains confounding. More importantly, contradictory behavior of low conductivity for thinner films but correspondingly high water uptake has been observed. This begs the question – which result is realistic and why are we seeing such a difference? This thesis will attempt to solve this conflict. Limited data on swelling of films as a function of humidity is available. No study has reported the simultaneous measurement of water uptake and swelling. Finally, there are no reported work on the effect of ionomer equivalent weight on water uptake and swelling properties on thin films.

Chapter 3

Experimental Techniques: Theory and Application

3.1 Introduction

In this chapter, the key experimental techniques employed to characterize the ionomer thin films are presented. A brief theory/principle of the measurement technique and the application of each instrument are provided.

3.2 Characterization techniques

3.2.1 Quartz Crystal Microbalance (QCM)

Mass change measurement by QCM: Quartz crystal microbalance is a useful technique for measuring change in mass of a substrate or a film on a substrate arising from either adsorption or absorption. Fundamentally, during the measurement the frequency of a quartz crystal resonator is monitored/measured. The oscillation of the crystal is effected by application of a controlled external alternating voltage. The change in frequency of the resonator can occur due to changes in the density-viscosity of the medium to which the resonator is exposed or due to absorption/adsorption or desorption of material from the surface or film over the surface of resonator. For rigid films, Sauerbrey equation permits the correlation of change in frequency to mass gained/lost per unit area. The Sauerbrey equation can be used to calculate the mass of the film deposited on the electrode surface by assuming that the film is an extension of the underlying crystal. The Sauerbrey equation can be found below. Change in frequency is proportional to change in mass by a sensitivity factor (C_f) which is constant for a 5 MHz AT-cut quartz crystal.

The Sauerbrey equation requires the film to be uniform, rigid and thin, and is applicable when the

change in frequency of the mass is less than 2% of the frequency of the unloaded crystal (5 MHz).

$$\Delta f = -\frac{2f_0^2}{A\sqrt{\rho_q\mu_q}}\Delta m \quad (3.1)$$

$$\Delta f = -C_f\Delta m \quad (3.2)$$

where f_0 is the resonant frequency of blank quartz crystal, A is the area of the working electrode, ρ_q and μ_q are the density and shear modulus of quartz.

Density of polymer films: The density of the film can be calculated by dividing the thickness obtained using ellipsometry by the mass (per area) of film obtained using the QCM. The dry film mass can be obtained by subtracting the resonant frequency of blank substrate at dry condition from the resonant frequency of the crystal after film preparation at dry condition. The frequency change can then be converted to mass using the Sauerbrey equation.

$$\rho_{f,dry} = \frac{\Delta m_{dry}}{t_{f,dry}} \quad (3.3)$$

3.2.2 Variable Angle Spectroscopic Ellipsometry (VASE)

In this thesis, variable angle spectroscopic ellipsometry was used to determine the thickness and optical properties of ionomer films. It is capable of measuring the thickness of nanometer-scale layers. Thus, it is being used in wide areas of research including semiconductors, flat panel displays, biosensors, and optical coating industries.⁵⁰ The working principle behind ellipsometry is quantifying the change in the polarization of light as it reflects or transmits

through a material. Polarized light is generated from a source and directed towards the material at various angles. The light reflected from the material and its various interfaces within is captured and analyzed by the detector and the change in polarization is used to determine the thickness and optical properties of the material. The polarization change is represented by two parameters, psi (ψ) and delta (Δ), which are the amplitude ratio and phase difference respectively. A typical ellipsometry configuration is shown in Figure 3.1.

Polarized light is defined as having a known parallel (p) and perpendicular (s) orientation and phase. A typical light source, also known as unpolarized light generates electromagnetic wave with random orientation and phase. The polarizer converts unpolarized light into polarized light by making the orthogonal waves to have the same amplitude and phase. The resulting orientation of the light is linear. When light interacts with a material, the p- and s- components change resulting in an ‘elliptical’ shape consisting of orthogonal waves of arbitrary amplitude and phase. This is where the name ellipsometry comes from.

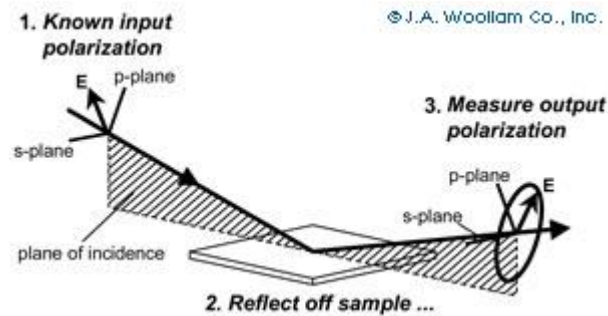


Figure 3.1: Typical ellipsometry configuration. Figure is taken from reference [50].

VASE does not provide the thickness and optical properties directly from the measurement. It only provides the complex reflectance ratio, ρ , of the sample, which is related to the two parameters by Equation 3.1. In order to obtain the thickness and optical properties of the

material, the user must select an appropriate optical model to fit the parameters over a wide range of wavelengths. The goodness of fit is quantified in terms of the Mean Squared Error (MSE). Parameters such as the thickness, roughness, uniformity, and refractive index (RI) can be obtained. The data analysis steps taken are shown in Figure 3.2.

$$\rho = \tan(\psi)e^{i\Delta} \quad (3.4)$$

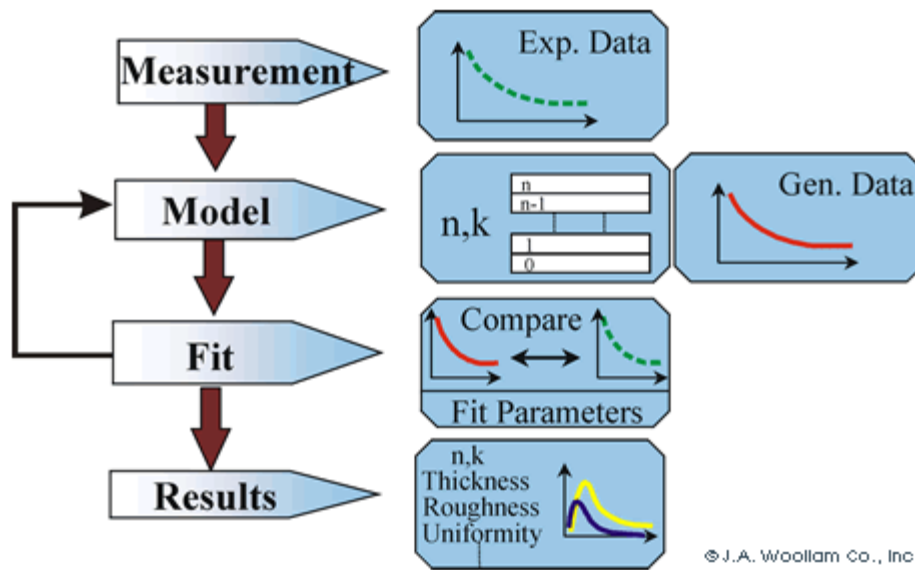


Figure 3.2: Flowchart of ellipsometry data analysis. Figure is taken from reference [51].

The Cauchy model was used to obtain the thickness and refractive index of thin ionomer films. It is commonly used for transparent materials and expresses the refractive index, n , of the material as a function of the wavelength of light, λ_{light} shown in Equation 3.5. The refractive index is the real part of the complex refractive index which is expressed as $\tilde{n} = n + ik$. The complex part, k , which is called the extinction coefficient, measures the amount of light absorbed by the material. For this model, it is assumed that there is no absorption, thus $k(\lambda_{light}) = 0$.

$$n(\lambda_{\text{light}}) = A + \frac{B}{\lambda_{\text{light}}^2} \quad (3.5)$$

where A and B are Cauchy parameters.

An alternate model, such as the Effective Medium Approximation model was tested by *Paul*⁵² to compare the thickness of the film using different models. He concluded that regardless of the model, the thickness of the film was similar. Therefore, in this thesis, only the Cauchy model will be presented.

3.2.3 Atomic Force Microscopy (AFM)

Atomic force microscopy is a type of scanning probe microscopy useful for determining the morphology and roughness of the surface of thin ionomer films. A cantilever with a sharp tip scans the surface of the material while a laser beam is being reflected from the top to a photo detector, which records its movement. As the tip experiences movement due to the force variation between the tip and the surface, the intensity of the reflected beam change. The change in intensity can be analyzed to show a height deviation or deflection force depending on a constant force or constant height mode of the scanner. The force experienced by the tip is calculated with Hooke's law and its dependence on the tip-surface distance is shown in Figure 3.3.

In constant force mode, or contact mode, the tip operates in the repulsive regime as shown in Figure 3.3. The tip is in direct contact with the surface. In constant height mode, or non-contact mode, the tip operates in the attractive regime. Tapping mode is a hybrid of the two

previous modes. The tip is vibrating at a fixed frequency and as the tip comes in contact with the surface, the disturbance in frequency can be analyzed to determine the height of the sample.

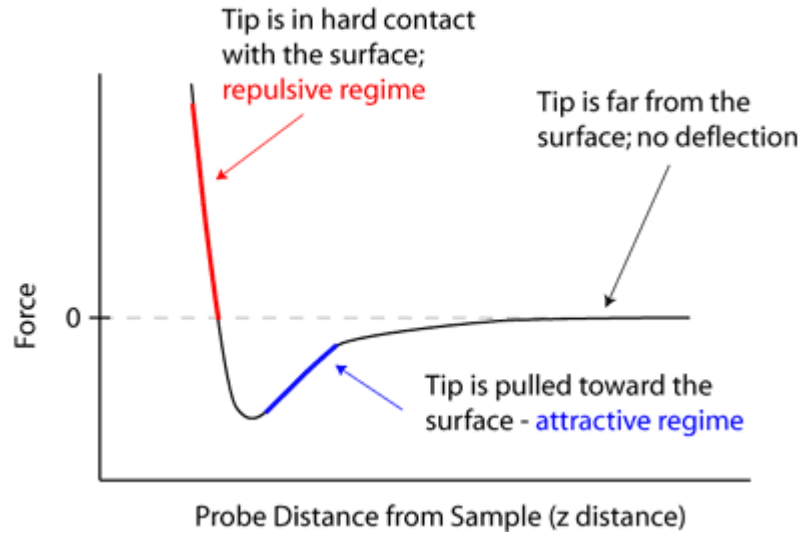


Figure 3.3: Force experienced by tip versus distance of tip to surface. Figure is taken from reference [53].

3.2.4 Goniometer

Goniometer is a useful tool for studying the wetting property of liquids on a sample surface.⁵⁴ By placing a drop of liquid onto the surface, the contact angle can be obtained. Using water as the liquid, one can study whether the surface is hydrophilic or hydrophobic. The instrumentation is presented in Figure 3.4.

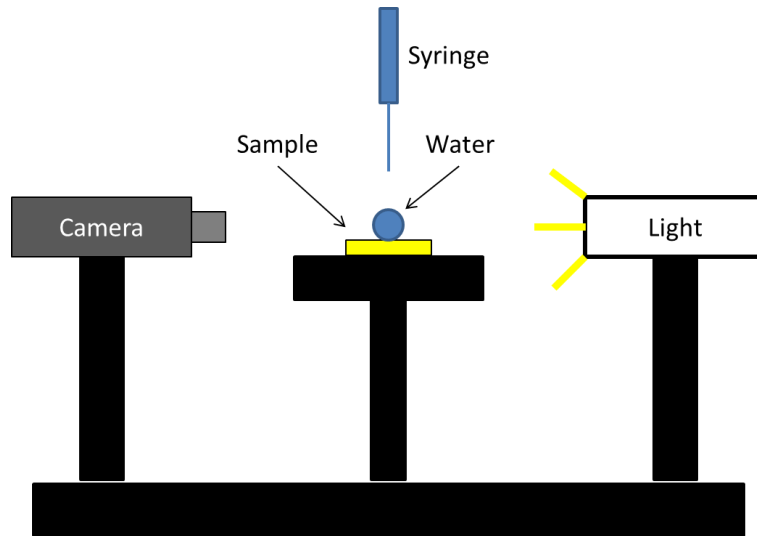


Figure 3.4: Instrumentation of goniometer (contact angle measurement).

After the water droplet is placed on the sample surface, the image is captured by the camera. The DROPimage software (Ramé-hart) can then analyze the image and obtain the contact angle directly. The measured contact angle can be employed by a suitable model, e.g. Young's equation to obtain the surface energy:

$$\gamma^{sv} = \gamma^{sl} + \gamma^{lv} \cos \theta \quad (3.6)$$

where θ is the contact angle, γ^{sv} and γ^{lv} are the solid and liquid surface free energy, and γ^{sl} is the surface-liquid interfacial free energy.

Typically, hydrophobic surfaces exhibit high water contact angle ($\theta > 90^\circ$) while hydrophilic surfaces exhibit low water contact angle ($\theta < 90^\circ$).

3.2.5 Electrochemical Impedance Spectroscopy (EIS)

Electrochemical impedance spectroscopy is a useful tool to investigate the protonic resistance within the film. Impedance measurements are performed by applying a single-frequency voltage to the sample or device of interest contained within or connected to two electrodes. The current generated experiences a shift in phase and amplitude due to the resistance, or more correctly the impedance, of the sample. When the measurement is carried out over a range of frequencies, a spectrum of impedance as a function of frequency results. This is the basis of impedance ‘spectroscopy’. The impedance result is usually represented by a Nyquist plot as shown in Figure 3.5.

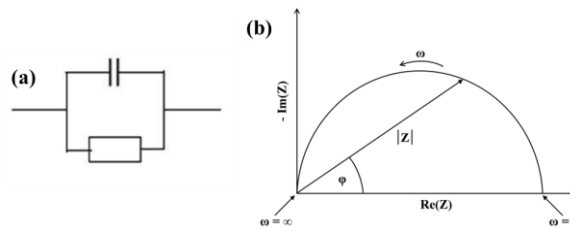


Figure 3.5: Impedance presentation of (a) Equivalent circuit and (b) Nyquist plot.

In this work, a comb-type inter-digitated electrode upon which the polymer film was deposited was employed. Using an appropriate model for the setup, the resistance of the film can be calculated and converted to conductivity using the following formula,⁵²

$$k_f = \frac{1}{R_f} \frac{d}{l(N-1)t} \quad (3.7)$$

where k_f is conductivity of the film and R_f is fitted resistance of the film. d , l , and N represents space between IDA electrodes (100 μm), length of teeth (0.8 cm) and number of electrodes (100) respectively. t is the thickness of the film.

3.3 Summary

The fundamental principles behind the main instruments used in this thesis have been described. Further experimental procedure and measurement protocol including but not limited to the above instruments will be presented in later chapters.

Chapter 4

Fabrication and Characterization of Sub-Micron Thin Ionomer Films

4.1 Introduction

In this chapter, the fabrication and characterization of sub-micron thin ionomer films are described in detail. A thorough run-through starting from the cleaning protocol of the blank substrate to the physical characterization of the films is presented. All substrates, unless otherwise specified, were pre-cleaned using the same cleaning protocol. The blank substrate was characterized using atomic force microscopy (AFM) for roughness and goniometer for water contact angle. The fabricated films were characterized using the quartz crystal microbalance (QCM) for dry mass, ellipsometer for thickness and refractive index (RI), AFM for roughness and the goniometer for water contact angle. Since the properties that are being studied are temperature and humidity sensitive, the validity of the experimental setup is proven. Issues encountered at each step of the experiment are discussed.

4.2 Fabrication of film

As discussed in Chapter 2, polymer film properties can be thickness- and substrate-dependent. Sub-micron thin ionomer films of thicknesses ranging from 16 nm to 155 nm were prepared on quartz crystals of varying working electrode surfaces using two different preparation methods: self-assembly and spin-coating.

4.2.1 Substrate cleaning

All films were fabricated on a 5 MHz quartz crystal (QC) (Tangidyne, Greenville, SC), which was AT-cut and 1 inch in diameter as shown in Figure 4.1. To remove surface contamination prior to film fabrication, the substrates were subjected to a strict cleaning protocol. QCs were immersed in acetone for 20 min followed by rinsing with acetone, IPA and DI water several times. The QCs were then dried with clean dry air. All types of substrate were subjected to the same cleaning procedure.

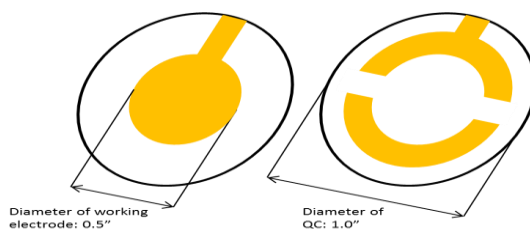


Figure 4.1: Schematic of front (left) and back (right) design of quartz crystal for QCM measurements. Drawing is not to scale.

4.2.2 Ionomer dispersion preparation

Commercially available 5 weight percentage (wt%) Nafion[®] stock solution (LQ-1105, 75/20 w/w alcohol to water, EW 1100) was purchased from Ion Power, USA. The stock solution was diluted to desired concentrations by addition of isopropyl alcohol (IPA) (Sigma-Aldrich) to prepare Nafion[®] dispersions. Dispersions were sonicated for 5 min and equilibrated for at least 24 h to bring the dispersions down to its lower aggregation state.

4.2.3 Self-assembly method

QCs were placed inside a crystal holder (Maxtek, Teflon[®]) exposing only the front side with the working electrode. The crystal holder was fully immersed in the ionomer dispersion and sealed for 12 h to allow for self-assembly as shown in Figure 4.2. The holder was taken out from the solution and the QC was dried with clean dry air for 30 min prior to further drying in the vacuum chamber at 40 °C and low vacuum overnight (10 – 15 h).

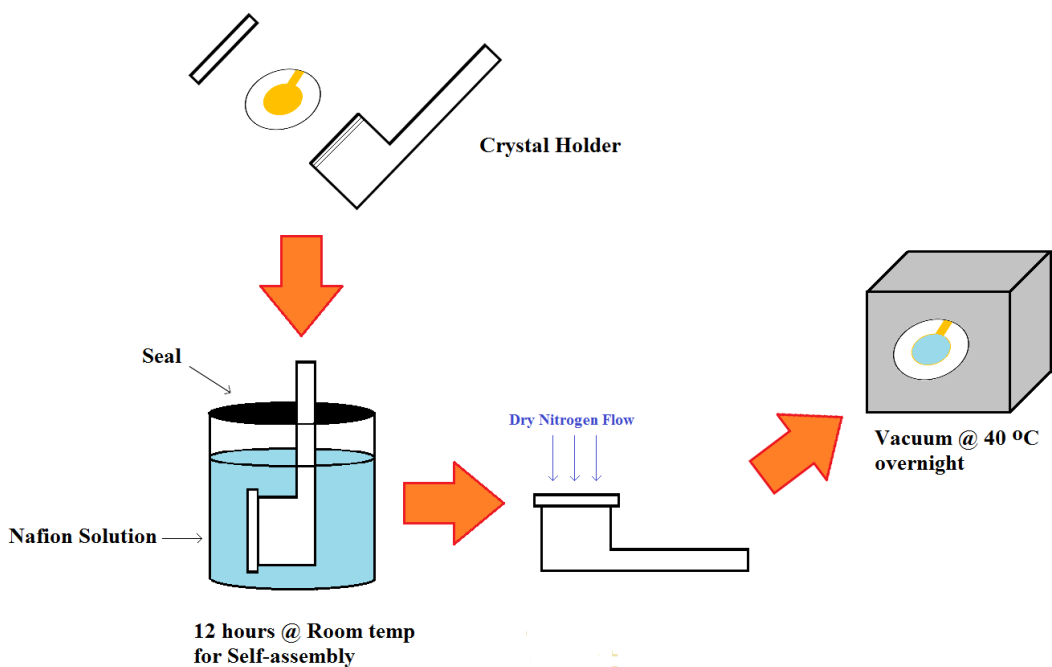


Figure 4.2: Self-assembled Nafion[®] thin film preparation on quartz crystal.

4.2.4 Spin-coating method

A commercial spin coater (WS-650MZ-23NPPB, Laurell Technology Corporation®) was employed for spin-coating of polymer films. For film fabrication, the working electrode of the crystal was placed on the spin coater stage, 0.1 mL of diluted ionomer dispersion of known ionomer concentration was injected onto the working electrode of the crystal and spun for 30 seconds at 5000 RPM. The spin-coated films were subjected to the same drying protocol as the self-assembled films.

4.3 Characterization of film

4.3.1 QCM measurement for ionomer film mass determination

Resonant frequency of QCs under dry air flow (0% RH) at 25 °C before and after film fabrication was measured. The resulting frequency change was converted to dry film mass using the Sauerbrey equation.

4.3.2 Ellipsometry measurement

Ellipsometry measurements were performed on QCs with and without film-coating. The blank substrate measurement was carried out to obtain optical constants for the underlying substrate layer required for fitting subsequent ellipsometer data with a multi-layer model. Measurements were done at three different angles (55, 65 and 75 degrees). All measurements were performed in an open environment where the relative humidity varied in the 10 - 20 % range. To obtain the thickness of films, the focusing probe with ~300 microns spot size, was

employed to measure the thicknesses at 13 different locations of the electrode and used to determine the average thickness and standard deviation.

4.3.3 AFM measurement

AFM images were obtained to study the surface features (roughness and phase contrast) of blank substrates and the thin films. All measurements were performed at ambient conditions in tapping mode by Dr. Paul in our research group.

4.4 Results and Discussions

Unless otherwise stated, all results presented in this section refer to spin-coated films on Au.

4.4.1 Dry film mass

To obtain the dry mass of films, the frequency change that occurred due to film fabrication was recorded and converted to mass change using the Sauerbrey equation. For blank substrate measurements, the resonant frequency under dry air flow at 25 °C was recorded after the cleaning protocol. After films were deposited onto the substrate and dried overnight, the resonant frequency was recorded again under the same condition.

Frequency measurements of QCM were performed in an environmental chamber. A schematic representation of the setup is shown in Figure 4.3. All experiments were performed at 25 °C. The temperature control was ± 0.1 °C. The humidity inside the cell containing the crystal

and holder was controlled with two flow controllers, one of which allowed the flow of air through bubbler containing water. The temperature and humidity were recorded at all times using two probes (SHT71, Sensirion AG Switzerland). A sample profile for humidity and temperature during the measurement is shown in Figure 4.4. Subjecting a humidity change causes a change in frequency. The stability of the frequency when exposed to a humidity step-change can be observed in Figure 4.5. It took about 15 minutes for the frequency to stabilize. All frequency changes were given at least 30 minutes for equilibration to be reached.

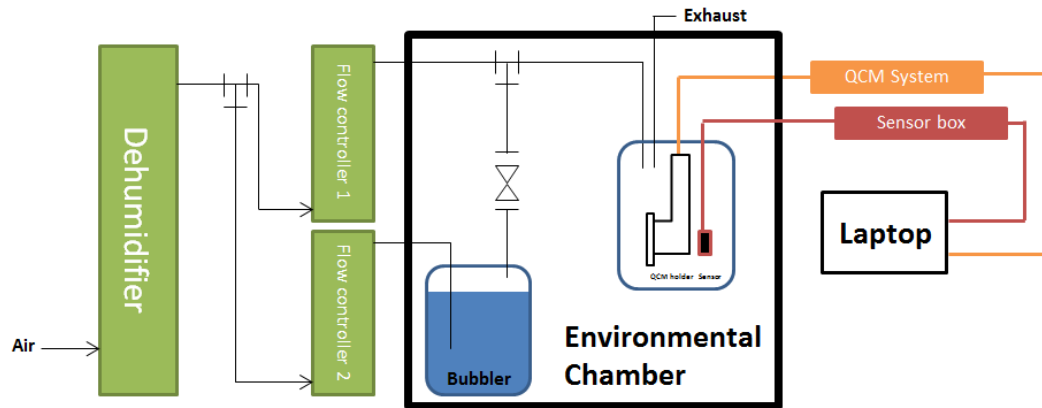


Figure 4.3: Experimental setup for QCM measurements.

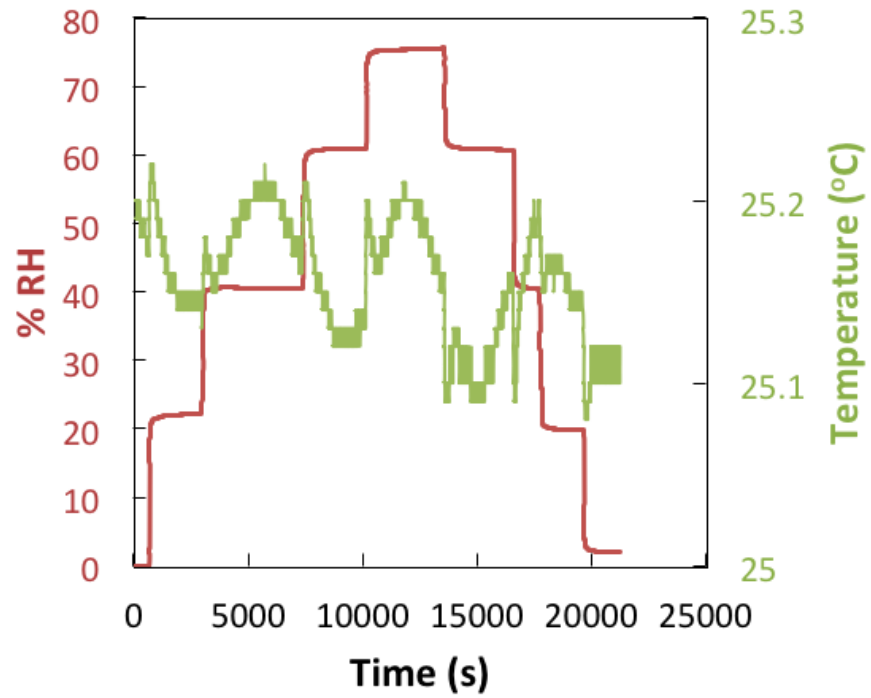


Figure 4.4: Representative RH and temperature profiles during a QCM experimentation.

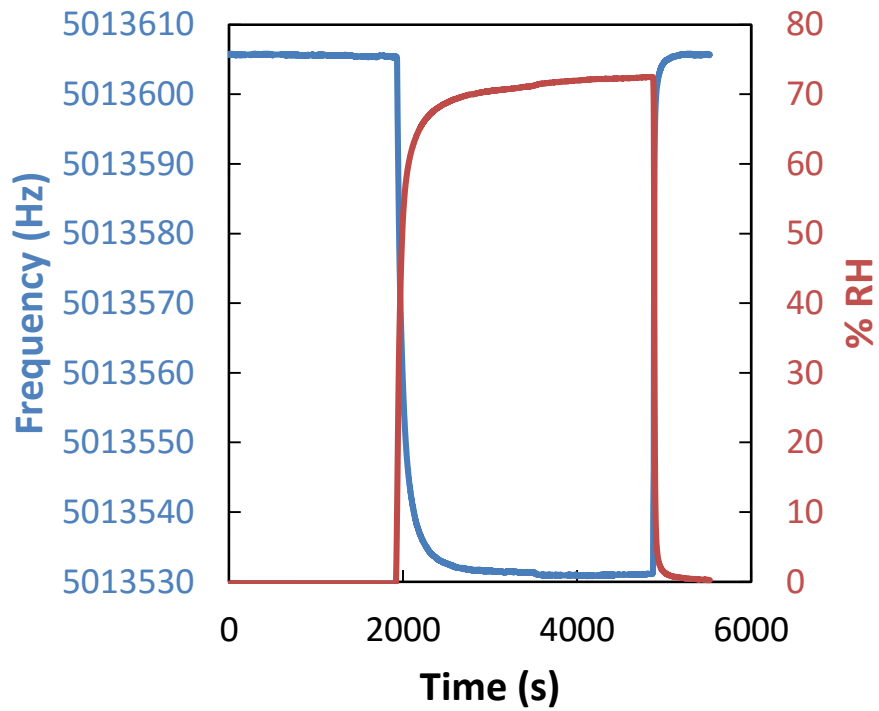


Figure 4.5: Frequency and RH stability during a humidity step change.

To obtain the dry mass of the film, it is necessary to ensure stable reading in dry (0% RH) conditions. As well, it is important that repeatable values of resonant frequency of unloaded and ionomer loaded crystals are obtained. While QCM measurements were performed with the crystal placed in a crystal holder, it was noticed that every time the holder was assembled and disassembled, there was a slight deviation in frequency. These frequency changes, while not significant compared to the frequency change due to film fabrication (<10% for thinnest film) still was a cause of concern. This issue is significant as it carries over to the calculation of hydration number. To compensate for the error, the resonant frequency was averaged out of 5 measurements; each time disassembling and assembling the setup. The film mass as a function of dispersion wt% for all Nafion® films prepared is shown in Figure 4.6. The graph shows a linear trend between film mass and concentration (wt%) of Nafion in the dispersion. The error bars represent 1 standard deviation of the 5 measurements, which is denoted as system error. It is to be noted that the large variation for 3.0, 4.0 and 5.0 wt% dispersions are due to ageing of the dispersion. It was noticed that dispersions that were dormant in the fridge showed signs of decrease in volume. The exact nature of this phenomenon was not studied and to eliminate this issue all subsequent dispersions were prepared the day before film preparation.

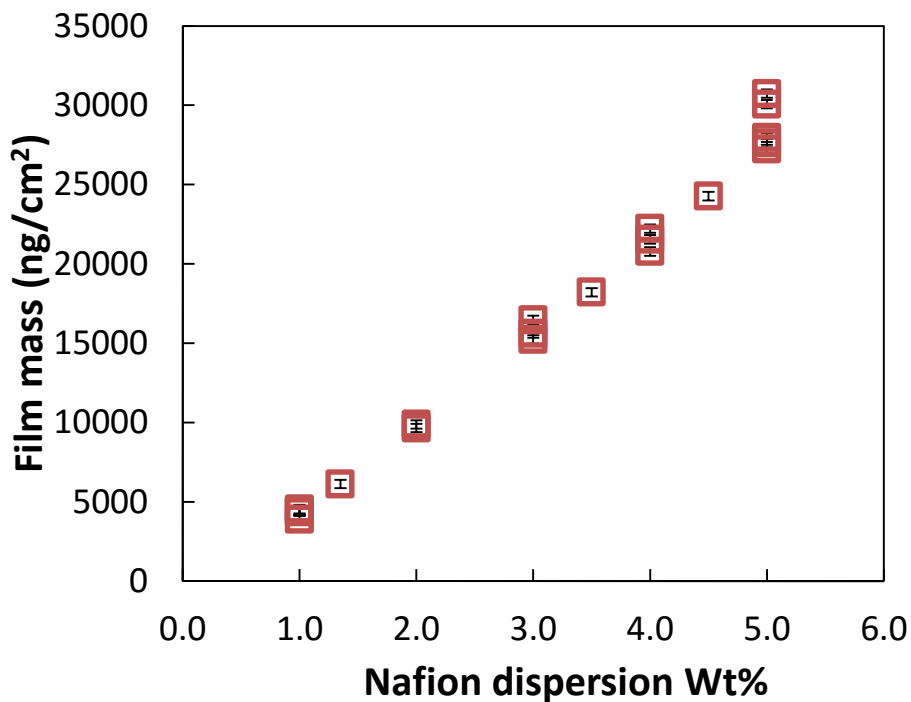


Figure 4.6: Dry film mass as a function of dispersion wt% of spin-coated films. The error bars indicate system error.

4.4.2 Film uniformity: thickness and roughness

4.4.2.1 Thickness

To investigate the uniformity of films, ellipsometry measurements were performed on 13 different points on films on the working electrode. Thickness of films was obtained by fitting ellipsometry data using a simple Cauchy model for optical property of Nafion. Prior to film deposition, the blank substrate was measured to obtain its psi and delta values. This data was used as the underlying substrate layer for the ellipsometry modelling. In the table below, the ellipsometry measurements of the various blank substrates and a diagram of its corresponding

layer are presented in Figure 4.7. For the metal (Au and Pt) substrates, because light is only reflected, a B-spline model was employed to verify that the surface is the corresponding metal. A B-spline model is a convenient data-analysis technique, which simply defines the optical properties of the layer by connecting a set of cubic polynomial splines. The thickness of these layers is not calculated. For the SiO₂ layer, the underlying substrate layer was Au with an additional Si layer on top. The quartz layer in all substrates is not modelled as light does not travel through the Au or Pt layers.

Ellipsometry measurement

Corresponding layer

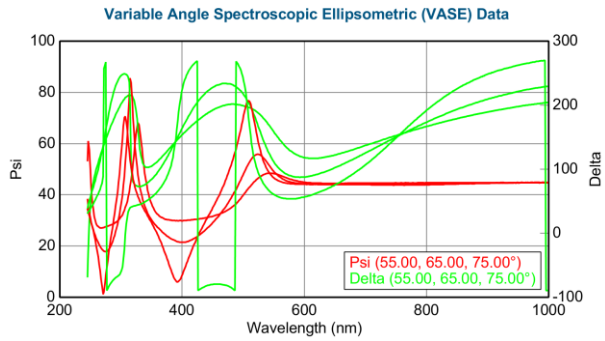
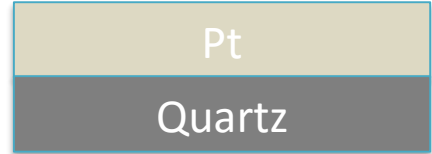
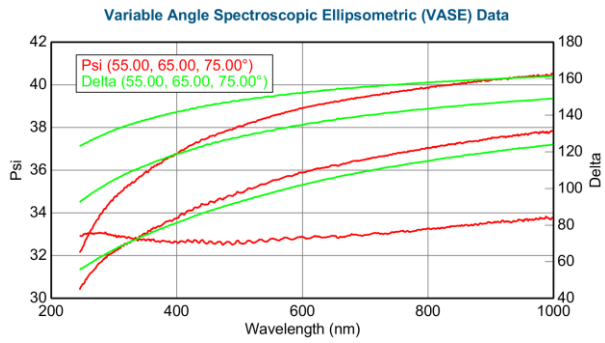
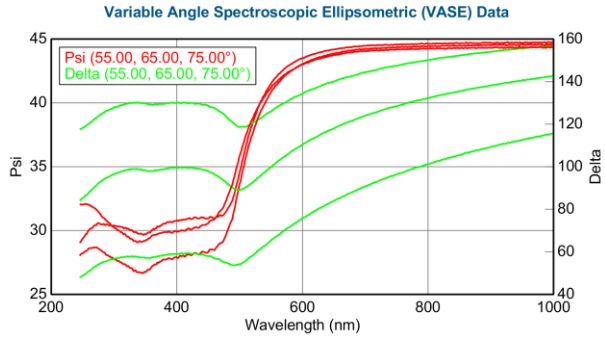
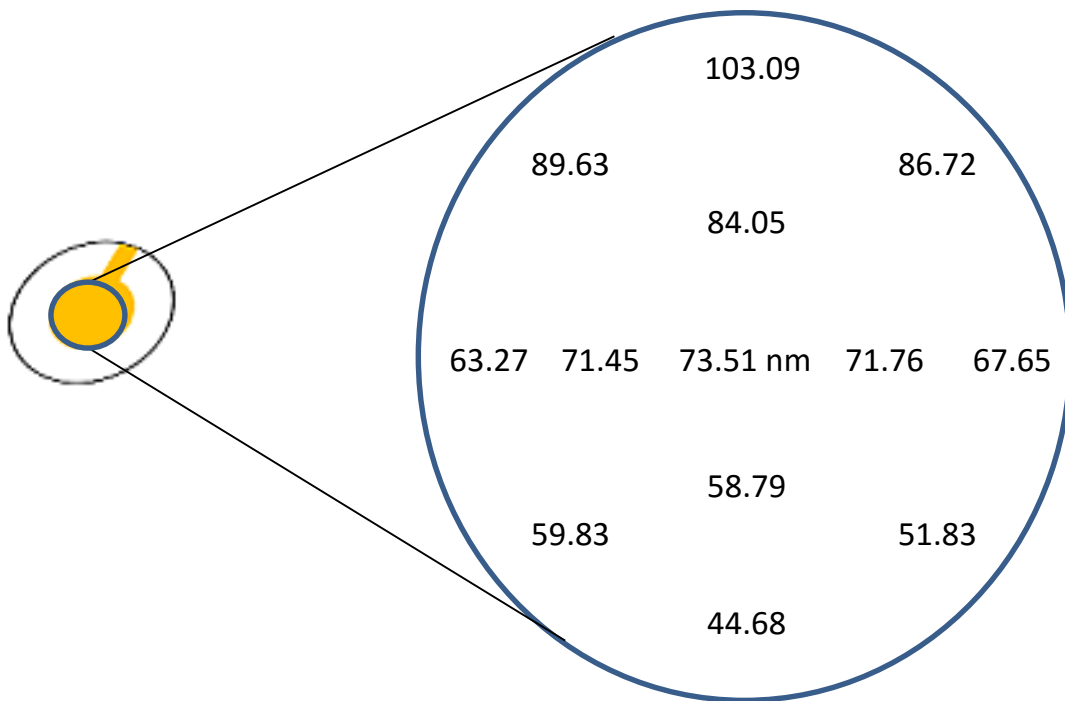


Figure 4.7: Ellipsometry measurement and diagram of corresponding layer for Au (top), Pt (middle), and SiO₂ (bottom) substrates.

Initially, films were prepared using the self-assembly method. However, thickness measurements showed that all films were non-uniform. Figure 4.8 shows the results for measurements performed on a sample self-assembled film. Thickness gradually decreases from the top to the bottom, displaying a variation of almost 60 nm. From further investigation we were able to identify that the issue was caused during the initial drying stage of the film. To remove the excess solvent from the substrate, the entire holder was tilted 45° and nitrogen was flowed from the top-to-bottom in a sweeping motion. This tilting motion was causing the films to have this non-uniform feature. Unfortunately, if the excess solvent were not evaporated with the holder being tilted there would be residual left above the ionomer layer causing other issues. This



fundamental problem could not be fixed. Thus an alternative spin-coating method was employed.

Avg. thickness	71.3 nm
1 St. dev	16.3 nm

Figure 4.8: Thickness measurements performed on self-assembled Nafion film.

After switching to the spin-coating method and developing a new protocol, the issue was resolved. Figure 4.9 shows the thickness measurements on a sample spin-coated film. Unlike the self-assembled film, it can be seen the standard deviation in thickness was within 2 %. For even the thickest films prepared using spin-coating, the standard deviation did not exceed 5 %.

Avg. thickness	77.3 nm
1 St. dev	1.3 nm

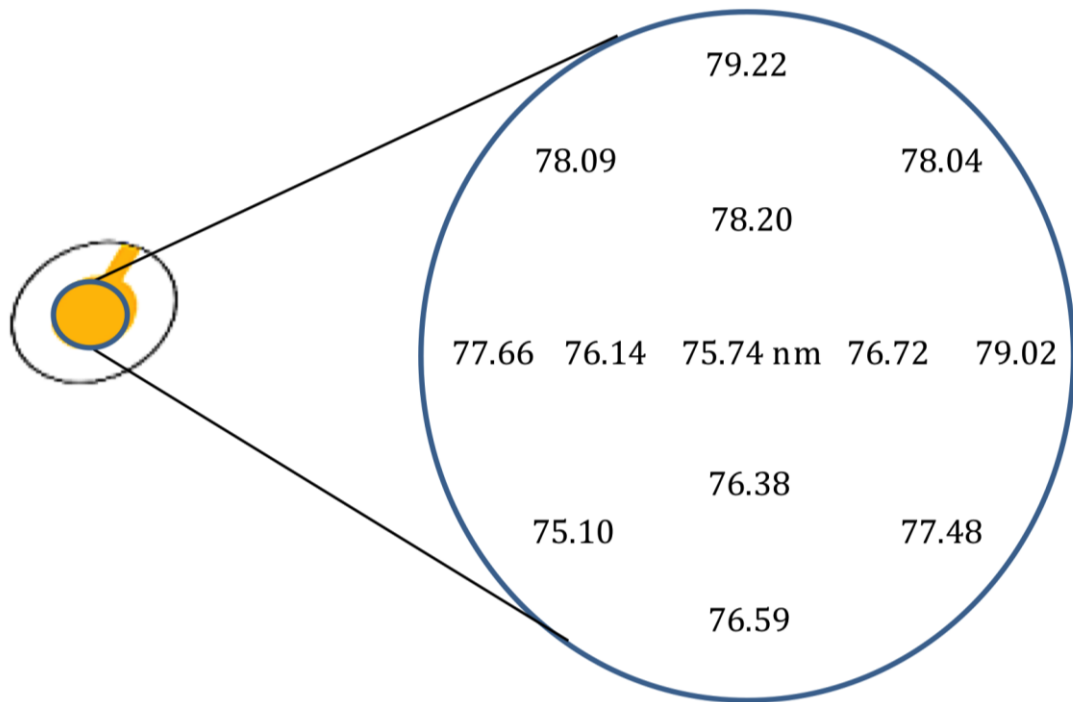


Figure 4.9: Thickness measurements performed on ~77 nm thick spin-coated Nafion film.

The film thickness as a function of dispersion wt% for all Nafion® films prepared is shown in Figure 4.10. Once again, the graph shows a linear trend between film thickness and dispersion wt%.

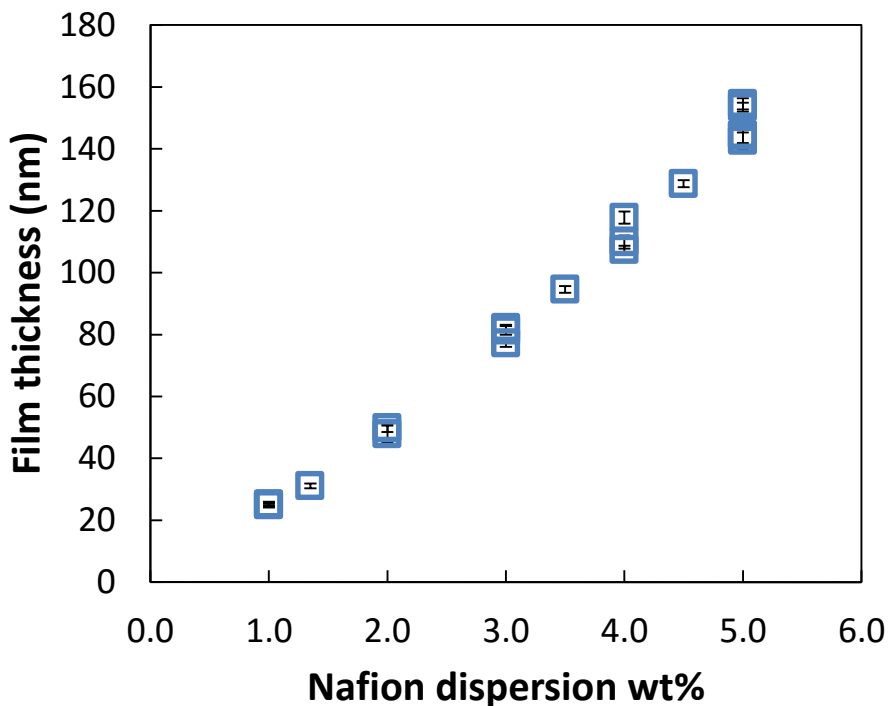
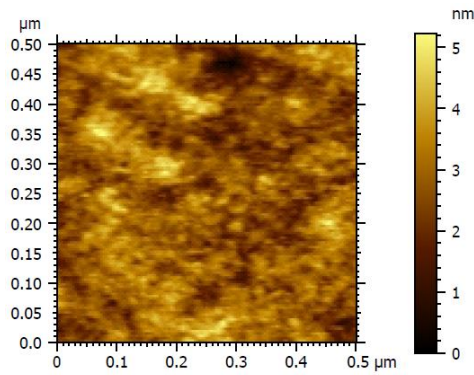


Figure 4.10: Film thickness as a function of dispersion wt% of spin-coated films. The error bars indicate spatial variation.

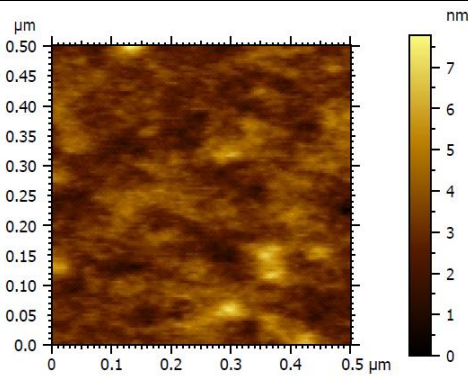
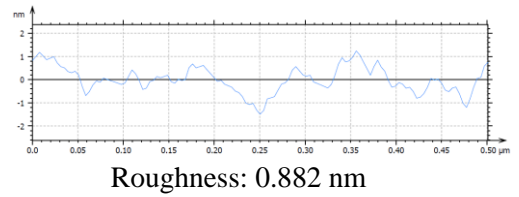
4.4.2.2 Roughness

Roughness of films was investigated using the AFM. To avoid damaging the samples, AFM imaging was performed after all thickness and water uptake measurements were finished. All films were dried extensively prior to imaging to minimize the effect of residual water. AFM image of the thinnest films on respective substrates is presented in Figure 4.11. The roughness was calculated by the Pico Image Elements 7.1 software. All films show very smooth surfaces

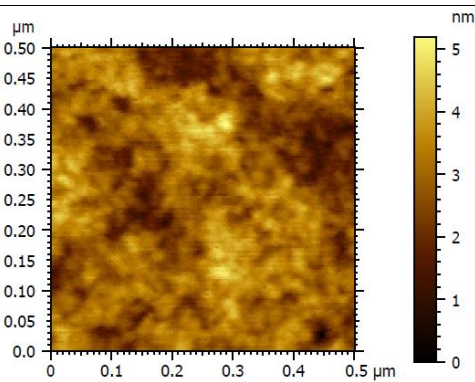
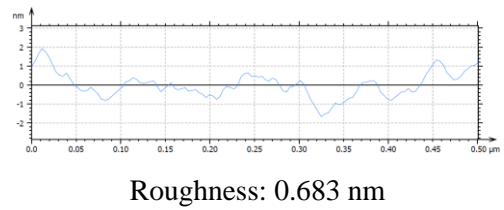
and the roughness calculated from the line scan shows a deviation of less than 5 % from the film thickness.



(a) 26 nm film on Au



(b) 20 nm film on Pt



(c) 25 nm on SiO₂

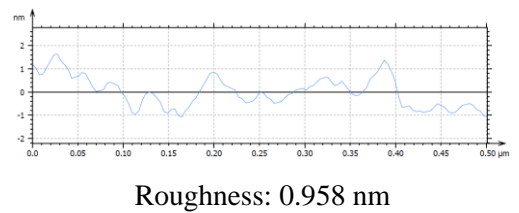


Figure 4.11: AFM image (left) and typical line-analysis (right) for films on (a) Au, (b) Pt, and (c) SiO₂

4.4.3 Thickness-dependent density and refractive index

Using the mass obtained by QCM and thickness by Ellipsometer, the thickness-dependent density and refractive index (RI) was obtained. The density of dry Nafion[®] membrane has been reported to be between 1.8 and 2.0 g/cm³. The RI of dry Nafion[®] membranes has been reported to be about 1.36^{55,56} within a spectral range of 500-600 nm. Figure 4.12 shows a close relationship between density and RI of the films. For thicker films (>80 nm) the RI is very close to that of the membrane at 1.36. The slight deviation of the RI from the value of 1.36 is identically observed in the density. When the RI is 1.36, the corresponding density is roughly 1.93 g/cm³. This close relationship between RI and density is expected since both are obtained by simultaneous fit to the ellipsometry data.

As the films get thinner (25-50 nm), interesting trends emerge. For the 50 nm films, while the RI is similar to that of the membrane, its density is relatively higher. For the 30 nm film, while the density is relatively similar, its RI is comparably lower. The thinnest films (~25 nm) exhibit a significant decrease in both density and RI. *Paul et al*³⁵ observed a similar trend for films below 10 nm thickness. As observed for thicker films, the drop in RI can be attributed to the drop in density. As the density of the films decrease, there is higher voidage or free volume within the polymer causing a decrease in RI.

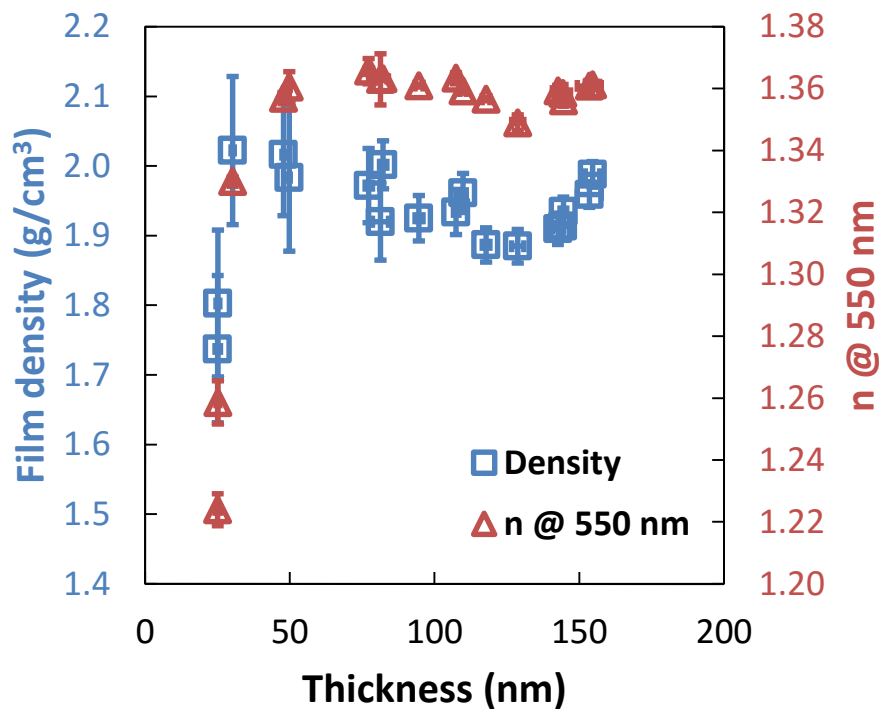


Figure 4.12: Thickness-dependent density (□) and refractive index (Δ) of Nafion® films prepared on Au QCs. Error bars indicate system error.

The properties of films on Pt substrates are shown in Figure 4.13. The RI of thicker films is close to 1.36. The thinnest film (19 nm) has an RI of 1.31 which is the same drop observed previously on Au substrate. However, unlike the thinnest film on Au, there is no significant drop in density for the 19 nm film. In addition to this observation, the density between samples of similar thickness varies significantly while the RI is reproducible. The density of ~50 nm films vary from 1.9 to 2.1 g/cm³ while the density of ~150 nm films vary from 1.8 to 2.0 g/cm³. In order to identify this variability, the blank Pt substrate was investigated. AFM on the surface of the blank Pt surface showed presence of ‘peaks’. Figure 4.14 shows an AFM line-analysis of a sample blank Pt substrate which shows two islands of ~ 7 nm peaks. These peaks might be responsible for the variation in density that we are observing. Unfortunately, it was not possible to probe the entire area of the Pt substrate so the roughness of the substrate was not considered.

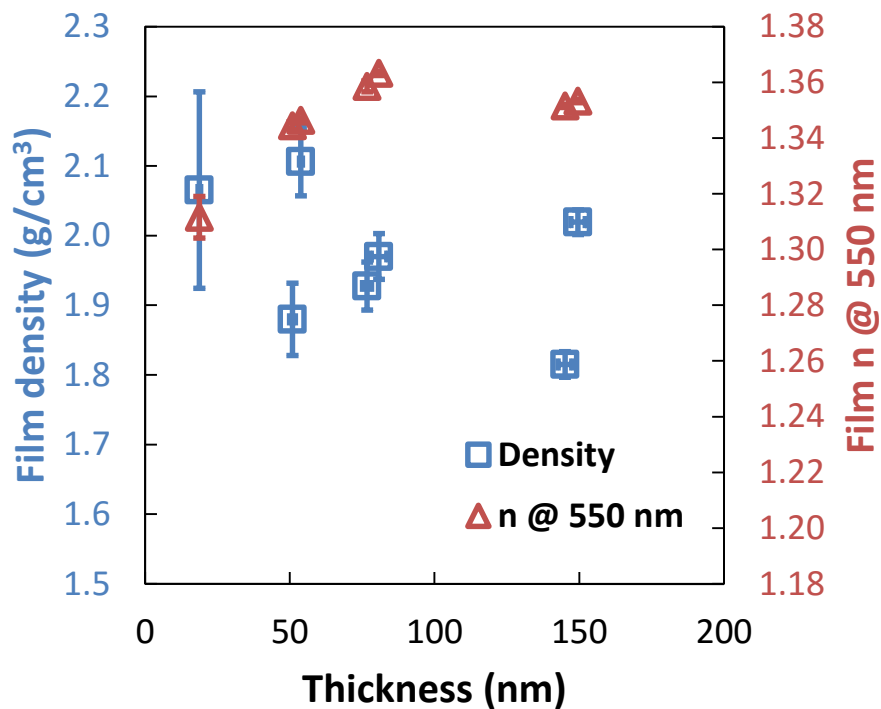


Figure 4.13: Thickness-dependent density (\square) and refractive index (Δ) of Nafion[®] films prepared on Pt QCs. Error bars indicate system error.

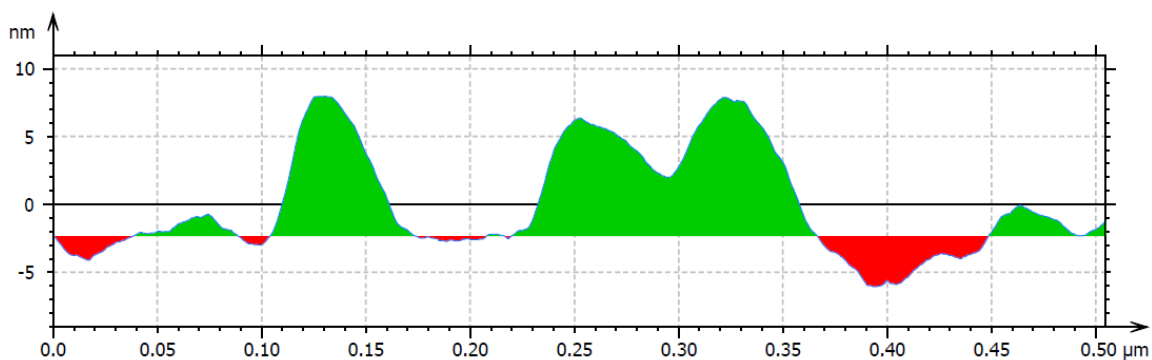


Figure 4.14: Line-analysis of samples blank Pt substrate showing high degree of roughness.

4.4.4 Water contact angle (WCA)

In addition to obtaining the surface roughness of the films using the AFM, the wetting properties of each substrate and film was obtained using the contact angle goniometer. By

obtaining the contact angle of the liquid (water), it is possible to identify whether the surface is hydrophilic or hydrophobic. Surface that exhibit WCA below 90° are said to have a hydrophilic surface while hydrophobic surfaces exhibit WCA above 90° . All our blank substrates showed WCA $\sim 90^\circ$ indicating hydrophobic surfaces.

The surface wettability of all films spin-coated onto QCs showed comparable values to the blank substrate. This indicates that all our films have a hydrophobic surface. This is comparable to the reported value of Nafion[®] membranes.⁵⁷ Meanwhile, it was reported by *Paul*⁵² that films of thickness <55 nm on SiO₂/Si wafers exhibited hydrophilic surfaces. However, even for our thinnest film (~ 20 nm) the surface wettability showed a hydrophobic surface. The reason for this discrepancy can be attributed to the differences in the substrate. Nafion films on carbon and gold surfaces have been observed to be hydrophobic.

4.5 Conclusions

In this chapter, we introduced two different film preparation methods: self-assembly and spin-coating. The films were characterized using QCM and ellipsometry for its dry mass and thickness. The ellipsometry measurement showed non-uniformity in self-assembled films which lead us to use the spin-coating method. A strict protocol was followed during film preparation and a linear trend between thickness and dispersion wt% was observed.

The spin-coated films on gold electrodes of the QCs showed uniform and smooth hydrophobic surfaces for all thicknesses and substrates as confirmed by AFM and goniometer. Using data obtained from the QCM and ellipsometry, the thickness-dependent density and RI was obtained. The density of thicker (>55 nm) Nafion[®] films on Au were between 1.8 and 2.0 g/cm³ and were closely related to its RI. The thinner (<55 nm) films on Au exhibit a sharp drop in both

density and RI. The density and RI trend for films on Pt were different and inconsistent which is attributed to the presence of random peaks on the blank Pt substrate.

Chapter 5

Thickness and Substrate-dependent Water Uptake Properties

5.1 Introduction

Proton conductivity is an important property of the ionomer as the primary function in the CL.³⁻⁷ As stated in Chapter 2, the intrinsic property is not the same in the thin film form compared to the membrane form. The structure and water uptake affect proton conduction and the former are thickness- and substrate-dependent. Previously, our group reported significantly depressed proton conductivity of Nafion[®] *ultra-thin* films on SiO₂ supported films compared to the membrane.⁶ However, when the water uptake was measured by Hickner group (Penn State Univ., USA), an opposite trend of higher water uptake for lower thickness was observed; thin films (4-10 nm) exhibited significantly higher water uptake compared to the membrane. The discrepancy between these results needs to be clarified. Furthermore, the effect of thickness and substrate (SiO₂, Au, and Pt) on water uptake is reported in this chapter.

5.2 Anomalous water uptake on SiO₂ substrate

In this work, thin films on SiO₂ substrates prepared by spin coating were characterized for water uptake at various RH and 25 °C. It must be noted that the vacuum-dried thin film was assigned a λ value of zero. *Krttil et al*³² reported that for Nafion[®] membranes, drying for a short amount of time could lead to residual water with $\lambda = 1.5$ at dry conditions. In order to address this issue, all films were dried extensively in the vacuum oven for a prolonged period of time as mentioned in section 4.2.3. The water uptake data for spin-coated films with thicknesses ranging

from 16 to 146 nm are presented in Figure 5.1 in addition to the previously reported data. Our data shows that, in agreement with the previously reported data, water uptake is significantly higher than that of the membrane. For a simpler comparison, water uptake of films at 75% RH has been presented in Figure 5.2. We also observe that water uptake decreases with increasing thickness and our data fills in the gap between the previously reported data adequately. While it verifies that the previously reported data is not wrong, it does not explain the discrepancy between high water uptake and low proton conductivity.

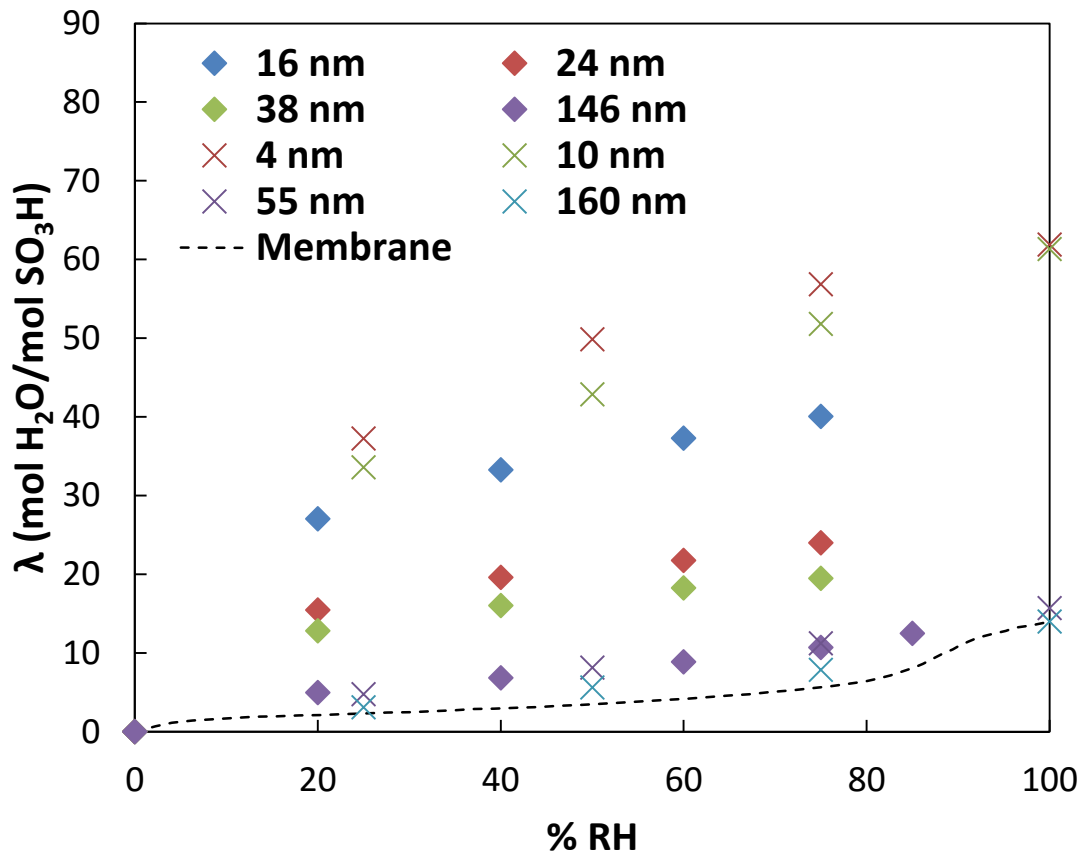


Figure 5.1: Water uptake of Nafion® films on 300 nm SiO₂ substrate (◇). Data reported by Modestino et al⁶ (X) are also included.

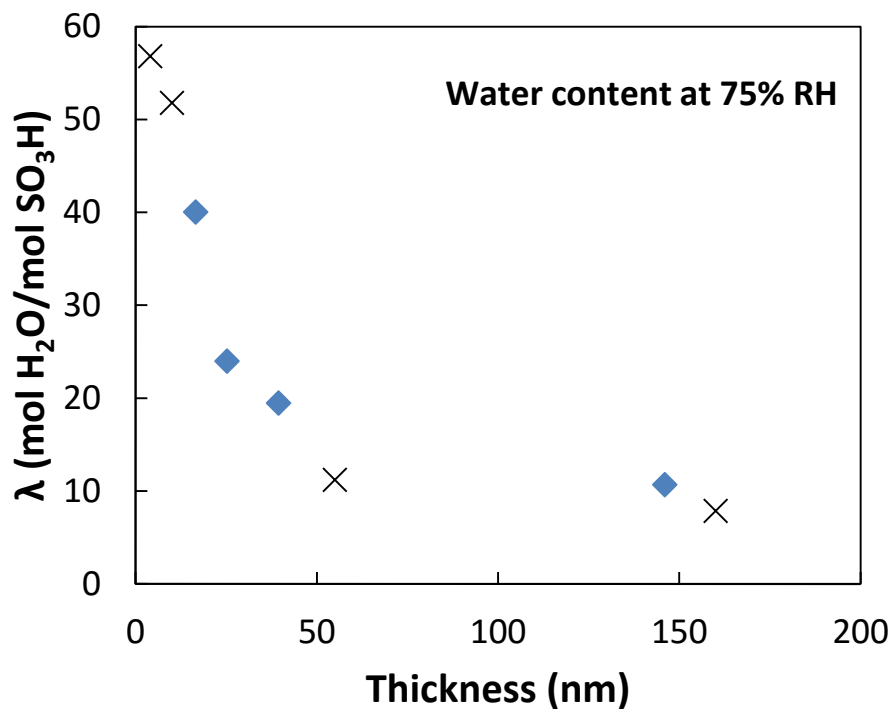


Figure 5.2: Water uptake of Nafion® films on 300 nm SiO₂ substrate (◇) at 75% RH. Data reported by Modestino et al⁶ (depicted by symbol X) are also included.

Initially, the high water uptake was attributed to the contribution of interfacial water on the ‘observed’ water uptake. It was hypothesized that the interfacial water will not change with the SiO₂ layer thickness, provided it was dense. If the sputtered SiO₂ layer was nanoporous, then films on different thicknesses of SiO₂ layer would exhibit different amounts of water uptake. All previously reported data in this work have been on thin films prepared onto 300 nm SiO₂ layer on Au. In order to investigate the effect of SiO₂ layer thickness, QCs with 100 nm SiO₂ layer on Au were purchased. Water uptake data for films with thicknesses ranging from 25 – 83 nm at 75% RH are presented in Figure 5.3. Interestingly, films of similar thicknesses (25 and 40 nm) exhibit water uptake value greatly different. This result is unexpected; how is the thickness of the SiO₂ layer below the film affecting water uptake of the film? Due to limitations in studying the nano-

structure of the films, the focus was shifted toward the blank substrate. Experiments were carried out on blank SiO₂ substrates to verify if they were the root cause of this issue.

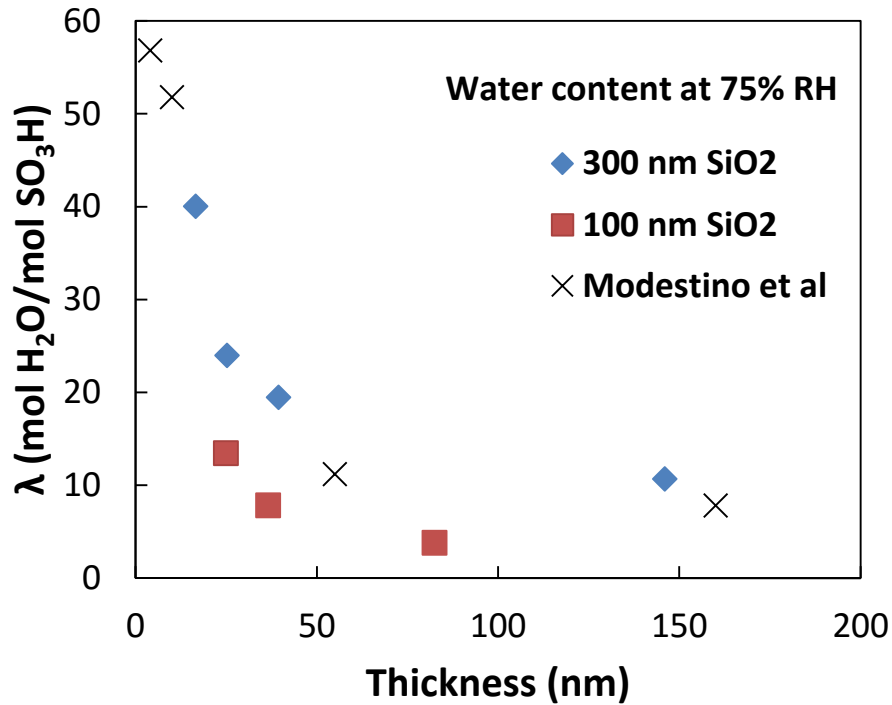


Figure 5.3: Water uptake of films on 100 nm SiO₂ substrate (□) at 75% RH added to Figure 5.2.

The water uptake of blank substrates is plotted in Figure 5.4. The Au and Pt substrates adsorbed negligible amount of water, equivalent to forming a water layer of roughly 0.7 nm on the surface at 75% RH. *Lee and Staehle*⁵⁸ reported roughly 3 nm water layer formation on films on Au at the same condition. The SiO₂ substrates on the other hand adsorbed a significant amount of water. At 75% RH, the observed water uptake on 100 and 300 nm SiO₂ layer corresponds to a water layer of 8 and 18, nm respectively. Water adsorption on SiO₂ substrate has been attributed to the presence of silanol groups at the surface.⁵⁹ *Asay and Kim*⁶⁰ reported that at 100% RH, a 3 nm multilayer of water can form on native oxide films. The high multilayer forming on our QC substrate suggests presence of pores. The SiO₂ substrates that were used in this thesis were

prepared by sputter-deposition and it has been reported that sputter-deposited SiO₂ layers exhibit highly-connected open pores as large as 2.6 nm.⁶¹ The ratio of water adsorption on 100 nm to that on 300 nm SiO₂ layer is almost 3 at all RH providing further evidence of the porosity. Attempts were made to investigate the porosity of the SiO₂ layer of our substrate but were unsuccessful. A confocal microscope was employed, and while initial results looked promising, they were deemed unfit due to the sensitivity of the instrument.

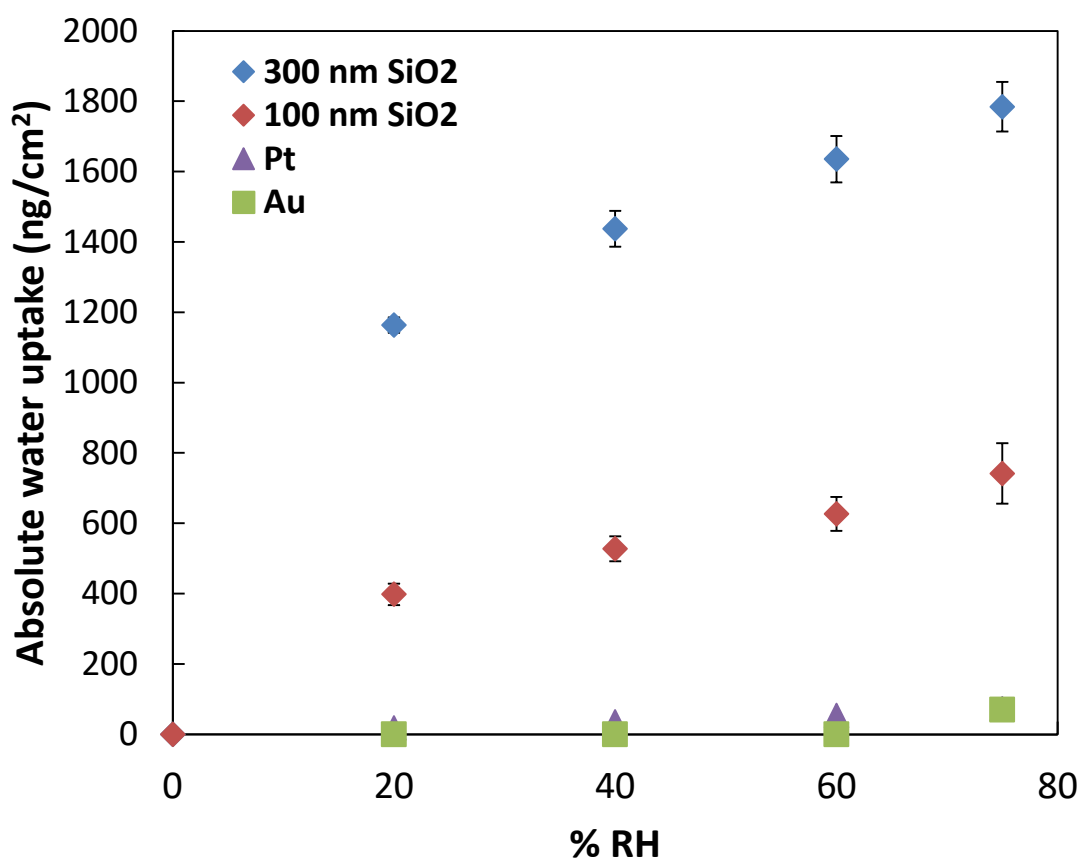


Figure 5.4: Comparison of water uptake of blank substrates. Error bars indicate sample-to-sample variation.

5.2.1 Corrected versus non-corrected λ

To obtain the correct water uptake for films on SiO₂ substrates, the water adsorption on blank SiO₂ substrates must be taken into account. Prior to film fabrication, the water uptake of blank SiO₂ was measured and recorded. After the film was prepared, the water uptake study was repeated. The corrected water uptake for films on SiO₂ substrates was obtained by subtracting the blank SiO₂ water uptake from the film water uptake,

$$WU_{corr} = WU_{with\ film} - WU_{without\ film} \quad (5.1)$$

where WU_{corr} is corrected water uptake, $WU_{with\ film}$ is water uptake of film and $WU_{without\ film}$ is water uptake of the blank SiO₂ substrate.

The uncorrected and corrected water uptake of 25 nm Nafion® films on 100 and 300 nm SiO₂ substrates are presented in Figure 5.5. The uncorrected water uptake for both films is much higher than the membrane water uptake. However, once the blank water uptake is taken into account, the corrected water uptake of both films is comparable and much lower than that of the membrane. Although the corrected water uptakes are not identical, the fact that they are comparable after correction indicates that the anomalous water uptake observed on SiO₂ substrate can be attributed to the blank SiO₂ adsorbing water.

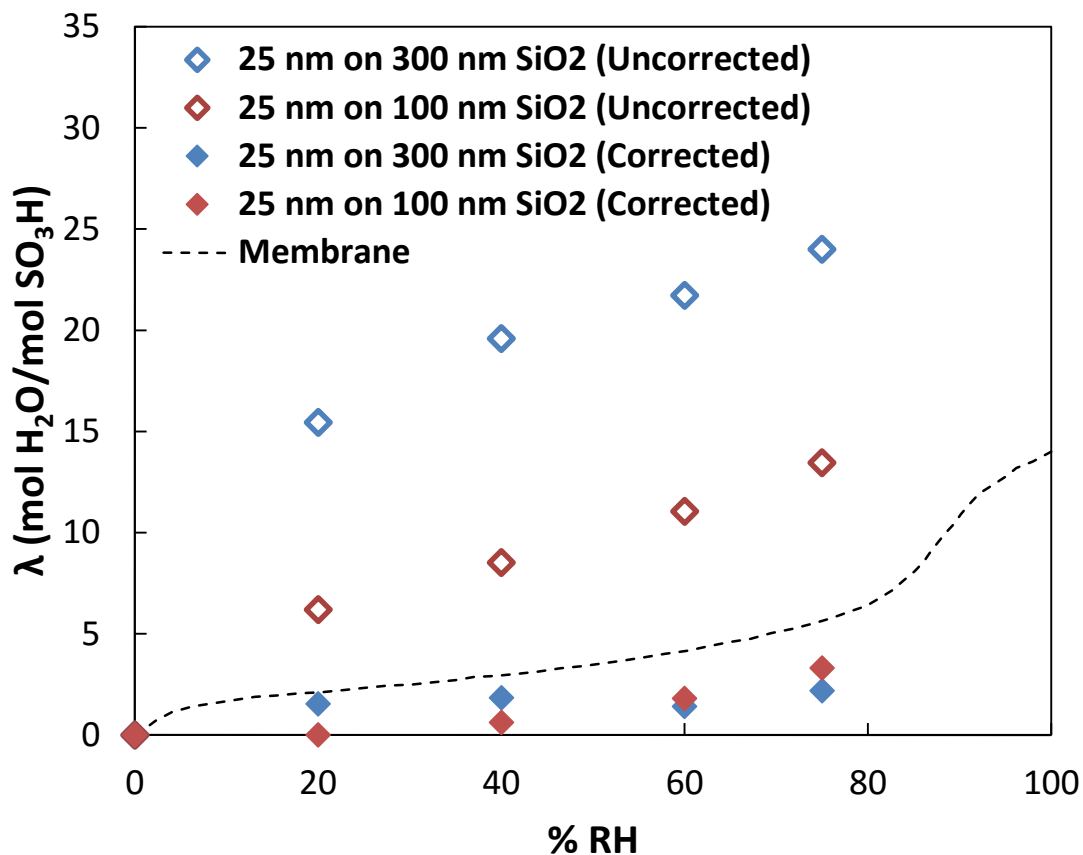


Figure 5.5: Uncorrected (open) and corrected (solid) water uptake of 25 nm films on 100 (red \diamond) and 300 (blue \square) nm SiO₂ substrate.

5.2.2 Substrate-effect on water uptake

Considering the reason underlying the anomalous water uptake of films on SiO₂ substrate has been discovered, the study on the effect of substrate can be investigated using the corrected water uptake. Figures 5.6 to 5.8 compare the water uptake of <55, 80, and 150 nm films on Au, Pt, and SiO₂ respectively. The reason for plotting <55 nm films together is explained later in the chapter. In Figure 5.6, the water uptake of <55 nm films on various substrates are plotted along with the water uptake of the CL reported by *Weber et al*⁵. The corrected water uptake of the 25 nm on SiO₂ is comparable to the water uptake of 25 nm on Au and 54 nm on Pt. They all exhibit

water uptake values lower than what is reported for the membrane. The water uptake of thin films is comparable to the CL water uptake at lower RH (< 40%) but adsorbs more at higher RH.

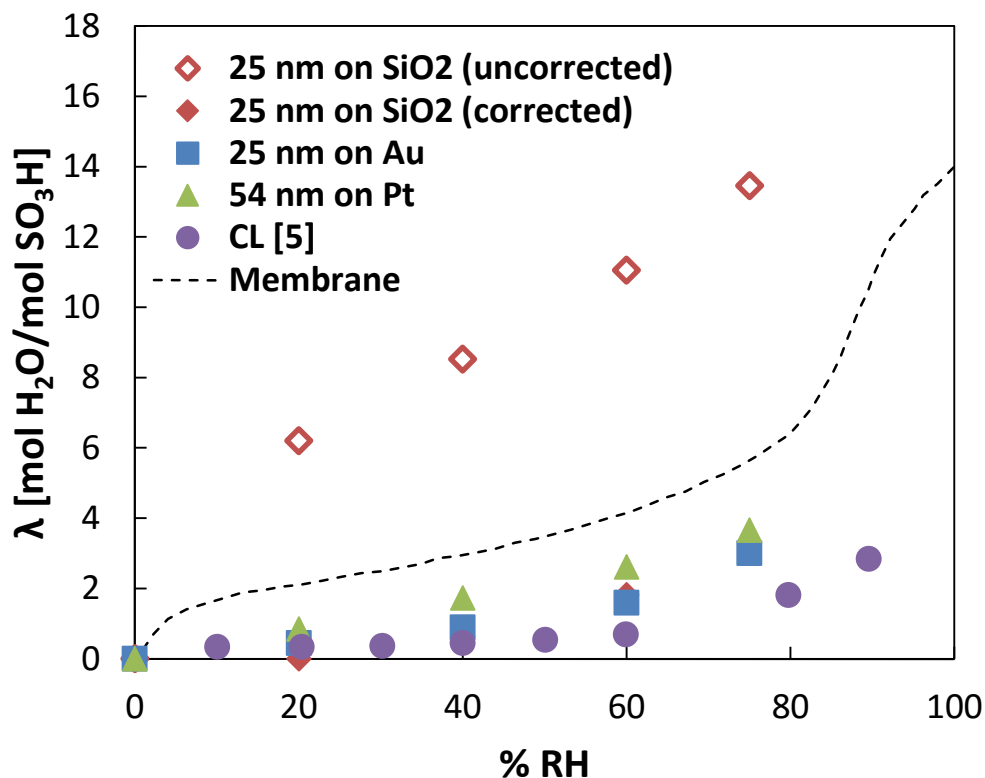


Figure 5.6: Water uptake of <55 nm films on Au (\square), Pt (Δ), and SiO₂ (\diamond) compared to WU of CL (\circ) taken from reference [5]. The uncorrected (open) and corrected (solid) data for film on SiO₂ substrate are presented.

In Figure 5.7, the water uptake of ~80 nm films on Au, Pt, and SiO₂ can be seen. For these films, after the water uptake of the 83 nm on SiO₂ is corrected, the values of all three films are very comparable. Similarly, in Figure 5.8 the water uptake of ~150 nm films are also comparable all exhibiting water uptake similar to that of the membrane. This suggests that water uptake of Nafion[®] thin films although dependent on substrate type are not as strong a function of substrate as previously reported⁶.

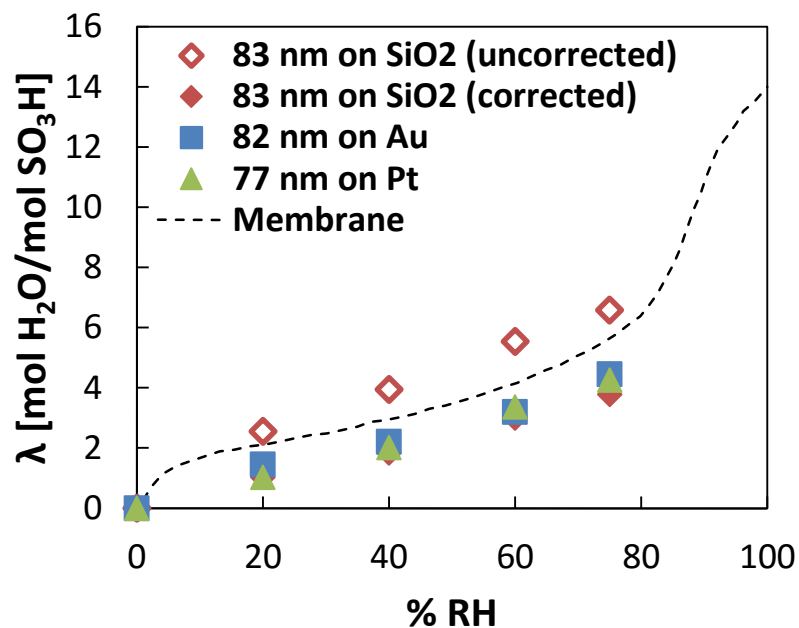


Figure 5.7: Water uptake of 80 ± 3 nm films on Au (\square), Pt (Δ), and SiO₂ (\diamond). The uncorrected (open) and corrected (solid) data for film on SiO₂ substrate are presented.

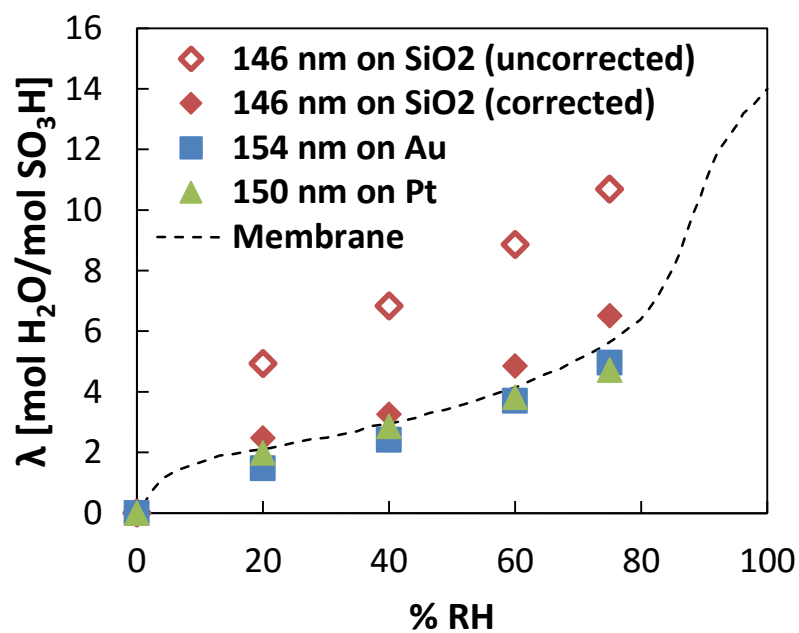


Figure 5.8: Water uptake of 150 ± 4 nm films on Au (\square), Pt (Δ), and SiO₂ (\diamond). The uncorrected (open) and corrected (solid) data for film on SiO₂ substrate are presented.

5.2.3 Correlating conductivity with water uptake

One of the main reasons for studying water uptake of films on SiO₂ substrate was to resolve the contradiction between low proton conductivity and high water uptake. Conductivity of two films, 25 and 83 nm were measured on interdigitated array (IDA) of Au electrode on SiO₂ using Electrochemical Impedance Spectroscopy (EIS).

A plot of conductivity versus corrected λ is shown in Figure 5.9. Due to the high water uptake of Nafion[®] membranes, proton conductivity at low λ is difficult to be obtained. However, if we extrapolate the membrane data to lower λ values, we can see that the thin film data no longer differs by 1 to 2 orders of magnitude. This indicates that the proton conductivity for Nafion[®] is a strong function of water content and less of morphology.

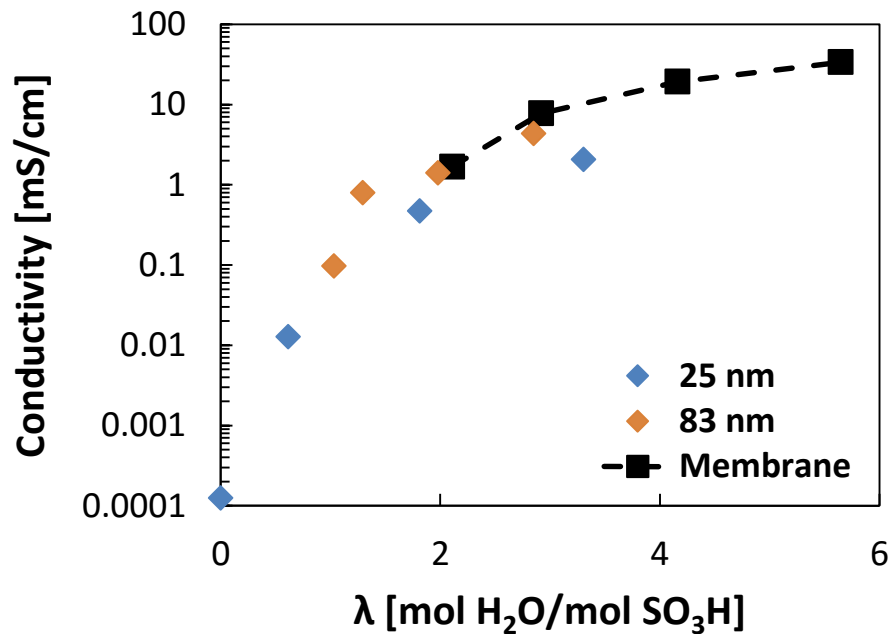


Figure 5.9: Conductivity versus λ of thin films on SiO₂ compared to membrane.

5.3 Equilibrium water uptake on Au substrate

Due to anomalous water uptake of blank SiO₂ substrates, the Au substrate was chosen to carry out the thickness-dependent water uptake of Nafion[®] thin films. Au substrates are ideal because they are inert and the blank substrate adsorbs insignificant amount of water. Films of thicknesses ranging from 25 nm to 154 nm were prepared and tested for water uptake between 25 and 75 % RH. Figure 5.10 shows the thickness-dependent mass water uptake of films at 20, 40, 60 and 75% RH. Here, mass water uptake indicates the absolute mass calculated from the change in frequency converted using the Sauerbrey equation. Water uptake increases with increasing thickness and shows a sigmoidal shape plateauing near 100 nm. At 20% and 40% RH, the 150 nm film shows lower water uptake than the 130 nm film. The reason for this behavior is not clear or obvious. One possibility could be the error introduced by the rigid film assumption that is the basis of Sauerbrey equation, which is employed to calculate the mass change from the observed frequency change of the QC. It has been stated by *Weber et al*⁶² that the structure of thin films on silicon substrates was greatly impacted below 100 nm. While they observed a difference in structure for Au, Pt, and carbon substrates, the structural change occurring below 100 nm could be independent of substrate. The observed water uptake data seems to suggest that the water uptake above 100 nm is an intrinsic property. The water uptake data were converted to hydration number and are plotted against RH in Figure 5.11.

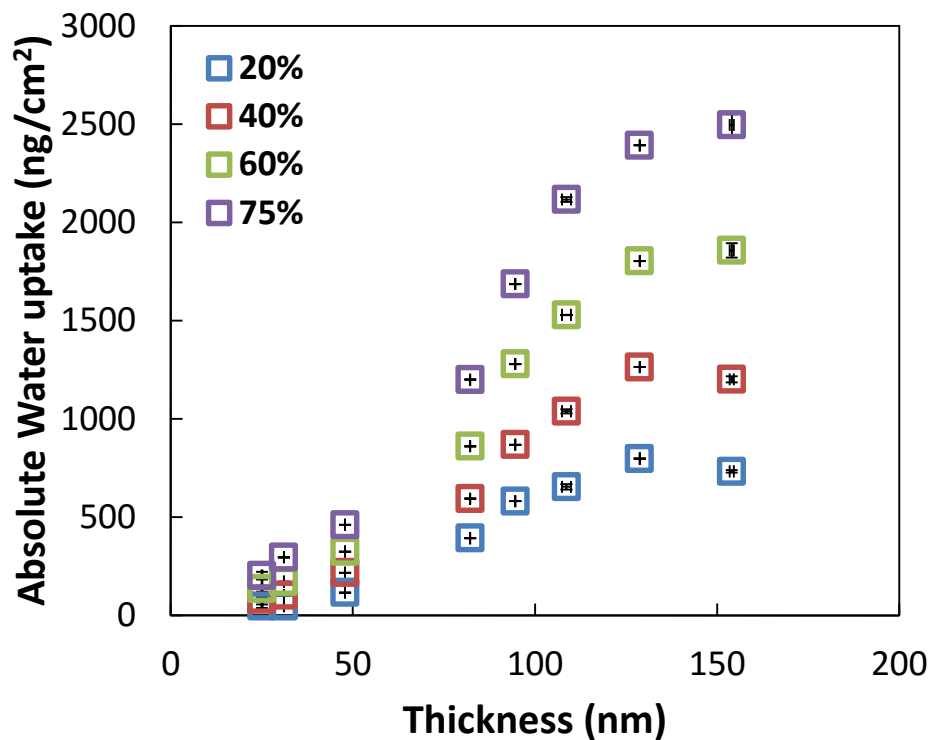


Figure 5.10: Thickness-dependent absolute mass water uptake at various RH of Nafion® thin films on Au. Error bars indicate sample-to-sample variation.

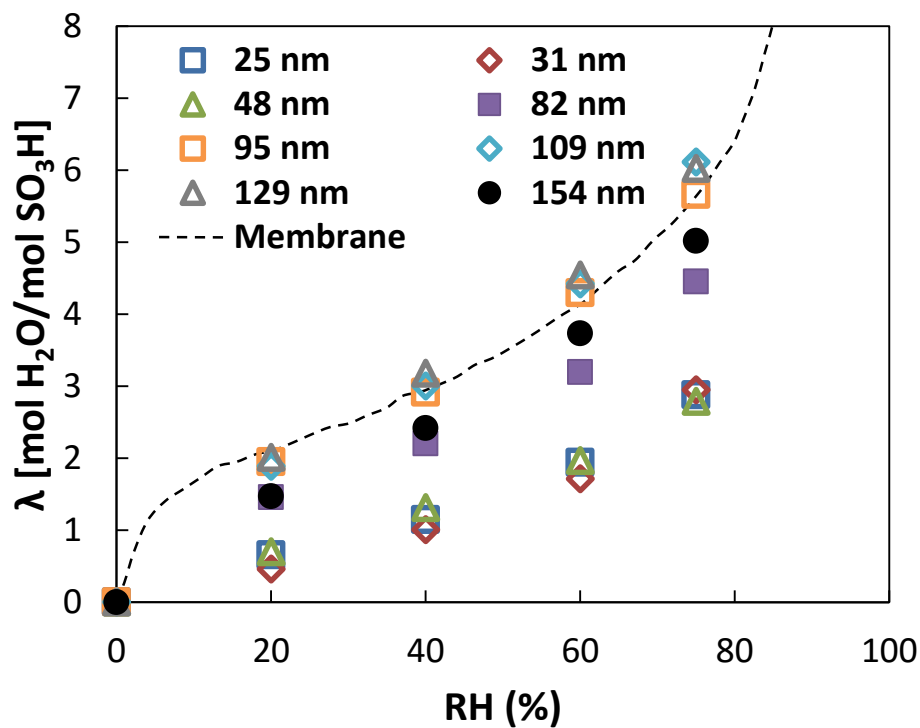


Figure 5.11: Water uptake for Nafion® films on Au substrate.

Figure 5.11 shows a general increase in λ with increasing thickness, in addition to three different 'clusters'. The thinnest films (25, 31, and 48 nm) show almost identical values that are much lower than that of the membrane. The 82 nm exhibited higher water uptake than the thinnest films but still lower than the membrane. The thicker films (96, 109, and 129) are comparable to membrane water content which was observed by other groups^{9,33,34}. The decrease in water content for the 154 nm was not investigated further.

The water uptake of 95, 109, and 129 nm films are slightly higher than the thickest 154 nm and are comparable to the membrane form. As mentioned earlier, the structure of thicker films (>100 nm) are expected to be similar, thus a similar water uptake is within expectation. The fact that we are observing slightly varying values for these films could be real, but one of the issues that might arise is the validity of the Sauerbrey equation for films >100 nm. *Vogt et al*⁶³ has reported that for thicker films, the Sauerbrey analysis might not be accurate as the viscosity of the film cannot be ignored. However, *Weber et al*⁶² have reported that for Nafion[®] films of thickness <600 nm, the Sauerbrey equation was valid stating that Nafion[®] experiences excessive viscoelastic losses at much greater thickness than pure polyelectrolytes. Due to limitations in studying the viscosity of the films, the Voigt analysis was not performed. Another contributing factor might be the sensitivity of the QCM. The main point is that water uptake of thin films does not exhibit water uptake higher than the membrane.

The water uptake trend observed in Figure 5.11 is comparable to the proton conductivity reported by our group⁵ on self-assembled films prepared on IDAs as shown in Figure 5.12. It was observed that conductivity of films below 55 nm were comparable to each other while the 160 nm film exhibited conductivity slightly lower than that of the membrane. The similar trend in water uptake and proton conductivity suggests that conductivity is mostly dependent on water content

rather than structure. To further verify this claim, film of thickness 78 nm was prepared and its conductivity was measured. A 23 nm film was also prepared and tested for comparison. In accordance with our water uptake property, the 78 nm film exhibited proton conductivity between the 23 and 160 nm films as presented in Figure 5.13. This further suggests that proton conductivity of Nafion® thin films are highly dependent on water content rather than structure.

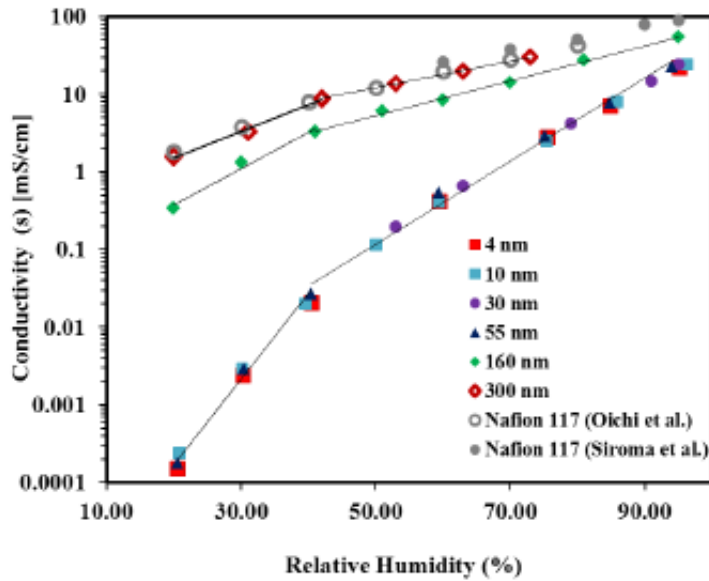


Figure 5.12: Proton conductivity of the Nafion® thin films of varying thicknesses 4-300 nm as a function of RH at 25 °C. Figure is taken from reference [8].

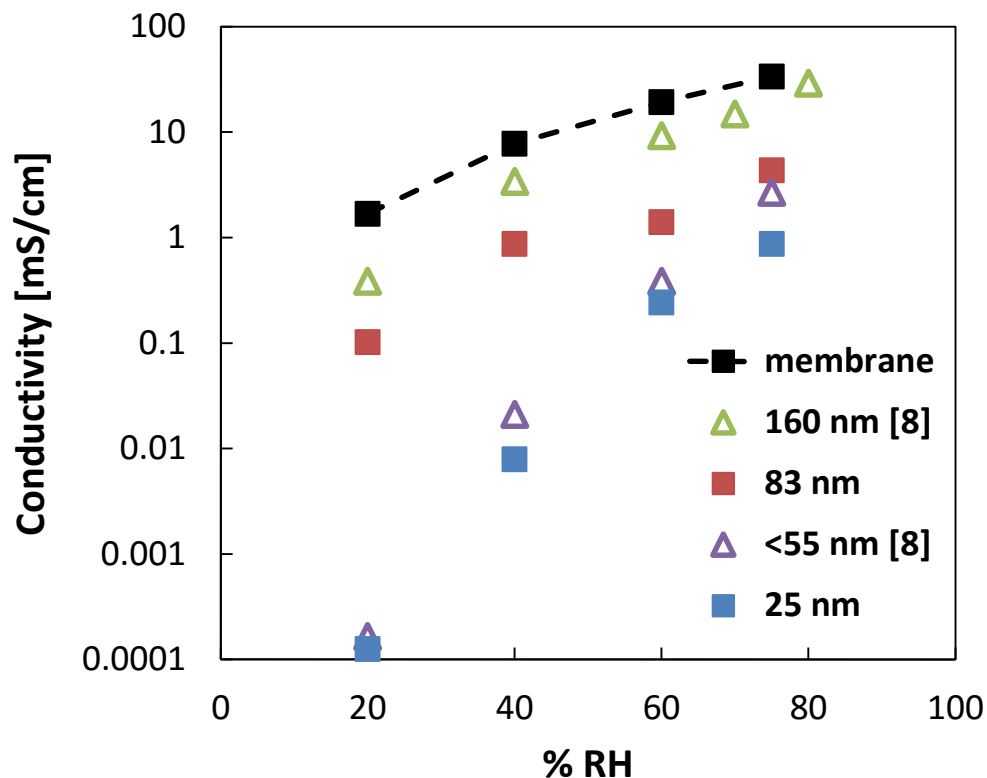


Figure 5.13: Proton conductivity of 23 and 83 nm Nafion[®] thin films at 25 °C as a function of RH. Data for <55, 160 nm, and membrane was taken from reference [8].

5.4 Equilibrium water uptake for Nafion films on Pt substrate

Thickness-dependent water uptake of Nafion thin films was also studied on Pt substrate. Thicknesses of films ranging from 20 to 150 nm were prepared and tested. It was reported by *Murthi et al*⁶⁴ that water uptake of thin films on Au and Pt were comparable. The mass water uptake versus thickness and hydration number versus RH can be seen in Figures 5.14 and 5.15. The general trend in mass water uptake is similar to that of thin films on Au. We see an increasing water uptake with increasing thickness, although the sigmoidal shape is less evident. Figure 5.15 also shows a similar trend with films on Au. We see an increase in water content

from 54 to 77 to 150 nm. The values are comparable to films of similar thickness on Au as expected.

The water uptake of the 20 nm film is notable. The water uptake property of the 20 nm film is even greater than that of the 77 nm at all RH. While some groups attributed this phenomenon to the change in film structure below 20 nm^{6,33}, the structure of the films was not a main focus of this thesis. Although this phenomenon was the main reason why the thickness-dependent water uptake study was started, producing sub 20 nm films were difficult with the spin-coating method. Attempts were made to produce 20 nm Nafion® films on Au but were unsuccessful.

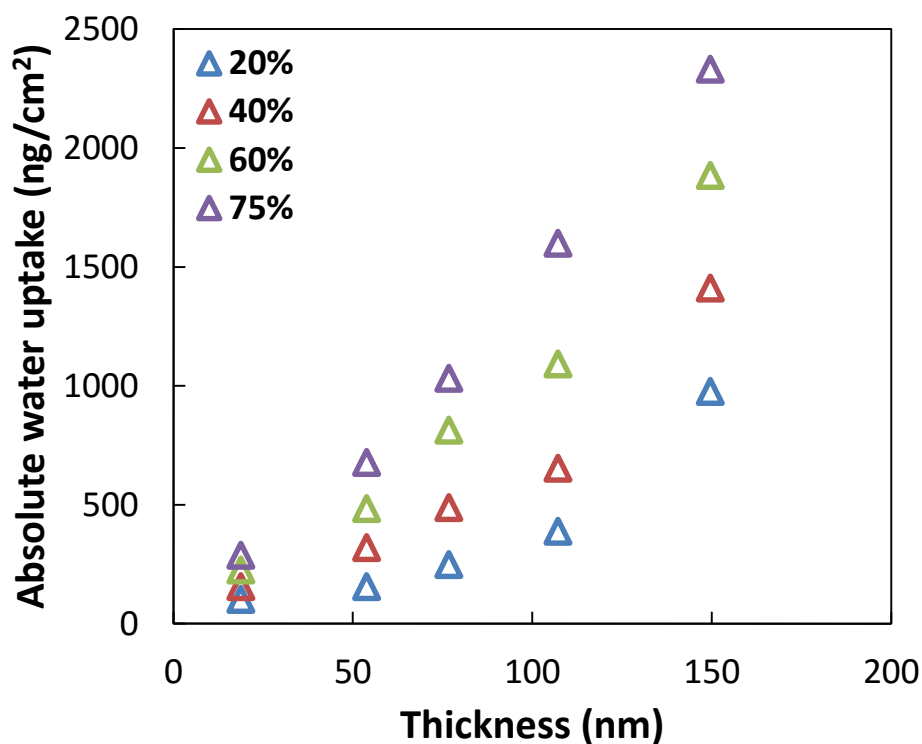


Figure 5.14: Thickness-dependent absolute mass water uptake at various RH for Nafion® thin films on Pt.

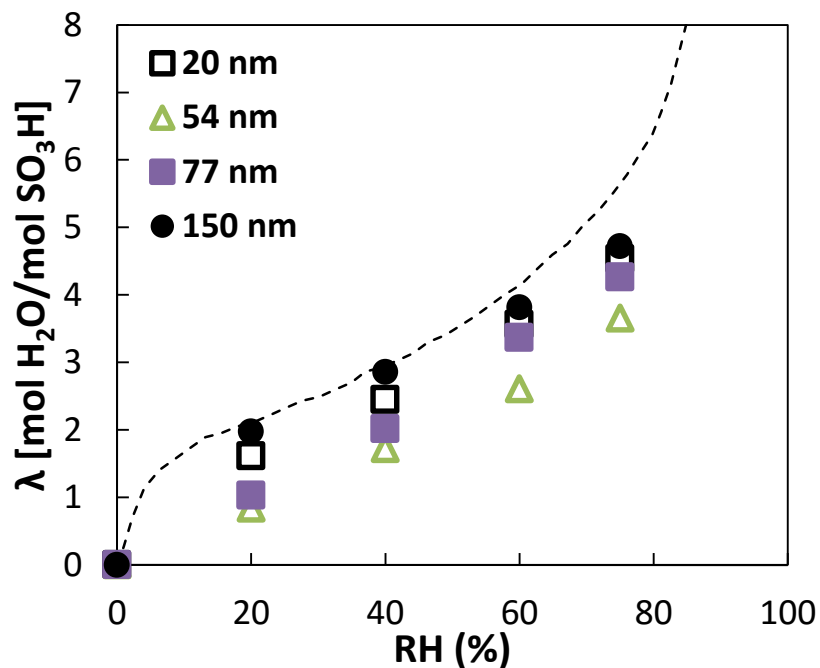


Figure 5.15: Water uptake for Nafion® thin films on Pt.

5.5 Conclusions

Thickness-dependent water uptake properties of Nafion® thin films were performed on SiO₂, Au, and Pt substrates. The discrepancy between low proton conductivity and high water uptake previously observed on SiO₂ substrates was resolved by taking into account the anomalous water uptake behavior of the blank substrate. Experiments with 300 nm and 100 nm SiO₂ layers indicated that they were highly porous and correcting the water uptake of the film by method of subtraction proved that water uptake of thin films on SiO₂, Au, and Pt was comparable. The effect of substrate on water uptake of Nafion® thin films was insignificant.

A systematic study on the effect of thickness of water uptake in Nafion® films on Au showed that higher volume (thickness) exhibited higher mass water uptake. When converted to

hydration number, a similar trend was observed showing comparable trends to proton conductivity reported previously. All films exhibited water uptake values lower or comparable to that of Nafion[®] membrane. The results indicate that proton conductivity is strongly dependent on water content rather than structure for films above 25 nm.

Equilibrium water uptake study of ionomer thin films on Pt substrate showed a similar trend observed for the Au substrate (150 > 77 > 54 nm). Furthermore, the result of the thinnest film (20 nm) provided evidence of some change in Nafion[®] thin films below 20 nm. This might suggest that proton conductivity in sub 20 nm films is not just dependent on water content, but also on structure. The phenomena observed in sub-20 nm films could not be studied on Au.

Chapter 6

Effect of Equivalent Weight on Water Uptake Properties

6.1 Introduction

As mentioned in Chapter 2, developing alternatives to Nafion[®] ionomers is an on-going area of research. The main goal is to reduce the price of production and increase performance of PEFCs. In order to achieve this goal, the new ionomer must retain the structural stability of Nafion[®] while improving the intrinsic properties. As reported in Chapter 5, proton conductivity is highly dependent on water content. While there has been literature on the effect of equivalent weight on water uptake properties in the membrane form, there are none in the thin film form. All literature has reported that lower EW resulted in higher or comparable water uptake at all conditions.³⁹⁻⁴³ This chapter attempts to verify if this is the case in the thin film form. Two different ionomers of equivalent weight 710 and 790 were provided in dispersion form by Automotive Fuel Cell Cooperation (AFCC), Burnaby. No prior knowledge of the new ionomers in the membrane form or thin film form is known.

6.2 Film preparation and characterization

PFSI710 and PFSI790 dispersions were conditioned in the same manner as Nafion[®] dispersion as outlined in section 4.2.2. Thin films were fabricated onto QCs using the spin-coating method as outlined in section 4.2.4.

PFSI710 thin films of thicknesses ranging from 22 – 93 nm and PFSI790 thin films of thicknesses ranging from 20 – 79 nm were spin-coated onto Au substrate. The thickness-dependent density and RI of these films are presented in Figures 6.1 and 6.2.

For PFSI710 films, the RI of thicker films (43, 48, and 93 nm) is comparably higher than Nafion[®] films at about 1.38. The thinnest film (23 nm) shows a much lower RI of 1.28 where the drop is similar to the behavior of Nafion[®] films. However, the density of all PFSI710 films is consistent around 2.0 g/cm³. While understandable for the thicker films, the thinnest film exhibiting comparable density but lower RI presents a similar issue as films on Pt substrate. The same trend can be seen for PFSI790 films. The RI is close to 1.39 for thicker films while it drops to 1.31 for the 20 nm film. The density of the thicker films (40, 55, and 79 nm) is again close to 2.0 g/cm³. This time, there is a slight increase in density for the thinnest (20 nm) film. No issues with the Au QC or films were observed. These results suggest that the structural properties of PFSI710 and PFSI790 thin films are comparable to Nafion[®] thin films up to 40 nm. The high density and low RI of the thinnest films are not fully understood at this moment.

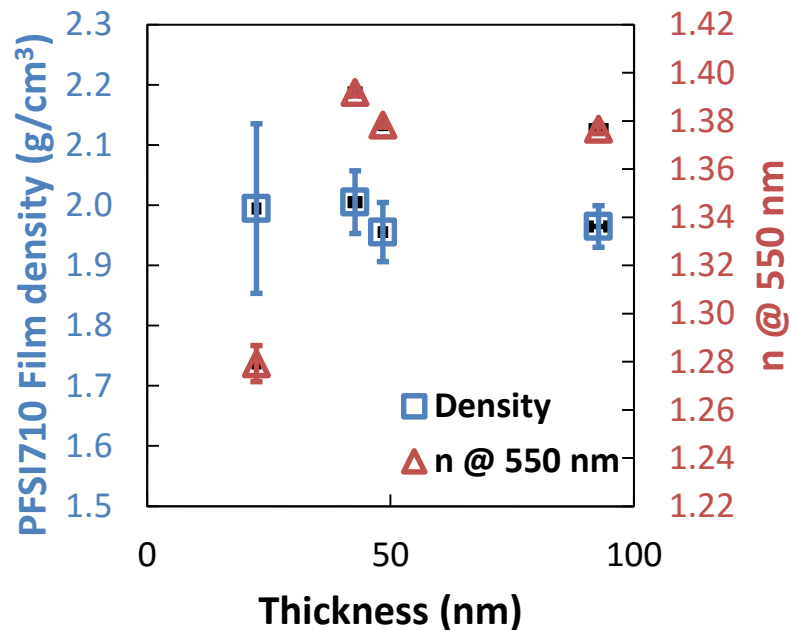


Figure 6.1: Thickness-dependent density (\square) and refractive index (Δ) of PFSI710 films prepared on Au QCs. Error bars indicate system error.

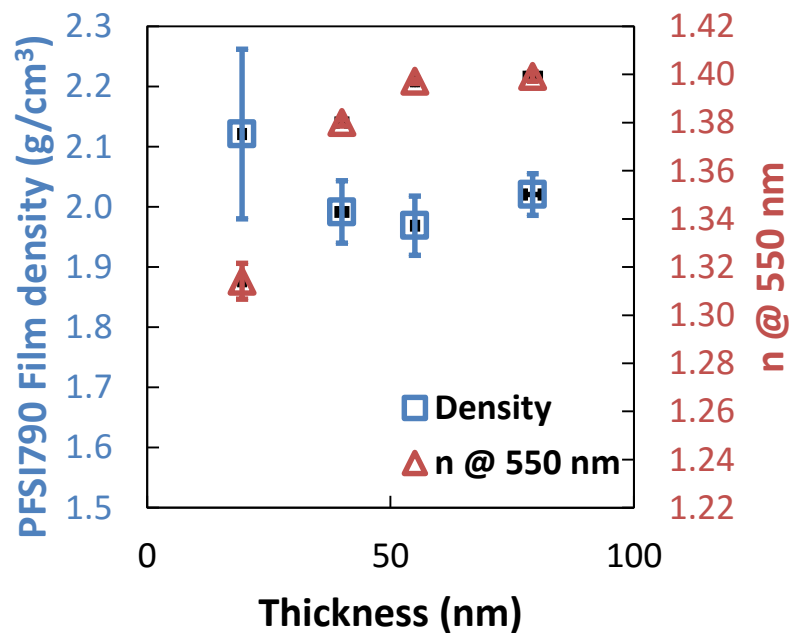


Figure 6.2: Thickness-dependent density (\square) and refractive index (Δ) of PFSI790 films prepared on Au QCs. Error bars indicate system error.

6.3 Water uptake properties

Water uptake properties of thin films of AFCC supplied ionomers were carried out in the same manner as Nafion[®] thin films. The mass water uptake data of each ionomer is presented in Figures 6.3 and 6.4. We observe an increase in water uptake with increase in thickness, similar to that of Nafion[®] thin films.

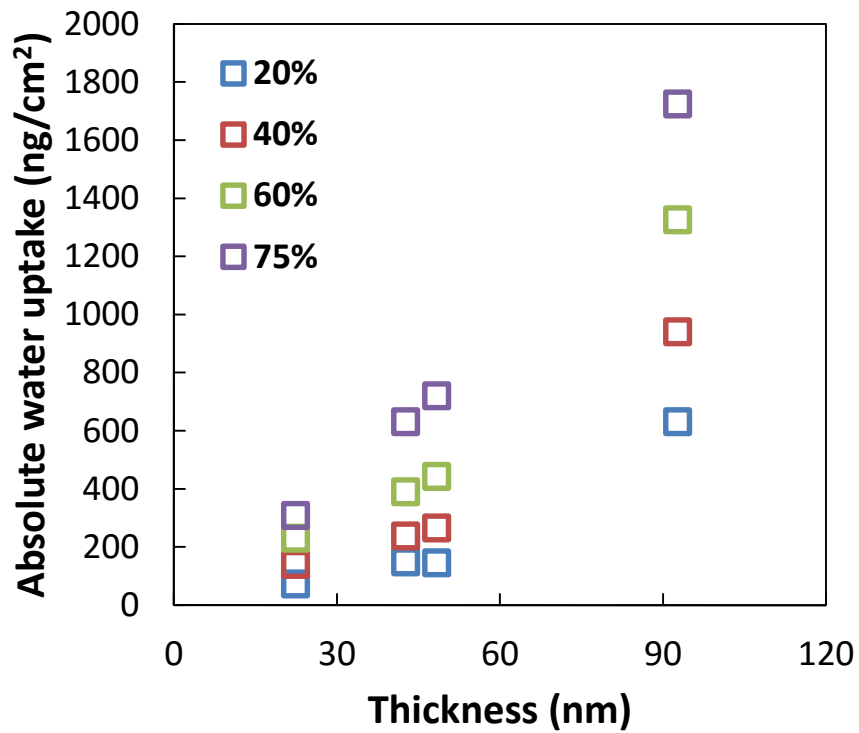


Figure 6.3: Thickness-dependent absolute mass water uptake at various RH for PFSI710 thin films.

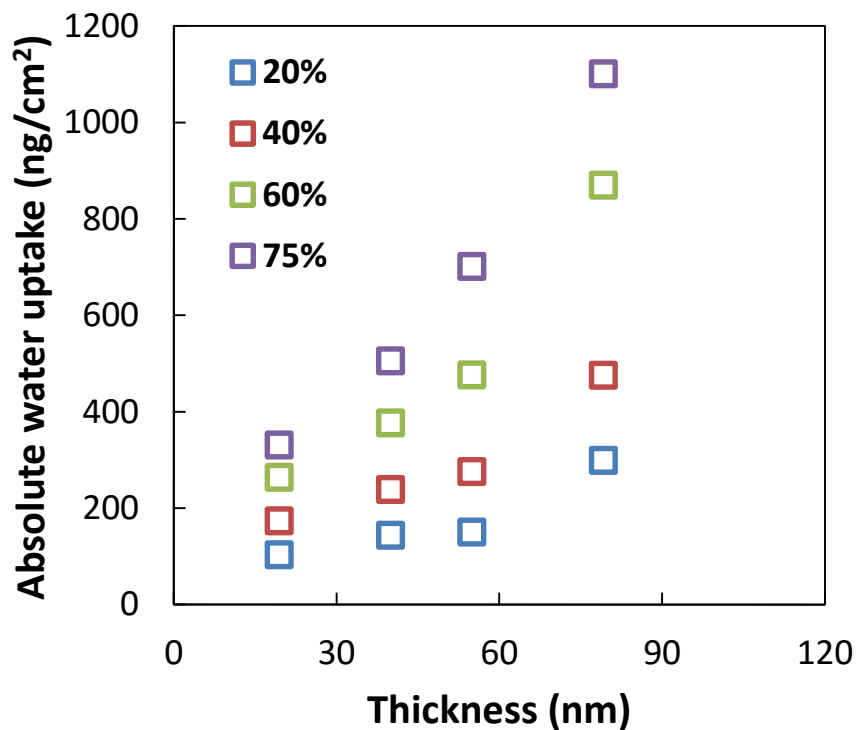


Figure 6.4: Thickness-dependent absolute mass water uptake at various RH for PFSI790 thin films.

The hydration numbers were calculated using the Sauerbrey analysis assuming $IEC = 1000/EW$ and are presented in Figures 6.5 and 6.6. The observed trend is very similar to Nafion® thin films. For PFSI710 films, the water uptake properties of 22 to 48 nm are comparable while the 93 nm showed higher water uptake compared to the thinner films. All films exhibited water uptake much lower than that of Nafion® membranes.

For PFSI790 samples, the trend is slightly different. While the 40 and 55 nm films show comparable water uptake properties, the 79 nm films exhibited slightly lower than expected values. The high water uptake of the 20 nm film, similar to what was observed for the 20 nm Nafion® film on Pt leads us to believe that the change in structure of films of sub 20 nm thickness

occurs in AFCC films as well. Further study on the structure of AFCC samples would shed light to this behavior.

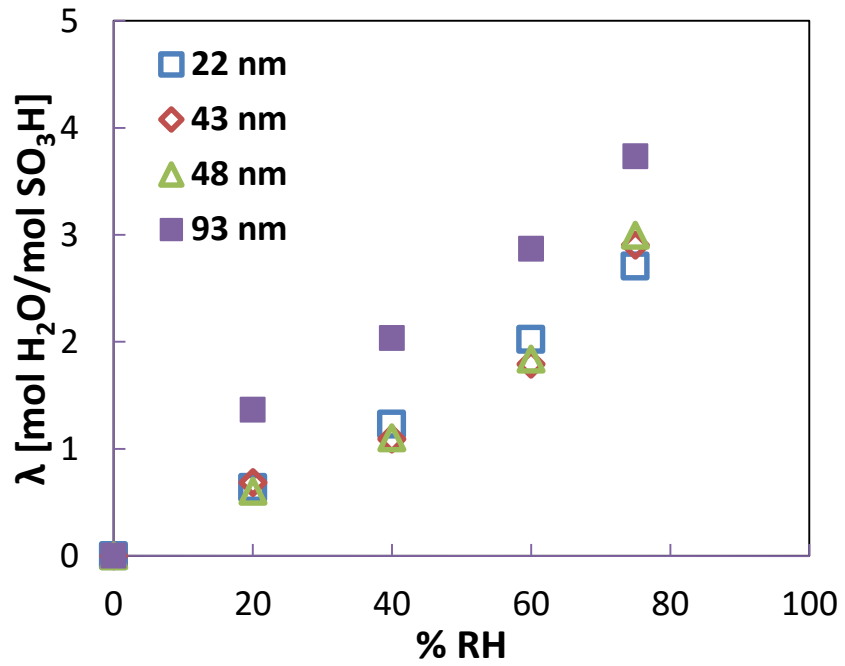


Figure 6.5: Water uptake for PFSI710 films on Au.

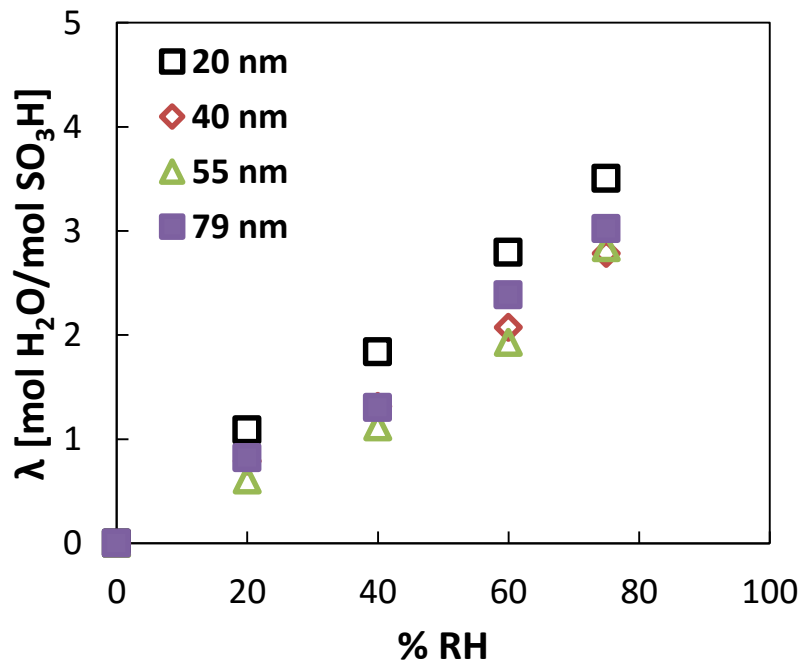


Figure 6.6: Water uptake for PFSI790 films on Au.

6.4 Comparison of Nafion[®], PFSI710 and PFSI790 thin films

For comparison of the 3 ionomers, the hydration number as a function of RH for films of similar thickness were plotted together. The results are presented in Figures 6.7 through 6.10. Figures 6.7 and 6.8 show data for the thinner films (<55 nm) whereas Figures 6.9 and 6.10 show the data for thicker films (>55 nm). We observe that for the thinner films, all ionomers exhibit similar water uptake properties at all humidities. The 20 nm PFSI790 was excluded as to eliminate the disordering effect of sub 20 nm films. This has been observed by *Zawodzinski et al*⁶⁵ as well when he compared the water uptake of Nafion[®] membrane, Dow membrane (EW 800) and membrane C (EW 900). Water uptake of the three types of membrane exhibited similar water uptake values at all RH. Only when the membrane was immersed in water did they see an increase in water uptake for the low EW membranes. All films exhibited hydrophobic surface properties as confirmed by the contact angle measurements. As the interfacial characteristic is stronger than the bulk characteristic, this might be the reason why we see similar water uptake for the thinner films.

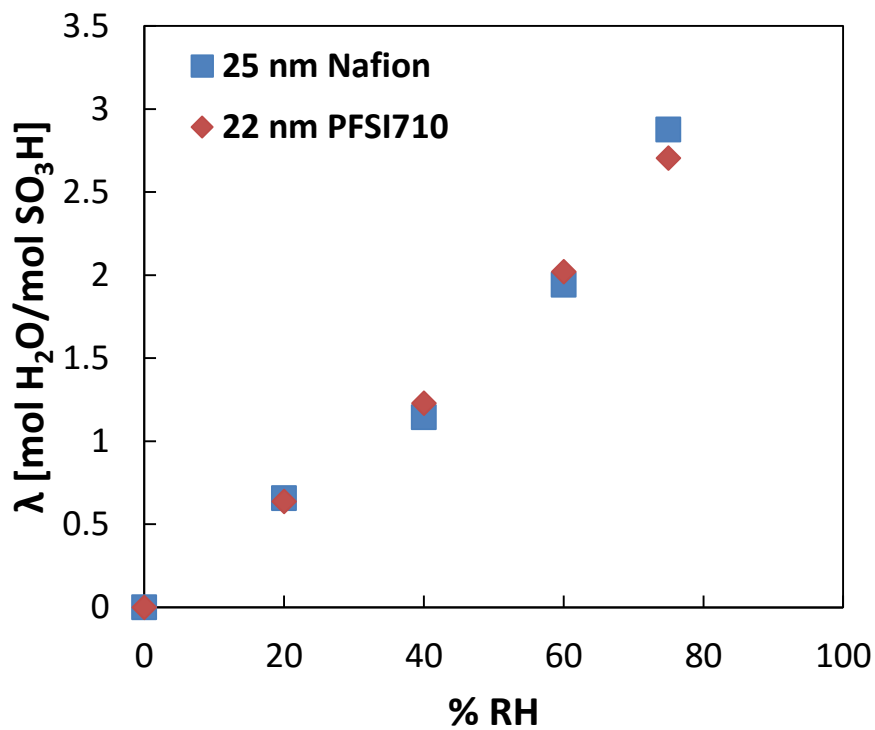


Figure 6.7: Water uptake of 23.5 ± 1.5 nm films on Au.

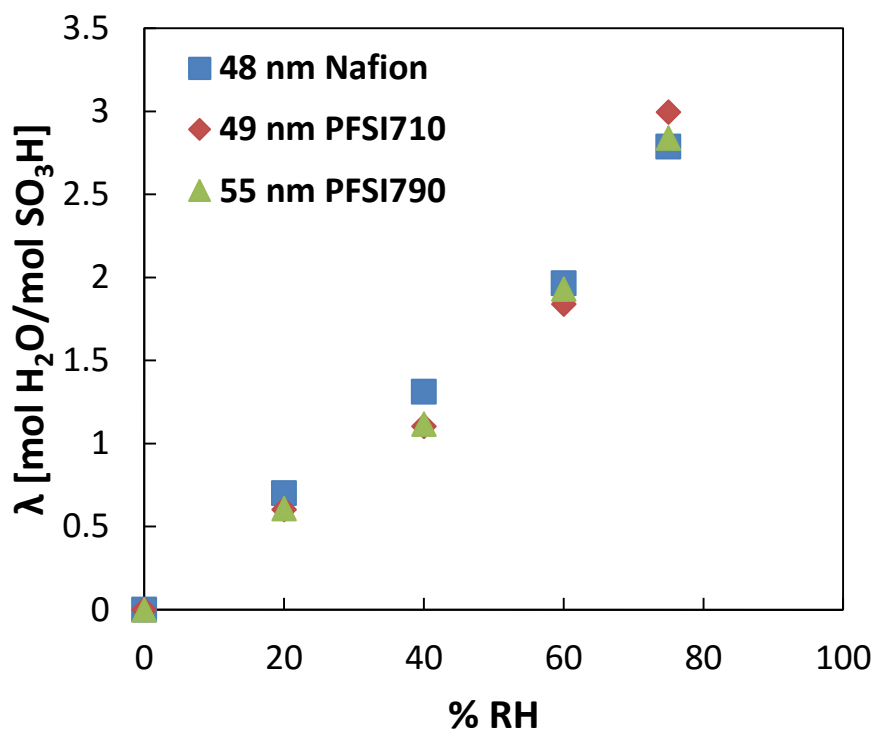


Figure 6.8: Water uptake of 50.7 ± 3.1 nm films of different ionomers on Au.

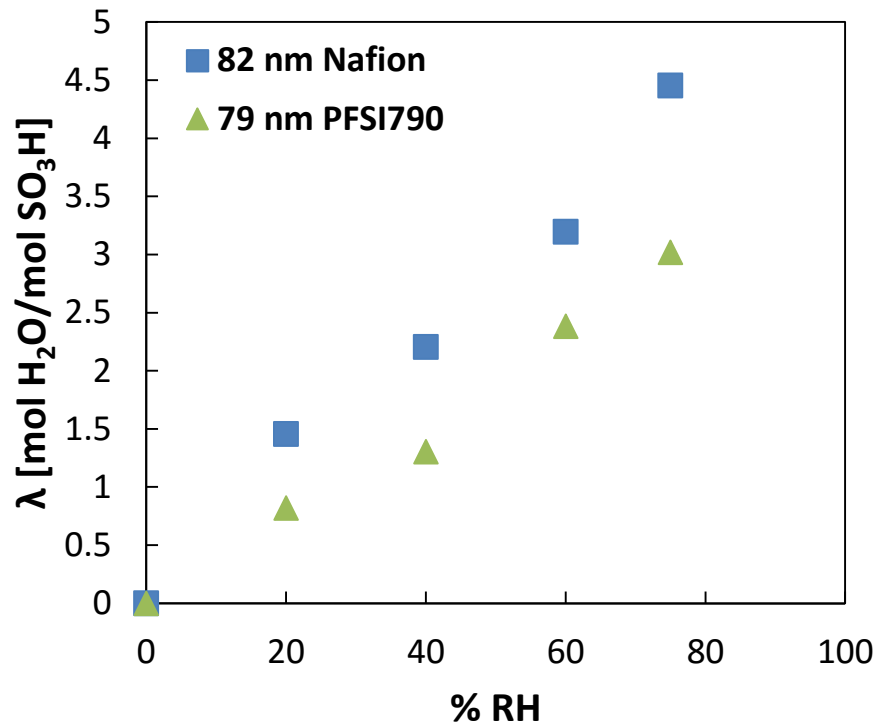


Figure 6.9: Water uptake of 80.5 ± 1.5 nm films on Au.

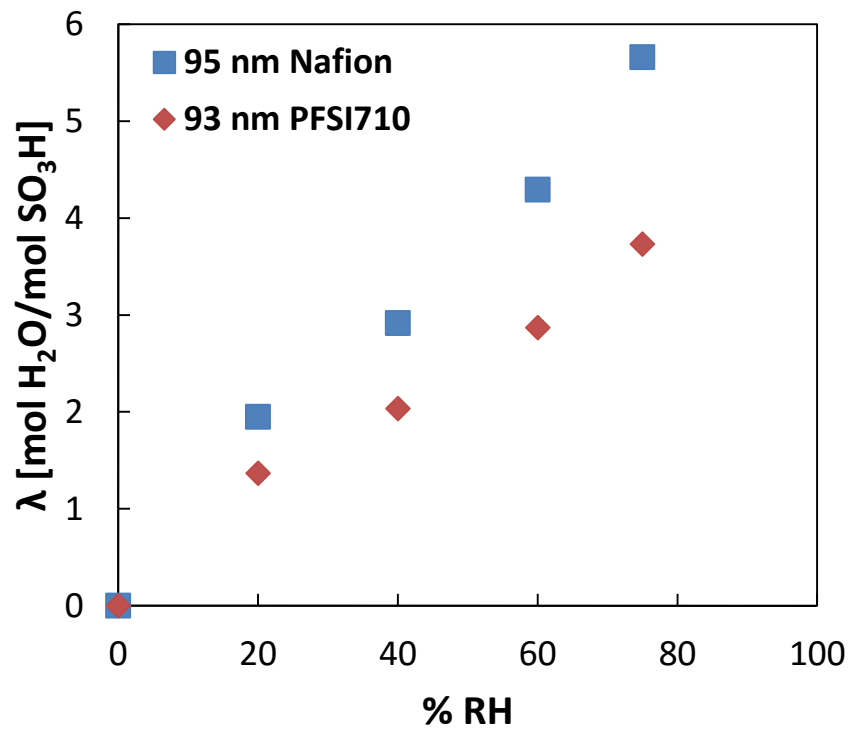


Figure 6.10: Water uptake of 94.0 ± 1.0 nm films on Au.

Interestingly, Nafion[®] films show higher water uptake for thick films (>55 nm). No literature for membranes has reported a decrease in water uptake as the EW of the ionomer gets lower. One reason for this interesting result could be the high crystallinity of low EW ionomers as observed by *Subianto et al*⁶⁶. A study of different ionomers using the SEM showed that SSC Aquivion (EW 830) might have greater physical crosslinking causing higher crystallinity. Decrease in water uptake due to crystallinity has been predicted and observed by various groups as well³⁵⁻³⁸. Since the thinner film exhibit similar water uptake, it suggests that the films with thickness greater 55 nm region are more strongly influenced by the crystallinity.

6.5 Conclusions

Thin films of two ionomers, PFSI710 and PFSI790, were fabricated onto Au QCs and characterized in this chapter. Thin films were fabricated onto Au substrates using the same protocol as Nafion[®] films. While the density of both samples was similar to that of Nafion[®] thin films, their RI was higher. Water uptake properties of both AFCC ionomers showed similar trends with respect to films thickness as that observed for Nafion[®] films; <55 nm films exhibited comparable water uptake to each other and then increased with thickness. The high water uptake of the thinnest PFSI790 film (20 nm) leads us to believe a similar change in structure is occurring similar to what was observed in Nafion[®] films on Pt. Films of similar thickness for the three ionomers were compared to study the effect of EW on water uptake.

While it has been reported that low EW leads to lower or comparable water uptake in the membrane form, it was found that this was not the case in the thin film form. While <55 nm films showed insignificant effect of EW on water uptake, comparison of thicker films (>55 nm) showed that Nafion[®] films absorbs more water than AFCC films. This has been attributed to the higher

crystallinity observed in low EW ionomers, which could be having a greater affect in the thin film form.

Chapter 7

Combined Water Uptake and Swellability Study of Sub-Micron Thin Ionomer Films and the Effect of Annealing

7.1 Introduction

Dimensional changes or swelling occur as water is taken up by the ionomer. The swelling properties of Nafion® membrane have been reported.^{3,6,9,34} As water fills up the hydrophilic domains, the pores expand and the ionomer experiences restructuring. The swelling properties of thin films might give us an idea on the structure. So far, studies on water uptake and thickness have been performed separately on separate equipment: QCM and ellipsometry.⁶ Using two separate instruments may cause a number of issues including but not limited to the time-dependent property changes of the ionomer. We present a new technique to simultaneously study mass uptake and swelling using the combined QCM and ellipsometry technique. The validity of the experiment is presented as well as initial measurements. The effect of thickness, EW, and annealing is reported.

7.2 Experimental setup

A custom stage for the ellipsometry was built to accommodate the quartz crystal holder. A metal base enveloping a quartz crystal holder was mounted on the ellipsometer. A humidity-temperature sensor was placed inside along with the crystal. The sensor was not in the way of the light path. A picture of the experimental setup is shown in Figure 7.1. To control the humidity, the holder was covered with a top with windows on each side for the light to enter and leave. Due

to the position of the windows, only one angle (65°) for ellipsometry measurements was obtained. It was confirmed previously that using one angle compared to three angles (55, 65, 75°) did not have a significant impact on thickness.



Figure 7.1: Combined QCM (water uptake) and ellipsometry (thickness) setup.

Typical profiles of the measured parameters are presented in Figures 7.2 and 7.3. The thickness, humidity, frequency and temperature during a step-change in humidity can be observed. Figure 7.2 shows the stability of the thickness measurement before and after a humidity step change from 0 – 20% RH. It took about 30 minutes for the thickness to stabilize after the humidity change was induced.

As mentioned previously, QCM measurements are very temperature sensitive. According to the operation manual, the frequency reading can change by 8 Hz for every 1 °C change. In the previous setup, the temperature was controlled to ± 0.1 °C. Unfortunately, due to the setup still

being fairly new and adjustment are still yet to be made, the temperature could not be controlled as well as we desired. Fluctuations in temperature were observed throughout the experiment and sometimes a temperature change of 1 °C was observed. In Figure 7.3, we can observe the fluctuation of frequency measurement before and after a humidity change. The ellipsometer calculated thickness fluctuation is in sync with the temperature fluctuation.

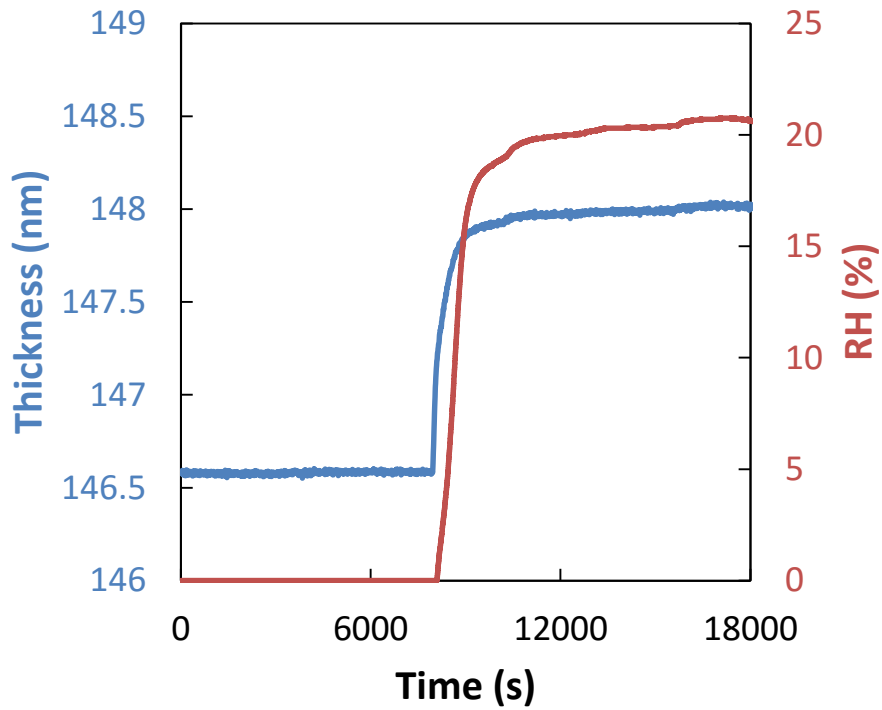


Figure 7.2: Sample thickness and humidity profile during a step-change in humidity.

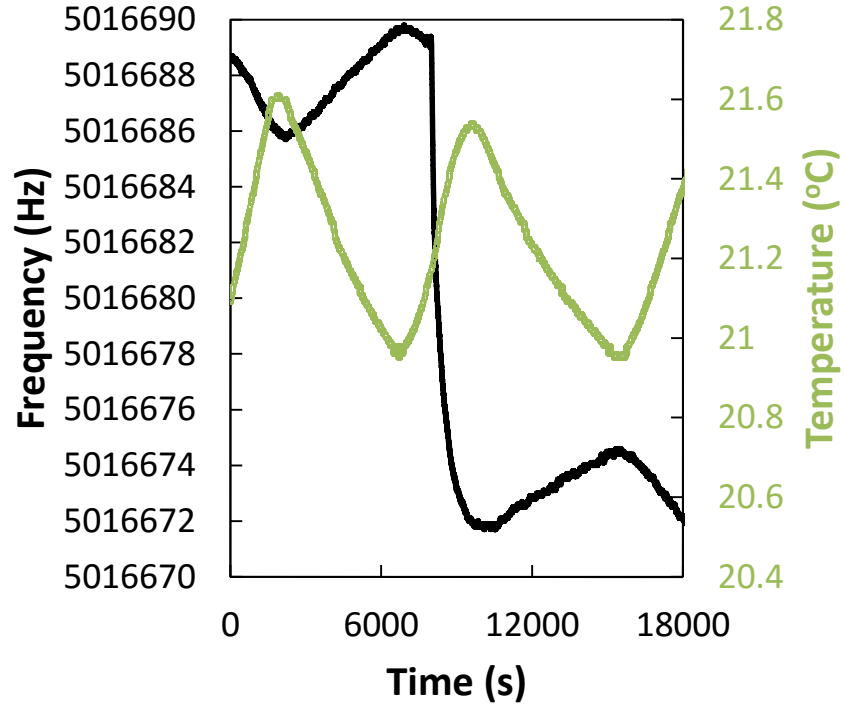


Figure 7.3: Sample thickness and temperature profile during a step-change in humidity.

In order to compensate for the effect of temperature, a simple temperature correction factor was added. The temperature correction factor, k_{sample} , of each quartz crystal was obtained by observing the frequency change with temperature change (at 20, 30, and 40 °C) prior to film fabrication. The values ranged from 4 to 10 Hz / °C. The temperature-corrected frequency was calculated by,

$$F_{T_corr} = F_{real} + k_{sample}(T_{real} - T_{initial}) \quad (7.1)$$

where F_{T_corr} is the temperature corrected frequency, F_{real} is the real frequency reading, T_{real} is the real temperature reading, and $T_{initial}$ is the temperature when the initial step change in humidity was introduced.

Comparison of the temperature-corrected frequency to the real frequency is presented in Figure 7.4. While this correction method was not perfect, the calculated frequencies result in a much stable response. All water uptake data presented in this chapter were calculated using the temperature-corrected frequencies if not stated otherwise.

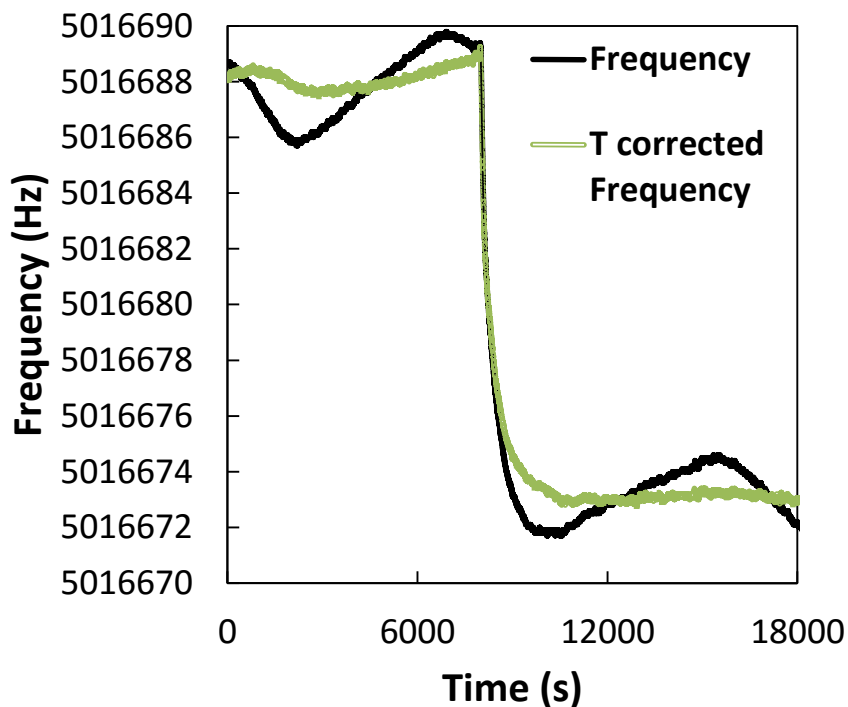


Figure 7.4: Sample frequency versus temperature-corrected frequency profile during a humidity step change.

Another issue that was encountered was the difference in thickness measurements of the film. The thickness of films that has been reported in this thesis was explained in Section 4.4.2.1. However, in-situ thickness measurement using the combined QCM-Ellipsometry setup showed a different thickness, typically 2~3 nm less than ex-situ measurement. Unfortunately, this problem was not solved. It is to be noted that all films have been reported with their ex-situ measurements but all calculations were done with the in-situ measurements in this chapter.

7.3 Water uptake and swelling properties of Nafion[®] films

Three different Nafion[®] films of thicknesses 25, 82, and 150 nm on Au were studied using the combined QCM-ellipsometry experimental setup. Figure 7.5 shows the plot of absolute swelling as a function of λ for Nafion[®] films on Au. Assuming one-directional swelling and no mixing, if all films experience the same swelling with same water content than the structure of the films could be said to be similar. Another group has made this assumption as well for thin films attributing it to lack of excess free volume or macroscale voids and confinement effects.⁹

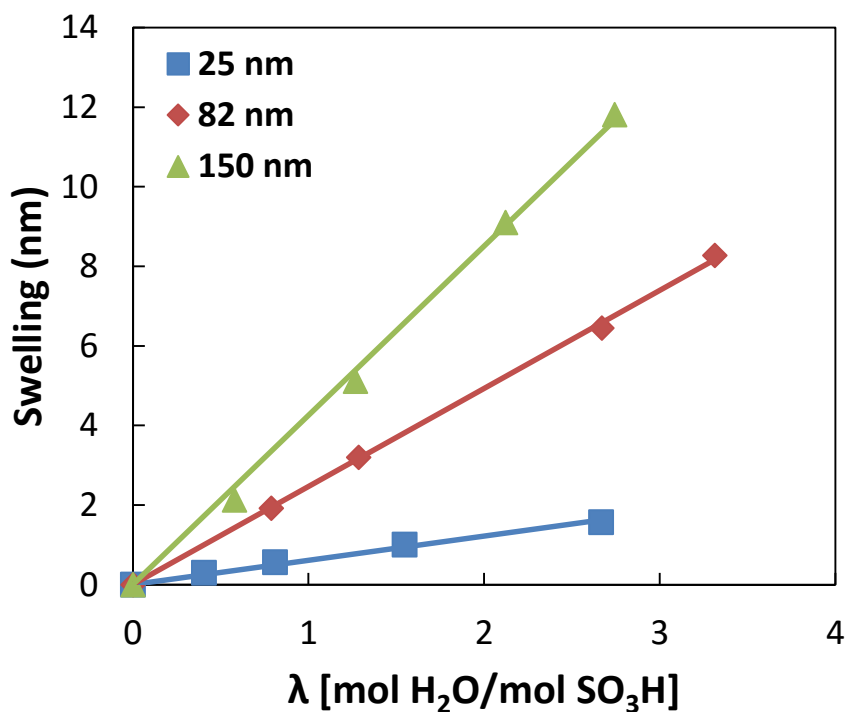


Figure 7.5: Swelling as a function of water content for untreated Nafion[®] films on Au.

All films experience a linear increase in swelling with λ . The difference in slope indicates that thicker films swell more than the thinner films with the same λ . If the assumptions stated above are true, the results could be correlated to the nano-structure of thin films proposed by

*Paul*⁵² in Figure 2.7. The thinnest (25 nm) film experiences the least swelling due to its high void fraction. As reported in Chapter 4, the density of the thinnest (25 nm) film was much lower than that of the thicker films. This suggests higher void fraction allowing the water molecule to be accommodated before the film experiences swelling. The discrepancy between the 82 and 150 nm film can be explained by the mixed-layer morphology. The bottom layer (<55 nm) of the film has higher voidage while the top layer (>55 nm) is denser. Due to the dense nature of the top layer, it would experience greater swelling.

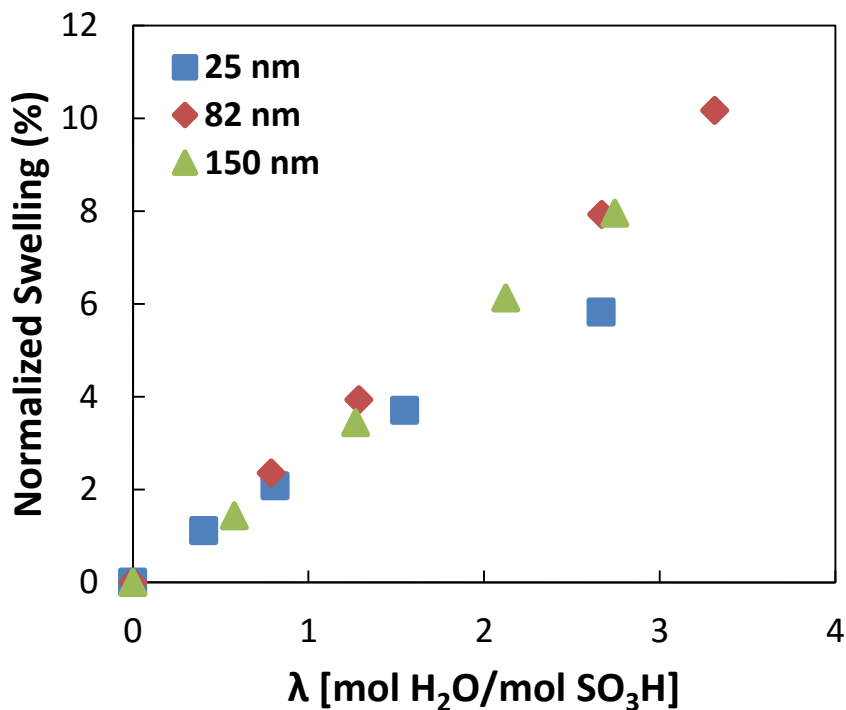


Figure 7.6 Normalized swelling as a function of water content for untreated Nafion[®] films on Au.

For comparison, normalized swelling (swelling/thickness of dry film) was plotted against λ as shown in Figure 7.6. Normalized swelling suggests that all films exhibit comparable swelling with the 25 nm film slightly lower swelling.

The above results were discussed assuming one-dimensional swelling with no mixing. One-dimensional swelling is assumed for thin films due to the significantly larger surface area compared to thickness. Furthermore, the ellipsometer is only capable of measuring thickness change in the z-direction (1-dimension), thus limiting our understanding of what is occurring inside the film. To further interpret the swelling behavior of the films and to examine the validity of one-dimensional swelling, the water uptake and thickness change data were related via equation 7.2

$$1 + (\lambda) \frac{\bar{V}_{H_2O}}{\bar{V}_o} - \frac{\bar{V}_{mix}}{\bar{V}_o} = \left(1 + \frac{\Delta L_{RH}}{L_o}\right)^m \quad (7.2)$$

where \bar{V}_{H_2O} and \bar{V}_o are molar volumes of water and polymer respectively, \bar{V}_{mix} is the volume of mixing, and m is the swelling dimension. The volume of mixing accounts for the non-ideal mixing of water and polymer phase and is mentioned to be present in Nafion® membranes.⁹

Using humidity-dependent λ and thickness change from the QCM and ellipsometer, respectively, the following was noted: (i) the swelling dimension was found assuming ideal mixing ($\bar{V}_{mix} = 0$) and (ii) the volume of mixing was found assuming 1-dimensional swelling (m=1). This was done because two separate instruments were used. With the new combined QCM+Ellipsometry setup, both the swelling dimension and volume of mixing will be solved simultaneously. Setting $1 + (\lambda) \frac{\bar{V}_{H_2O}}{\bar{V}_o}$ as y and $1 + \frac{\Delta L_{RH}}{L_o}$ as x, equation 7.2 can be rearranged to,

$$y = x^a + b \quad (7.3)$$

where a = m and b = \bar{V}_{mix}/\bar{V}_o .

Using TableCurve 2D (Systat Software Inc.), the swelling dimension and volume of mixing was obtained fitting the above exponential curve. The swelling dimension and volume of mixing for Nafion[®] films can be seen in Figure 7.7. The swelling dimension of all films is around 1 indicating that swelling is mostly in the z-direction. This can be interpreted as the films being affected by confinement effect. The volume of mixing is significantly lower than what is reported for the membrane and nearly close to 0 suggesting negligible non-ideal mixing.

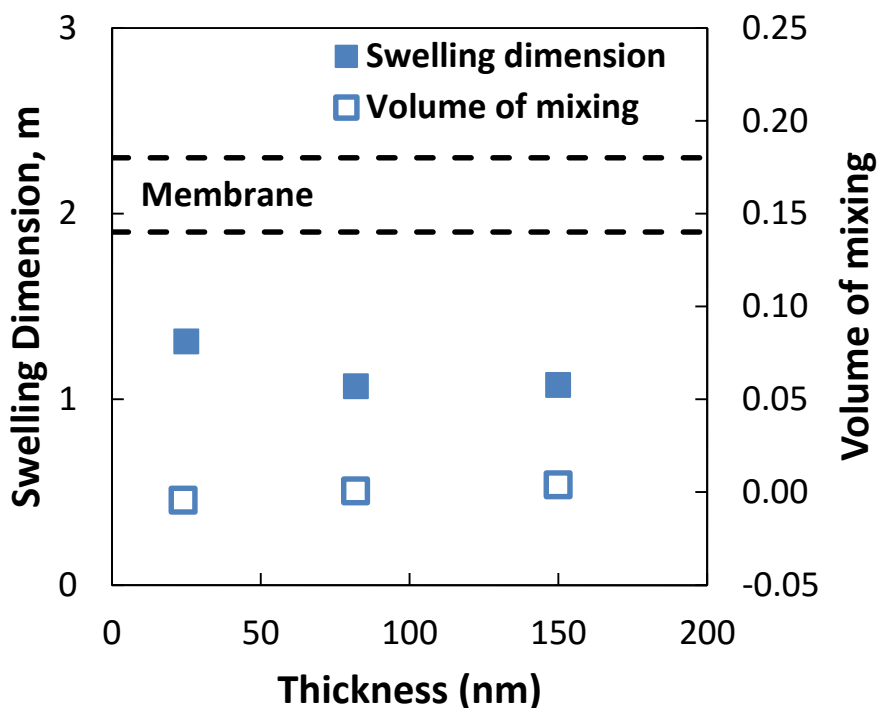


Figure 7.7: Swelling dimension (solid \square) and volume of mixing (open \square) of Nafion[®] thin films on Au. Dashed lines indicate range of volume of mixing for Nafion[®] membranes.

7.4 Water uptake and swelling properties of AFCC ionomer films

The water uptake and swelling properties of AFCC ionomer films were measured in the combined QCM and ellipsometry setup. The plots of swelling as a function of water content are presented in Figures 7.8 and 7.9. In both Figures, while not significant a thickness-dependent trend can be observed. For both ionomers swelling increases with increasing thickness. Furthermore, there is a clear difference in behavior between the thinner (< 55 nm) and thicker (> 55 nm) films for both samples. As mentioned in Chapter 6, AFCC ionomer films appear to be experiencing the same morphological changes around the 55 nm thickness similar to Nafion[®] films and this swelling behavior is a further evidence in support of this. Films of thicknesses <55 nm might have similar multi-lamellar structure, which is why similar swelling for the thinner films are observed.

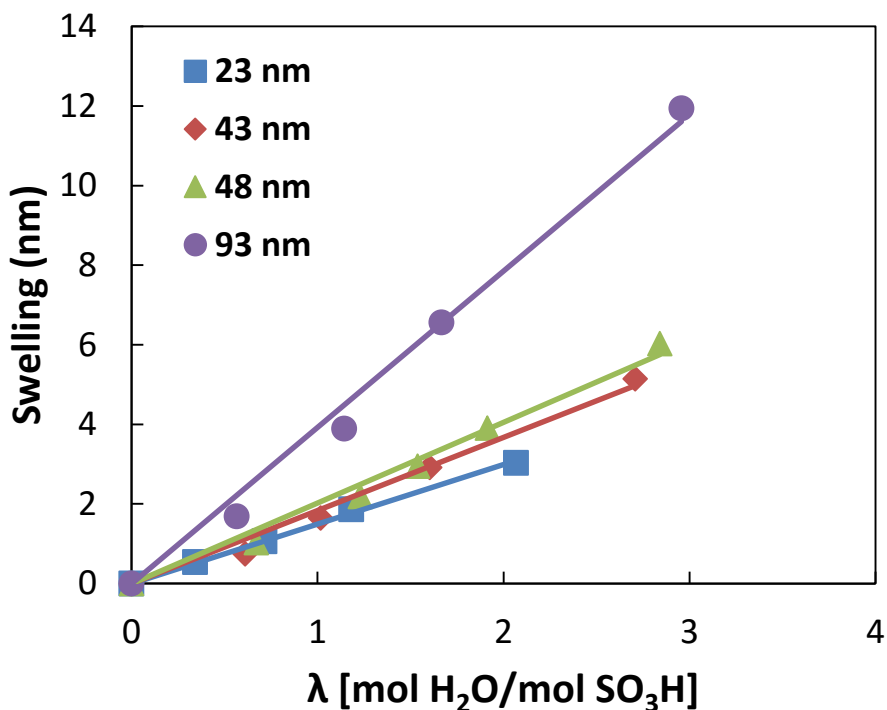


Figure 7.8: Swelling as a function of water content for untreated PFSI710 films on Au.

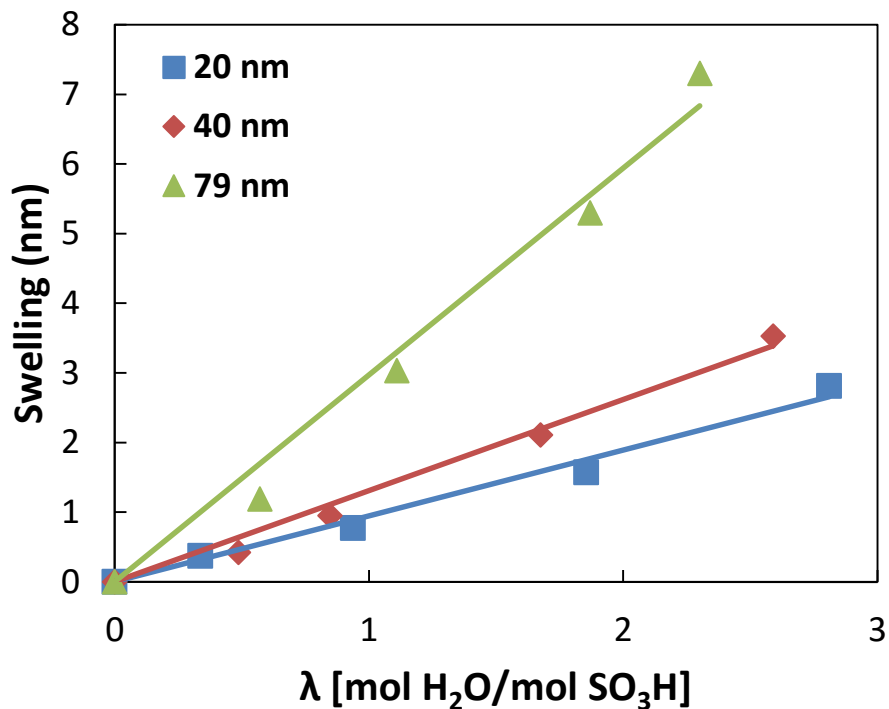


Figure 7.9: Swelling as a function of water content for untreated PFSI790 films on Au.

The swelling dimension and volume of mixing was investigated for the AFCC films as well. The results are presented in Figures 7.10 to 7.11. Most of the samples exhibit swelling dimensions very close to 1 suggesting the presence of confinement. One concern is the 23 nm PFSI710 film showing a dimensional swelling of less than 1, meaning that the film experienced more swelling than what was put in. This was not investigated further and thought to be the result of the error associated with the equipment. All AFCC films exhibit a volume of mixing close to 0, much lower than that of Nafion[®] membranes. Once again the assumption of 1-dimensional swelling and ideal mixing is reasonable.

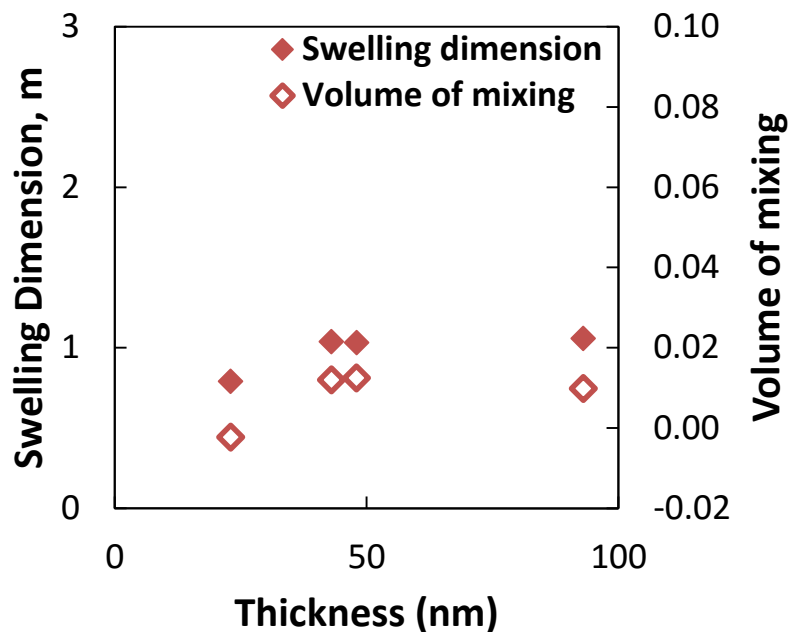


Figure 7.10: Swelling dimension (solid \diamond) and volume of mixing (open \diamond) PFSI710 thin films on Au.

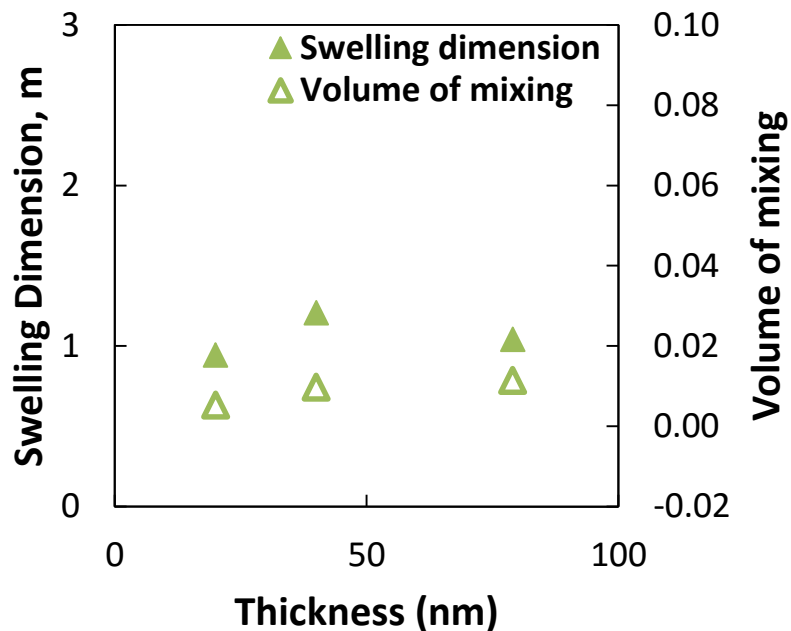


Figure 7.11: Swelling dimension (solid Δ) and volume of mixing (open Δ) PFSI790 thin films on Au.

A comparison of the thickness-dependent swelling dimension and volume of mixing for all films on Au were plotted in Figures 7.12 and 7.13. While no thickness-dependent trend was observed, the confinement effect and negligible non-ideal mixing was confirmed for ionomer thin films.

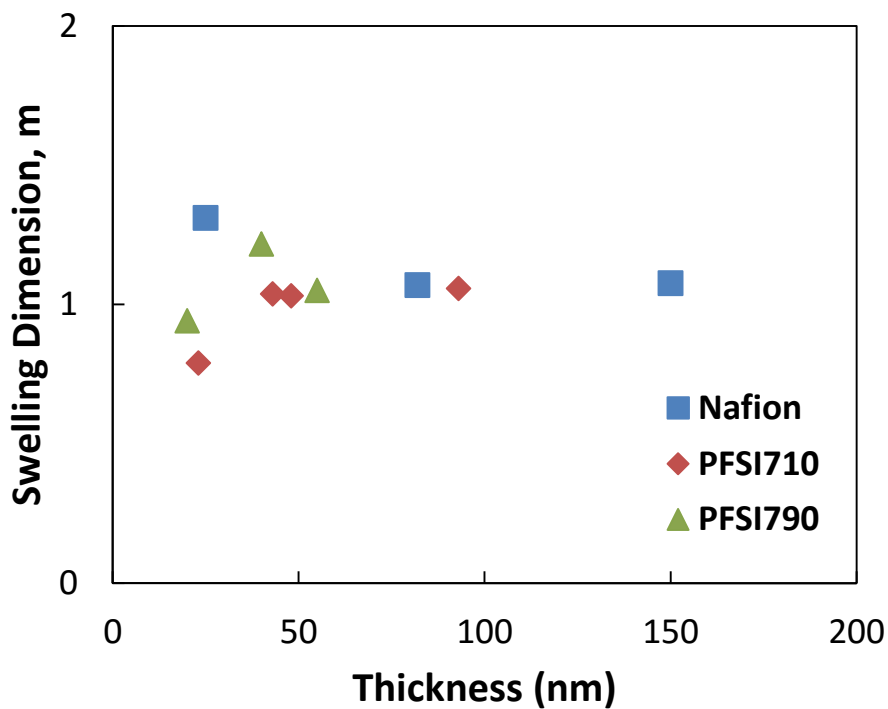


Figure 7.12: Swelling dimension of Nafion[®] (□), PFSI710 (◇), and PFSI790 (Δ) films on Au.

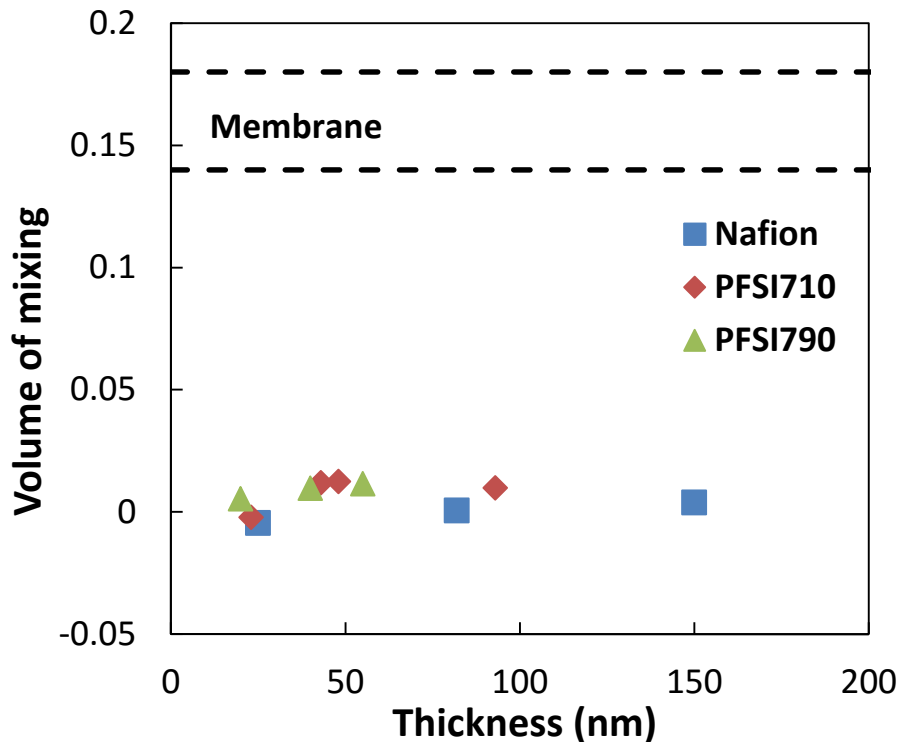


Figure 7.13: Volume of mixing for Nafion[®] (□), PFSI710 (◇), and PFSI790 (Δ) films on Au.

7.5 Effect of aging and thermal annealing on Nafion[®] films

The effect of annealing on the intrinsic properties of Nafion[®] was also of interest as mentioned in Chapter 2. After obtaining the untreated water uptake and swelling data, the films were subjected to a heat-treatment at 160 °C for 40 hours. 40 hours was chosen because it was found to be the minimum time required for the films to fully transition to a new state as observed in an ongoing study.⁶⁷ The annealed films were tested in the same manner as the untreated films.

It is useful to mention that the films tested using this setup were not freshly prepared. This is important because a differentiation between the effect of aging and of thermal annealing on water uptake/swelling must be made. Ageing of Nafion[®] has been reported by other groups^{34,68}

which reported a decrease in water uptake with ageing. The slow relaxation of the polymer was attributed for this phenomenon. Meanwhile, the effect of ageing on swelling has not been reported. To introduce the effect of ageing on Nafion[®] films, a single sample aged in an uncontrolled environment was tested at random. Figure 7.14 shows the depreciation of water uptake at all humidity for a 150 nm Nafion[®] film on Au as it is aged. Measurements were done in the environmental chamber introduced in Chapter 4 to ensure accurate measurements. To eliminate the effect of aging from the effect of annealing, the films were annealed as soon as the untreated film data was obtained. The water uptake of annealed films was measured as soon as the films cooled down after the annealing protocol.

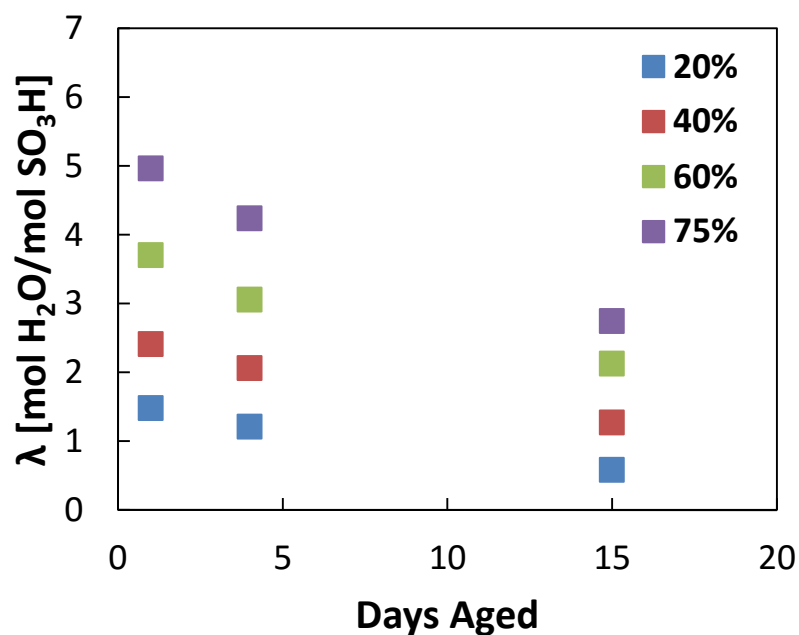


Figure 7.14: Effect of aging on water uptake for 150 nm Nafion[®] film on Au.

The annealed films were characterized for their thickness. Assuming the film mass did not change, the density of the annealed films was calculated. The density and thickness change

due to annealing are presented in Figure 7.15. The 25, 82, and 150 nm films experienced a 16, 12, and 19% increase in thickness respectively. No thickness-dependent trend was observed.

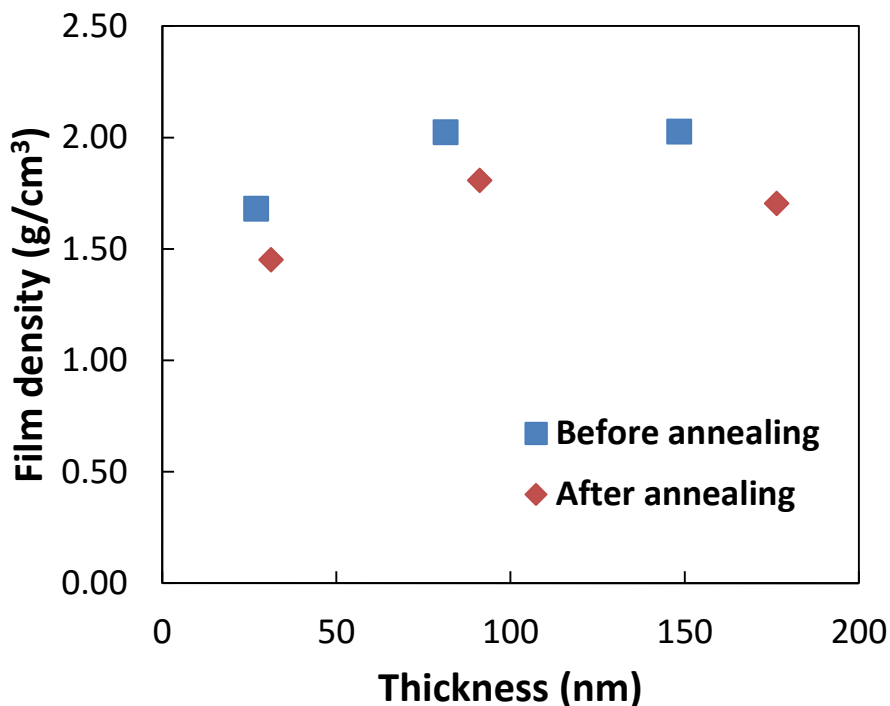


Figure 7.15: Density of Nafion[®] films on Au before and after thermal annealing.

Figures 7.16 to 7.18 show the water uptake and percentage swelling data for Nafion[®] films before and after annealing. For all films, there is a significant drop in both water uptake and swelling properties after annealing. While this result is consistent with the observed depreciation in proton conductivity by *Paul et al*³⁵, in theory, a decrease in density (increase in thickness) indicates higher void fraction within the film and should thus adsorb more water. This contradiction indicates that annealing the films does not simply inflate the film. Rather than a simple 1-dimensional increase in thickness, the internal structure or the surface is being altered.

No significant change in water contact angle was observed before and after annealing which suggests a structural change.

Earlier reports which observed similar results attributed the decrease in water uptake to the increase in crystallinity within the polymer that inhibits water uptake^{26,35-38}. The increase in crystallinity was confirmed by GISAXS studies.⁶² Once again, the depreciation in proton conductivity after annealing can be attributed to the decrease in water uptake for Nafion[®] thin films. Also, although *Paul et al*³⁵ reported that annealing only affects the water uptake of thicker films (>50 nm) this was not the case for our films. The discrepancy could be attributed to the difference in annealing time; 40 hours compared to 1 hour. Absolute swelling as a function of water content was plotted in Figure 7.19 for the annealed films. The trend is very comparable with the untreated films.

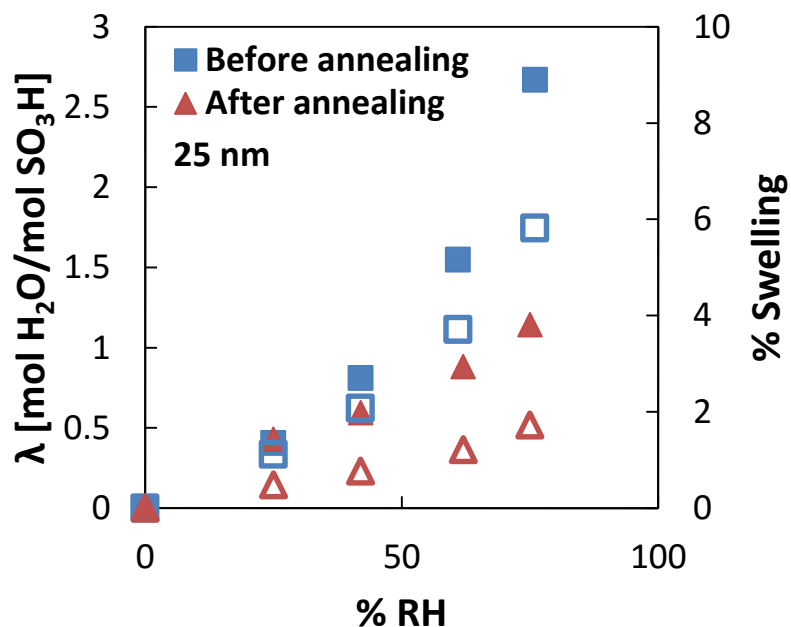


Figure 7.16: Water uptake (solid) and swelling (open) data for 25 nm Nafion[®] film on Au.

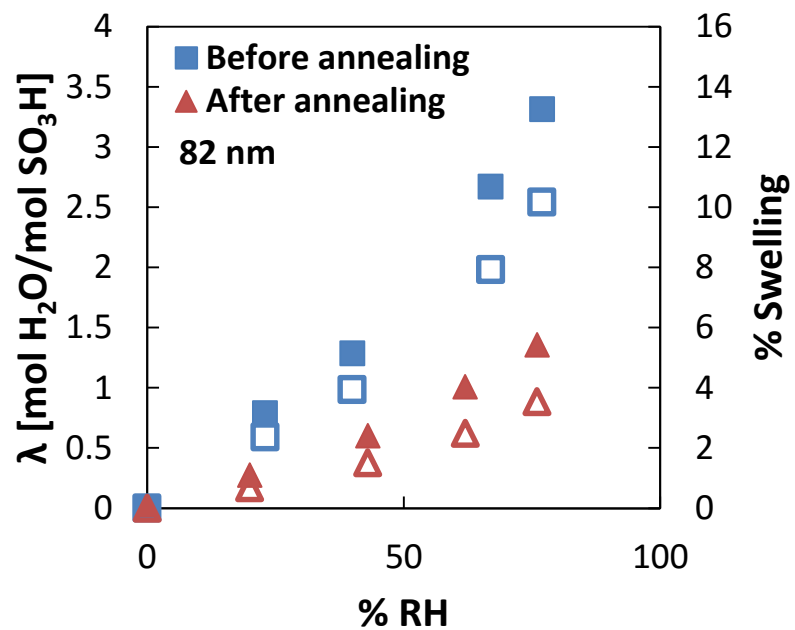


Figure 7.17: Water uptake (solid) and swelling (open) data for 82 nm Nafion[®] film on Au.

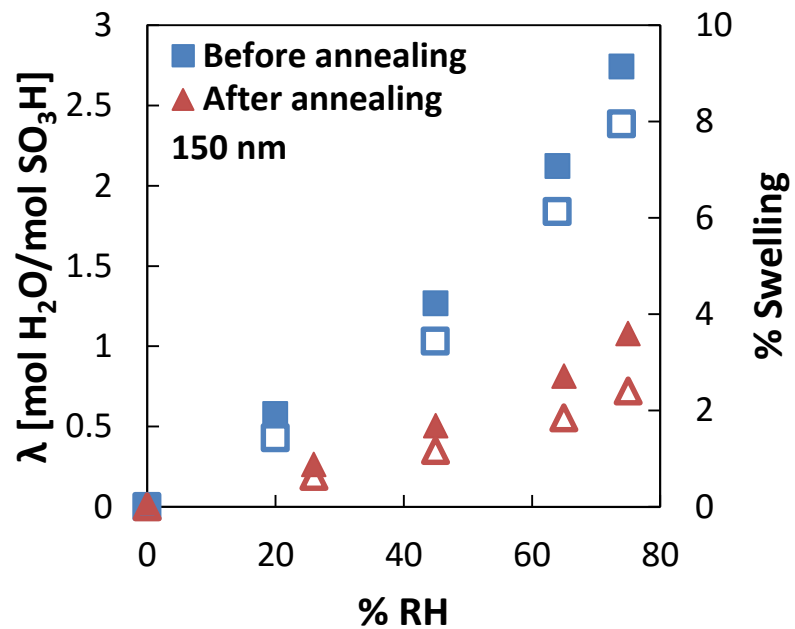


Figure 7.18: Water uptake (solid) and swelling (open) data for 150 nm Nafion[®] film on Au.

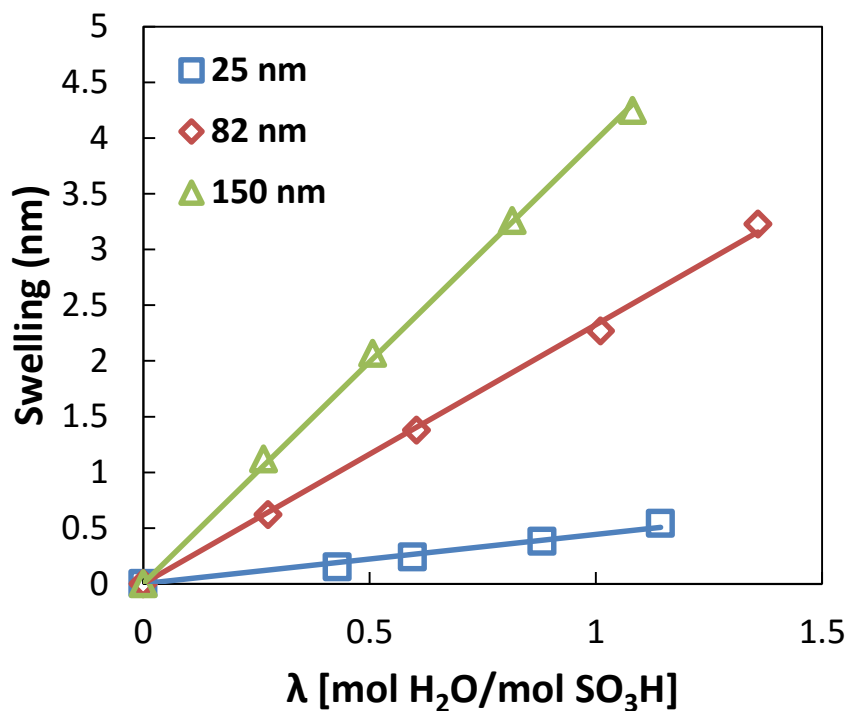


Figure 7.19: Swelling as a function of water content for annealed Nafion[®] films on Au.

The effect of annealing on each film has been plotted through Figures 7.20 to 7.22. While the 25 nm film shows a slight decrease in swelling per water uptake after annealing, the 82 and 150 nm films shows no difference. Annealing the films is inhibiting water uptake but with the same amount of water the films experience comparable swelling. This is interesting because if the film is crystallizing due to annealing, the film should exhibit less swelling with the same water uptake. The decrease in water uptake with similar swelling can be interpreted as the water molecules having a harder time penetrating the hydrophobic layer to the hydrophilic pores but once the pores fill up the film behaves in the same manner. This leads us to believe that annealing effects are mostly affecting the surface of the film, but as mentioned before no significant difference in water contact angle was observed. Since there are still errors associated with the frequency measurement of the QCM, further investigation is required to make a conclusion.

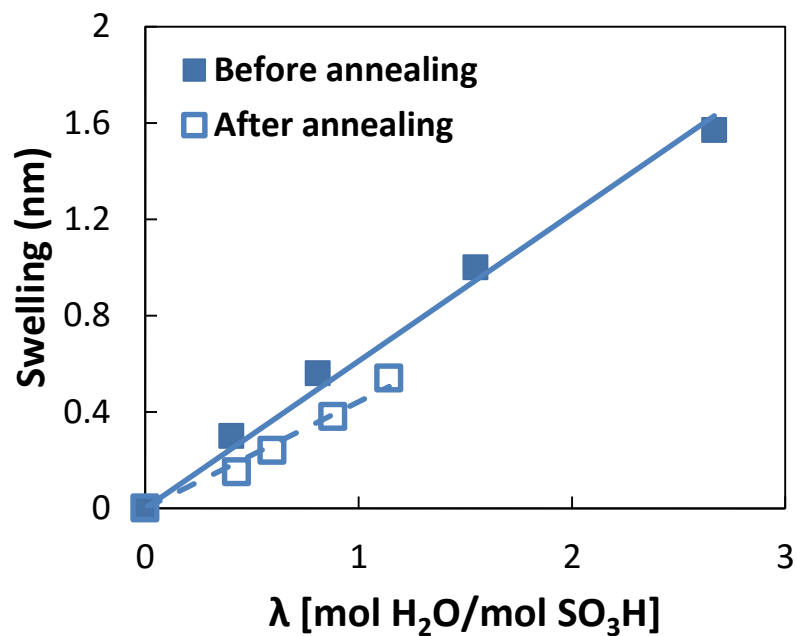


Figure 7.20: Effect of annealing on swelling as a function of water content for 25 nm Nafion[®] film on Au.

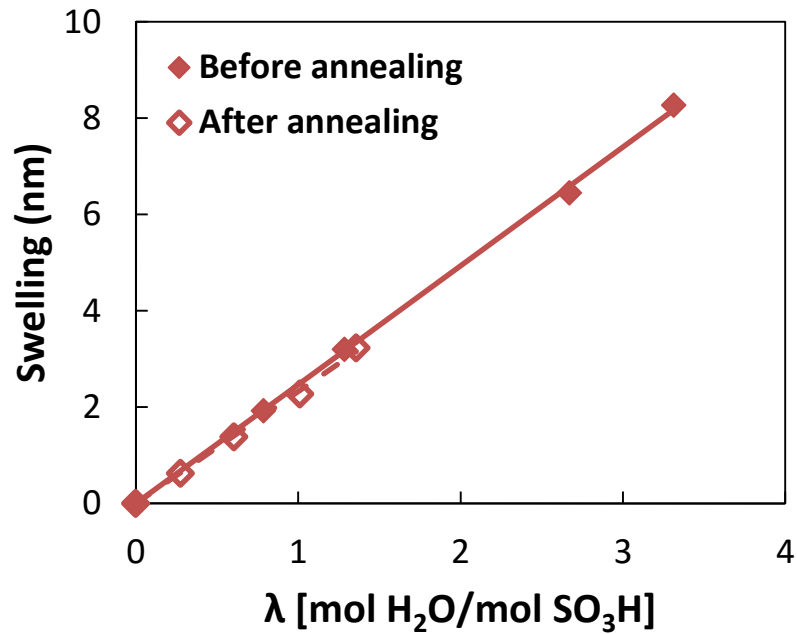


Figure 7.21: Effect of annealing on swelling as a function of water content for 82 nm Nafion[®] film on Au.

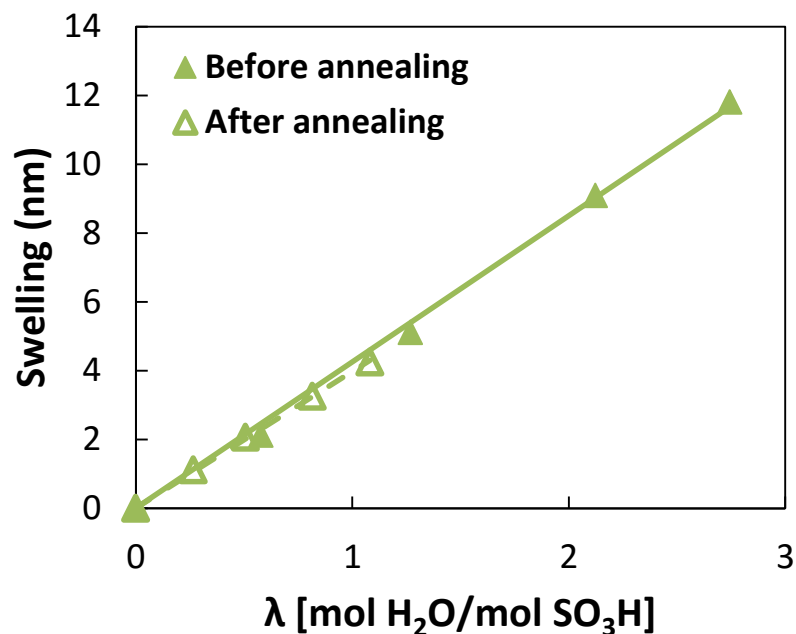


Figure 7.22: Effect of annealing on swelling as a function of water content for 150 nm Nafion® film on Au.

The swelling dimension and volume of mixing was investigated for the annealed films. The results are presented in Figure 7.23. For all films, the swelling dimension and volume of mixing did not change significantly. All swelling dimension and volume of mixing was close to 1 and 0 respectively. Unfortunately, no conclusion can be made from this results and the exact nature of the effect of annealing on water uptake and swelling must be investigated further.

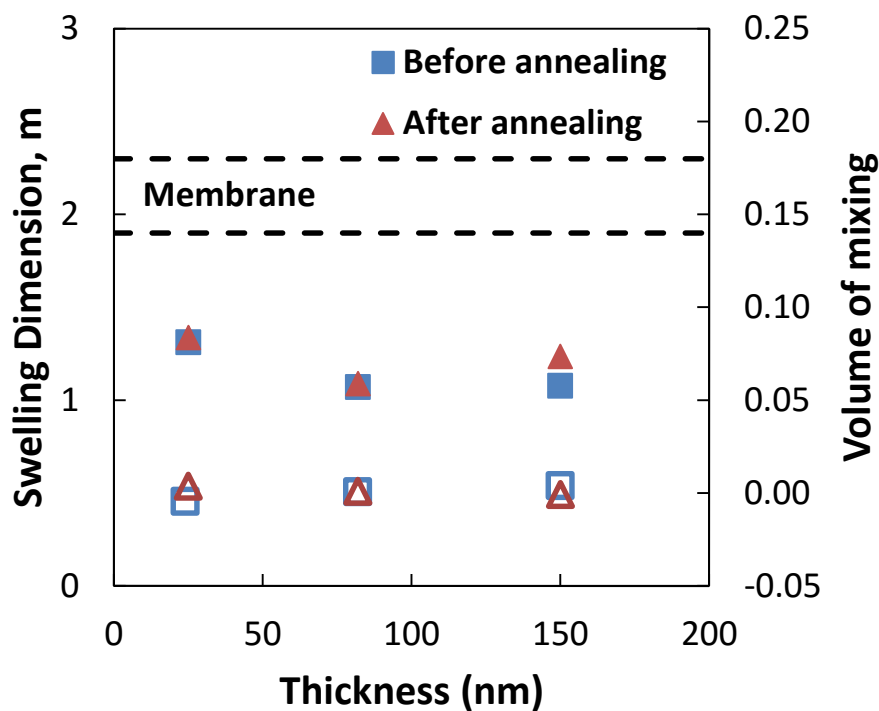


Figure 7.23: Swelling dimension (solid) and volume of mixing (open) of untreated (\square) and annealed (Δ) Nafion[®] thin films on Au. Dashed lines indicate range of volume of mixing for Nafion[®] membranes.

7.6 Conclusions

In this Chapter, a combined QCM-ellipsometry setup that was custom-made was introduced. Although further calibration is required, initial results show promising data. With the combined system, the water uptake and swelling property of ionomer thin films and the effect of thickness, EW, and annealing was investigated.

For all ionomers, swelling and λ showed a linear relationship and increased with thickness. A thickness-dependent trend similar to the water uptake property was observed. In

addition, the results further supported the proposed nano-structure of thin films by *Paul* for all ionomers. Investigation of swelling dimension and volume of mixing suggests the presence of confinement effect and negligible non-ideal mixing for thin films. No trend for EW was observed.

The effect of annealing in Nafion[®] thin films was significant on both the water uptake and swelling properties. Both properties faltered significantly after prolonged annealing. However, it was observed that swelling as a function of λ did not change after annealing as well as no significant difference in the swelling dimension and volume of mixing. The effect of annealing on Nafion[®] thin films requires further investigation until a conclusion can be made.

Chapter 8

Conclusions and Recommendations

8.1 Conclusions

Water uptake and swelling properties of thin ionomer films that play a crucial role in PEFCs were investigated in this thesis. The effect of thickness, substrate, EW, and annealing was studied. Thin films were prepared on quartz crystals and characterized using the QCM and ellipsometer: The QCM was employed to characterize the dry film mass and water uptake properties of the film, the ellipsometer for film thickness and optical properties, and combining the two techniques made it possible to study the density and swelling properties. Due to issues of non-uniformity of thickness of films created by self-assembly method on larger substrates ($> 1\text{ cm} \times 1\text{ cm}$), this thesis focused on spin-coated films. Spin-coating method of fabrication resulted in uniform and smooth thin films as confirmed by AFM. The density and RI of Nafion[®] thin films were strongly correlated for thicker ($>55\text{ nm}$) films exhibiting values close to that of the membrane. The drop in RI for thinner ($<55\text{ nm}$) films were observed although further study on density is required.

The discrepancy between high water uptake and low proton conductivity previously reported for Nafion[®] thin films on SiO₂ substrate was resolved by identifying the porous nature of the blank SiO₂. A simple subtraction method taking into account the blank SiO₂ substrate water uptake showed that water uptake was not strongly affected by substrate between Au, Pt, and SiO₂. A thickness-dependent study of Nafion[®] films on Au and Pt showed similar trends to previously reported proton conductivity trends which indicates that proton conductivity is strongly

dependent on water content. The increase in water uptake for sub-20 nm films was also observed on Pt.

The study on the effect of EW in the thin film form has not been reported yet in literature. Alternative dispersions provided by AFCC were prepared and characterized in the same manner as Nafion[®] films. The density and RI of AFCC samples showed comparably higher values than Nafion thin[®] films. The effect of thickness on each AFCC sample showed similar trends to that of Nafion[®] thin films indicating similar nano-structure. However, comparison of water uptake property between the various ionomers showed that interestingly Nafion[®] (highest EW) adsorbed more water at higher thicknesses (>55 nm). For thinner (<55 nm) the water uptake was comparable. This could be attributed due to the high crystallinity observed in low EW ionomers.

The swelling properties of ionomer thin films and the effect of annealing were studied using the customized QCM + ellipsometer setup. No thickness- and EW-dependent trend was observed, but investigation of the swelling dimension and volume of mixing indicated that confinement effect was evident for all ionomers thin films. Annealing Nafion[®] thin films greatly reduced its water uptake and swelling properties. However, a plot of swelling as a function of λ showed that annealing had almost no effect. The exact effect of annealing on thin film morphology needs further investigation.

8.2 Recommendations

While this thesis has introduced some new and interesting insight into ionomer thin films, further investigation is required to fully interpret the observations. While studying water uptake and swelling properties gives us a general idea on the response of ionomers in the thin film form when exposed to RH, it does not lend itself to fully clarifying the underlying physics of these

responses. As mentioned in Chapter 2, studying the kinetics of water uptake was a major focus of this thesis. However, due to limitations in controlling the humidity change this was not possible. If it is possible to instantaneously change the RH to a desired point, the response can be fully attributed to the film property which would allow us to obtain an understanding of the water uptake process and the morphology.

Furthermore, calibration regarding the preparation and characterization techniques will lead to better results. The main issue with studying the density of thin (<55 nm) films is the error associated with the QCM system. Due to the high variance in frequency reading due to assembly and disassembly of the holder, obtaining the exact dry film mass requires some fine-tuning. A method to prepare uniform and smooth thin film on QCs while inside the holder is required. Regarding the combined QCM + ellipsometer system, a method to control the temperature fluctuation to a minimum is also required due to the sensitivity of QCM to temperature.

Bibliography (or References)

1. United States Environmental Protection Agency. Regulations & Standards: Light-duty.
<http://www.epa.gov/otaq/climate/regs-light-duty.htm#new1>
2. European Commission. Reducing CO₂ emissions from passenger cars.
http://ec.europa.eu/clima/policies/transport/vehicles/cars/index_en.htm
3. Mauritz, K. A.; Moore, R. B. State of understanding of Nafion. *Chem. Rev.* **2004**, 104(10), 4535-4586.
4. Ohma, A.; Mashio, T.; Sato, K.; Iden, H.; Ono, Y.; Sakai, K.; Shinohara, K. Analysis of proton exchange membrane fuel cell catalyst layers for reduction of platinum loading at Nissan. *Electrochim. Acta.* 2011, 56(28), 10832-10841.
5. Kusoglu, A.; Kwong, A.; Clark, K. T.; Gunterman, H. P.; Weber, A. Z. Water uptake of fuel-cell catalyst layers. *J. Electrochem. Soc.* **2012**, 159(9), F530-F535.
6. Modestino, M. A.; Paul, D. K.; Dishari, S.; Petrina, S. A.; Allen, F. I.; Hickner, M. A.; Weber, A. Z. Self-assembly and transport limitations in confined Nafion films. *Macromolecules.* **2013**, 46(3), 867-873.
7. Holdcroft, S. Fuel cell catalyst layers: a polymer science perspective. *Chem. Mater.* **2013**, 26(1), 381-393.
8. Paul, D. K.; McCreery, R.; Karan, K. Proton Transport Property in Supported Nafion Nanothin Films by Electrochemical Impedance Spectroscopy. *J. Electrochem. Soc.* **2014**, 161(14), F1395-F1402.
9. Kusoglu, A.; Kushner, D.; Paul, D. K.; Karan, K.; Hickner, M. A.; Weber, A. Z. Impact of Substrate and Processing on Confinement of Nafion Thin Films. *Adv. Funct. Mater.* **2014**, 24(30), 4763-4774.

10. Gubler, L.; Scherer, G. G. A proton-conducting polymer membrane as solid electrolyte–function and required properties. *Adv. Polym. Sci.* **2008**, 215, 1-14.
11. Berg, P.; Promislow, K.; Pierre, J. S.; Stumper, J.; Wetton, B. Water management in PEM fuel cells. *J. Electrochem. Soc.* **2004**, 151(3), A341-A353.
12. Eikerling, M. Water management in cathode catalyst layers of PEM fuel cells a structure-based model. *J. Electrochem. Soc.* **2006**, 153(3), E58-E70.
13. More, K.; Borup, R.; Reeves, K. Identifying Contributing Degradation Phenomena in PEM Fuel Cell Membrane Electrode Assemblies via Electron Microscopy. *J. Electrochem. Soc. Trans.* **2006**, 3(1), 717-733.
14. Li, H.; Tang, Y.; Wang, Z.; Shi, Z.; Wu, S.; Song, D.; Mazza, A. A review of water flooding issues in the proton exchange membrane fuel cell. *J. Power Sources.* **2008**, 178(1), 103-117.
15. Dai, W.; Wang, H.; Yuan, X. Z.; Martin, J. J.; Yang, D.; Qiao, J.; Ma, J. A review on water balance in the membrane electrode assembly of proton exchange membrane fuel cells. *Int. J. Hydrogen Energy.* **2009**, 34(23), 9461-9478.
16. Jiao, K.; Li, X. Water transport in polymer electrolyte membrane fuel cells. *Prog. Energy Combust. Sci.* **2011**, 37(3), 221-291.
17. Hsu, W. Y.; Gierke, T. D. Ion transport and clustering in Nafion perfluorinated membranes. *J. Membr. Sci.* **1983**, 13(3), 307-326.
18. Schmidt-Rohr, K.; Chen, Q. Parallel cylindrical water nanochannels in Nafion fuel-cell membranes. *Nat. Mat.* **2007**, 7(1), 75-83.
19. Haubold, H. G.; Vad, T.; Jungbluth, H.; Hiller, P. Nano structure of NAFION: a SAXS study. *Electrochim. Acta.* **2001**, 46(10), 1559-1563.
20. Rubatat, L.; Gebel, G.; Diat, O. Fibrillar structure of Nafion: matching Fourier and real space studies of corresponding films and solutions. *Macromol.* **2004**, 37(20), 7772-7783.

21. Yakovlev, S.; Wang, X.; Ercius, P.; Balsara, N. P.; Downing, K. H. Direct imaging of nanoscale acidic clusters in a polymer electrolyte membrane. *J. Am. Chem. Soc.* **2011**, 133(51), 20700-20703.
22. McLean, R. S.; Doyle, M.; Sauer, B. B. High-resolution imaging of ionic domains and crystal morphology in ionomers using AFM techniques. *Macromol.* **2000**, 33(17), 6541-6550.
23. Gebel, G.; Aldebert, P.; Pineri, M. Structure and related properties of solution-cast perfluorosulfonated ionomer films. *Macromol.* **1987**, 20(6), 1425-1428.
24. Dura, J. A.; Murthi, V. S.; Hartman, M.; Satija, S. K.; Majkrzak, C. F. Multilamellar interface structures in Nafion. *Macromol.* **2009**, 42(13), 4769-4774.
25. Mohamed, H. F.; Kuroda, S.; Kobayashi, Y.; Oshima, N.; Suzuki, R.; Ohira, A. Possible presence of hydrophilic SO₃H nanoclusters on the surface of dry ultrathin Nafion[®] films: a positron annihilation study. *PCCP.* **2013**, 15(5), 1518-1525.
26. Bass, M., Berman, A., Singh, A., Konovalov, O., & Freger, V. Surface structure of Nafion in vapor and liquid. *J. Phys. Chem.* **2010**, B114(11), 3784-3790.
27. Zawodzinski, T. A.; Gottesfeld, S.; Shoichet, S.; McCarthy, T. J. The contact angle between water and the surface of perfluorosulphonic acid membranes. *J. Appl. Electrochem.* **1993**, 23(1), 86-88.
28. Paul, D. K.; Karan, K.; Docoslis, A.; Giorgi, J. B.; Pearce, J. Characteristics of self-assembled ultrathin Nafion films. *Macromol.* **2013**, 46(9), 3461-3475.
29. Zawodzinski, T. A.; Derouin, C.; Radzinski, S.; Sherman, R. J.; Smith, V. T.; Springer, T. E.; Gottesfeld, S. Water uptake by and transport through Nafion[®] 117 membranes. *J. Electrochem. Soc.* **1993**, 140(4), 1041-1047.
30. Choi, P.; Datta, R. Sorption in Proton-Exchange Membranes: An Explanation of Schroeder's Paradox. *J. Electrochem. Soc.* **2003**, 150(12), E601-E607.

31. Zhao, Q.; Majsztrik, P.; Benziger, J. Diffusion and interfacial transport of water in Nafion. *J. Phys. Chem. B.* **2011**, 115(12), 2717-2727.
32. Krtil, P.; Trojánek, A.; Samec, Z. Kinetics of water sorption in nafionthin films-quartz crystal microbalance study. *J. Phys. Chem. B.* **2001**, 105(33), 7979-7983.
33. Kongkanand, A. Interfacial water transport measurements in Nafion thin films using a quartz-crystal microbalance. *J. Phys. Chem. C.* **2011**, 115(22), 11318-11325.
34. Abuin, G. C.; Cecilia Fuertes, M.; Corti, H. R. Substrate effect on the swelling and water sorption of Nafion nanomembranes. *J. Membr. Sci.* **2013**, 428, 507-515.
35. Paul, D. K.; Karan, K. Conductivity and Wettability Changes of Ultrathin Nafion Films Subjected to Thermal Annealing and Liquid Water Exposure. *J. Phys. Chem. C.* **2014**, 118(4), 1828-1835.
36. Jung, H. Y.; Kim, J. W. Role of the glass transition temperature of Nafion 117 membrane in the preparation of the membrane electrode assembly in a direct methanol fuel cell (DMFC). *Int. J. Hydrogen. Energy.* **2012**, 37(17), 12580-12585.
37. Fujimura, M.; Hashimoto, T.; Kawai, H. Small-angle X-ray scattering study of perfluorinated ionomer membranes. 1. Origin of two scattering maxima. *Macromol.* **1981**, 14(5), 1309-1315.
38. Gebel, G.; Aldebert, P.; Pineri, M. Structure and related properties of solution-cast perfluorosulfonated ionomer films. *Macromol.* **1987**, 20(6), 1425-1428.
39. Viswanathan, B.; Helen, M. Is Nafion the only choice. *Bull. Catal. Soc. India.* **2007**, 6, 50-66.
40. Hickner, M. A.; Ghassemi, H.; Kim, Y. S.; Einsla, B. R.; McGrath, J. E. Alternative polymer systems for proton exchange membranes (PEMs). *Chem. Rev.* **2004**, 104(10), 4587-4612.

41. Heitner-Wirguin, C. Recent advances in perfluorinated ionomer membranes: structure, properties and applications. *J. Membr. Sci.* **1996**, 120(1), 1-33.
42. Ghielmi, A.; Vaccarone, P.; Troglia, C.; Arcella, V. Proton exchange membranes based on the short-side-chain perfluorinated ionomer. *J. Power Sources.* **2005**, 145(2), 108-115.
43. Hamrock, S. J.; Yandrasits, M. A. (2006). Proton exchange membranes for fuel cell applications. *J. Macromol. Sci. Part C: Polym. Rev.* **2006**, 46(3), 219-244.
44. Kreuer, K. D.; Schuster, M.; Obliers, B.; Diat, O.; Traub, U.; Fuchs, A.; Maier, J. Short-side-chain proton conducting perfluorosulfonic acid ionomers: Why they perform better in PEM fuel cells. *J. Power Sources.* **2008**, 178(2), 499-509.
45. Majsztrik, P. W.; Satterfield, M. B.; Bocarsly, A. B.; Benziger, J. B. Water sorption, desorption and transport in Nafion membranes. *J. Membr. Sci.* **2007**, 301(1), 93-106.
46. Ge, S., Li, X., Yi, B., & Hsing, I. M. Absorption, desorption, and transport of water in polymer electrolyte membranes for fuel cells. *J. Electrochem. Soc.* **2005**, 152(6), A1149-A1157.
47. Berens, A. R.; Hopfenberg, H. B. Diffusion and relaxation in glassy polymer powders: 2. Separation of diffusion and relaxation parameters. *Polym. J.* **1978**, 19(5), 489-496.
48. Satterfield, M. B.; Benziger, J. B. Non-Fickian water vapor sorption dynamics by Nafion membranes. *J. Phys. Chem. B.* **2008**, 112(12), 3693-3704.
49. Pantelic, N. Mass Transport Properties in Thin Ion-exchange Polymer Films and Related Phenomena. Ph.D. Thesis [Online], University of Cincinnati, Cincinnati, OH, **2007**.
https://etd.ohiolink.edu/ap/10?0::NO:10:P10_ACCESSION_NUM:ucin1179174207.
50. J.A. Woollam Co. Inc. Ellipsometry Measurements.
http://www.jawoollam.com/tutorial_4.html.
51. J.A. Woollam Co. Inc. Data Analysis. http://www.jawoollam.com/tutorial_5.html.

52. Paul, D. K. Structure and Properties of Self-assembled Sub-micron Thin Nafion® Films. Ph.D. Thesis [Online], Queen's University, Kingston, ON, September **2013**.
<http://qspace.library.queensu.ca/handle/1974/8410>.
53. Nanoscience Instruments, Inc. Atomic Force Microscopy Overview.
<http://www.teachnano.com/education/AFM.html>
54. Ramehart Instruments Co. Information on Contact Angle.
<http://www.ramehart.com/contactangle.htm>
55. Grot, W. Fluorinated ionomers [Online]; Elsevier Inc: Kidlington, Oxford, **2011**.
[https://books.google.ca/books?hl=en&lr=&id=E8H1Hwd5GXUC&oi=fnd&pg=PP1&dq=55.%09Grot,+W.+\(2011\).+Fluorinated+ionomers.+William+Andrew.&ots=F6eKZKD_rv&sig=3i8VQ4ZIRQoYwHt8xRTZOaOveao&redir_esc=y#v=onepage&q&f=false](https://books.google.ca/books?hl=en&lr=&id=E8H1Hwd5GXUC&oi=fnd&pg=PP1&dq=55.%09Grot,+W.+(2011).+Fluorinated+ionomers.+William+Andrew.&ots=F6eKZKD_rv&sig=3i8VQ4ZIRQoYwHt8xRTZOaOveao&redir_esc=y#v=onepage&q&f=false)
56. Bunkin, N. F.; Ignatiev, P. S.; Kozlov, V. A.; Shkirin, A. V.; Zakharov, S. D.; Zinchenko, A. A. Study of the phase states of water close to Nafion interface. *Water J.* **2013**, 4, 129-154.
57. Goswami, S.; Klaus, S.; Benziger, J. Wetting and Absorption of Water Drops on Nafion Films. *Langmuir.* **2008**, 24, 8627–8633
58. Lee, S.; Staehle, R. W. Adsorption of water on gold. *Corros. J.* **1996**, 52(11), 843-852.
59. Parida, S. K.; Dash, S.; Patel, S.; Mishra, B. K. Adsorption of organic molecules on silica surface. *Adv. Colloid Interface Sci.* **2006**, 121(1), 77-110
60. Asay, D. B.; Kim, S. H. Evolution of the adsorbed water layer structure on silicon oxide at room temperature. *J. Phys. Chem. B.* **2005**, 109(35), 16760-16763
61. Kobayashi, Y.; Zheng, W.; Chang, T. B.; Hirata, K.; Suzuki, R.; Ohdaira, T.; Ito, K. Nanoporous structure of sputter-deposited silicon oxide films characterized by positronium annihilation spectroscopy. *J. Appl. Phys.* **2002**, 91(3), 1704-1706

62. Modestino, M. A.; Kusoglu, A.; Hexemer, A.; Weber, A. Z.; Segalman, R. A. Controlling Nafion structure and properties via wetting interactions. *Macromol.* **2012**, 45(11), 4681-4688.
63. Vogt, B. D.; Lin, E. K.; Wu, W. L.; White, C. C. Effect of film thickness on the validity of the Sauerbrey equation for hydrated polyelectrolyte films. *J. Phys. Chem. B.* **2004**, 108(34), 12685-12690.
64. Murthi, V. S.; Dura, J.; Satija, S.; Majkrzak, C. Water uptake and interfacial structural changes of thin film Nafion® membranes measured by neutron reflectivity for PEM fuel cells. *J. Electrochem. Soc. Trans.* **2008**, 16(2), 1471-1485.
65. Zawodzinski, T. A.; Springer, T. E.; Davey, J.; Jestel, R.; Lopez, C.; Valerio, J.; Gottesfeld, S. A comparative study of water uptake by and transport through ionomeric fuel cell membranes. *J. Electrochem. Soc.* **1993**, 140(7), 1981-1985.
66. Subianto, S.; Cavaliere, S.; Jones, D. J.; Rozière, J. Effect of side-chain length on the electrospinning of perfluorosulfonic acid ionomers. *J. Polym. Sci. Part A: Polym. Chem.* **2013**, 51(1), 118-128.
67. Zhang, C. Thermal behavior of ionomer thin films, MSc Thesis (in progress), University of Calgary, Calgary AB.
68. Collette, F. M.; Lorentz, C.; Gebel, G.; Thominette, F. Hygrothermal aging of Nafion®. *J. Membr. Sci.* **2009**, 330(1), 21-29.

APPENDIX

For comparison of the 3 ionomers, the mass water uptake as a percentage of dry film mass is presented through Figures A1 to A4. We observe for thinner films (<55 nm) the low EW ionomer thin films absorb more water compared to Nafion® thin films at all humidity. However, for thicker (>55 nm) films this is not always the case. Interestingly, we observe that at certain humidity the water uptake of low EW ionomer thin films is either similar or even lower at sometimes compared to Nafion® thin films of similar thickness.

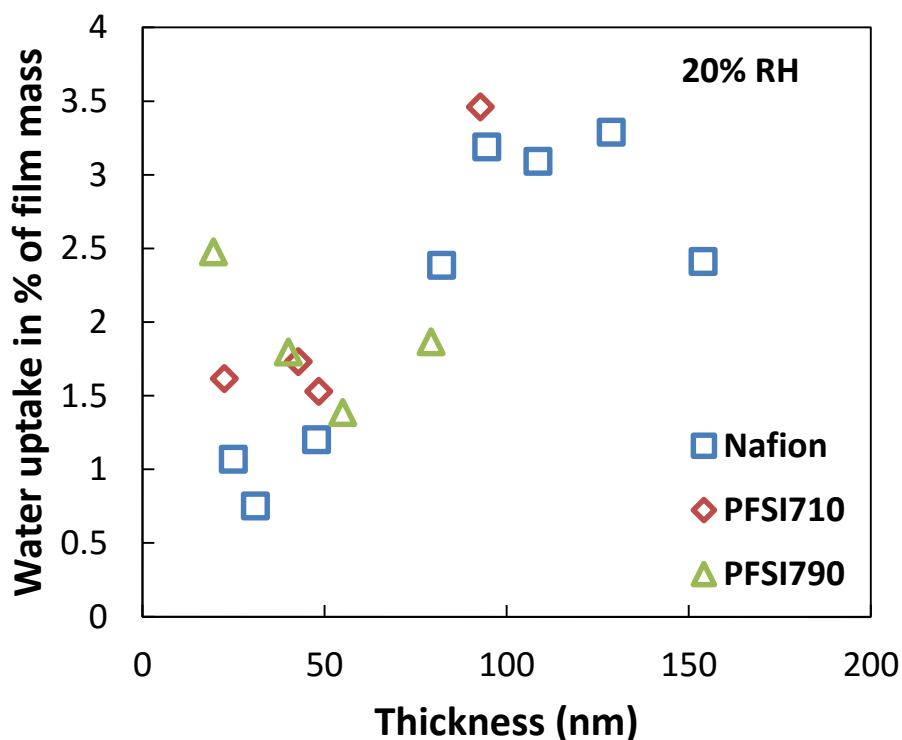


Figure A1: Thickness-dependent mass water uptake at 20% RH for thin films on Au.

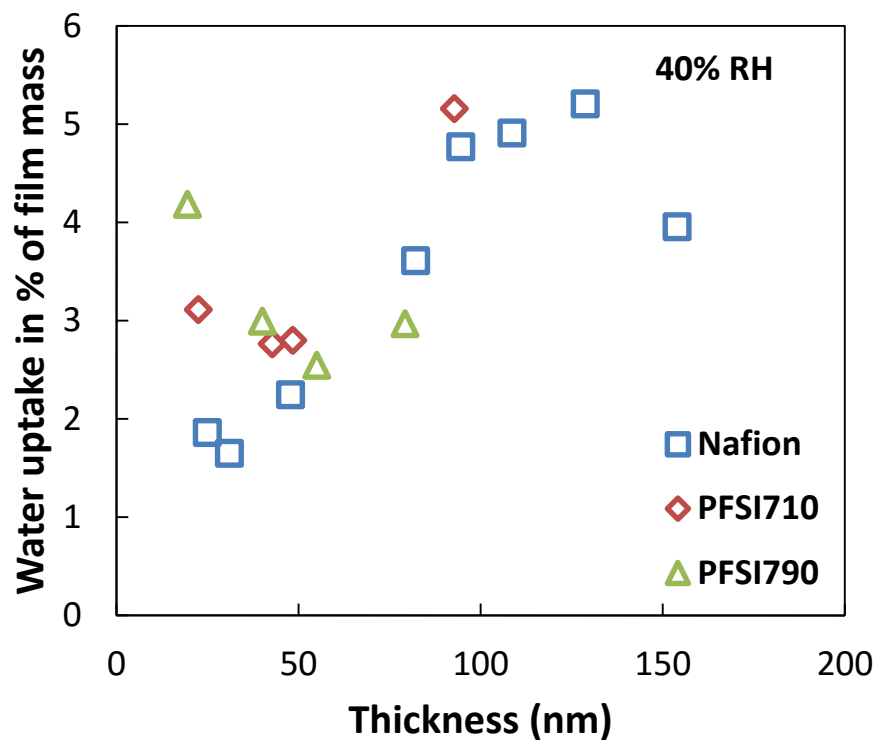


Figure A2: Thickness-dependent mass water uptake at 40% RH for thin films on Au.

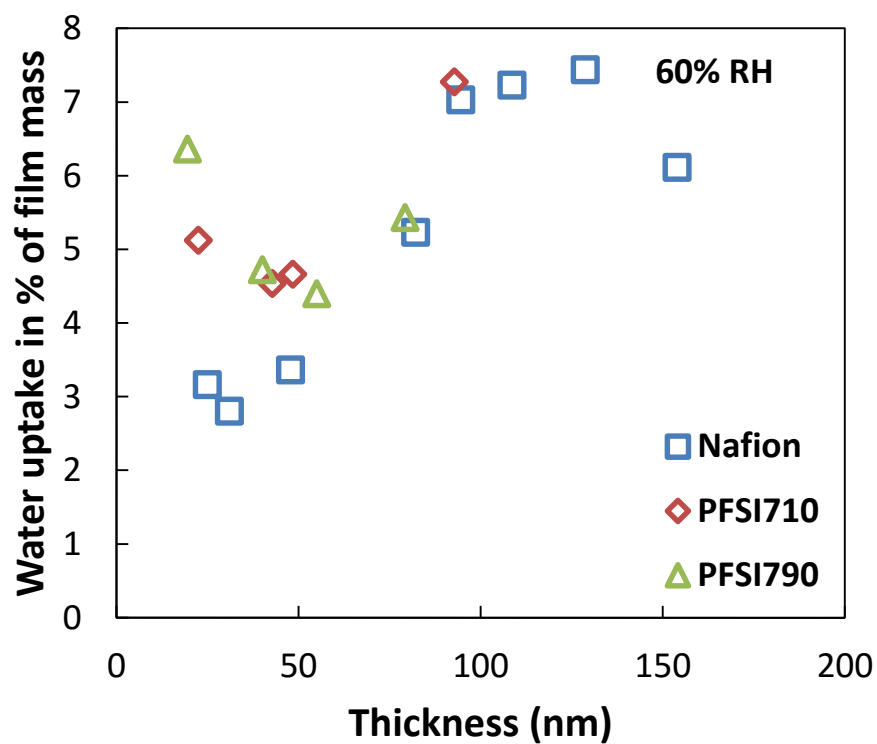


Figure A3: Thickness-dependent mass water uptake at 60% RH for thin films on Au.

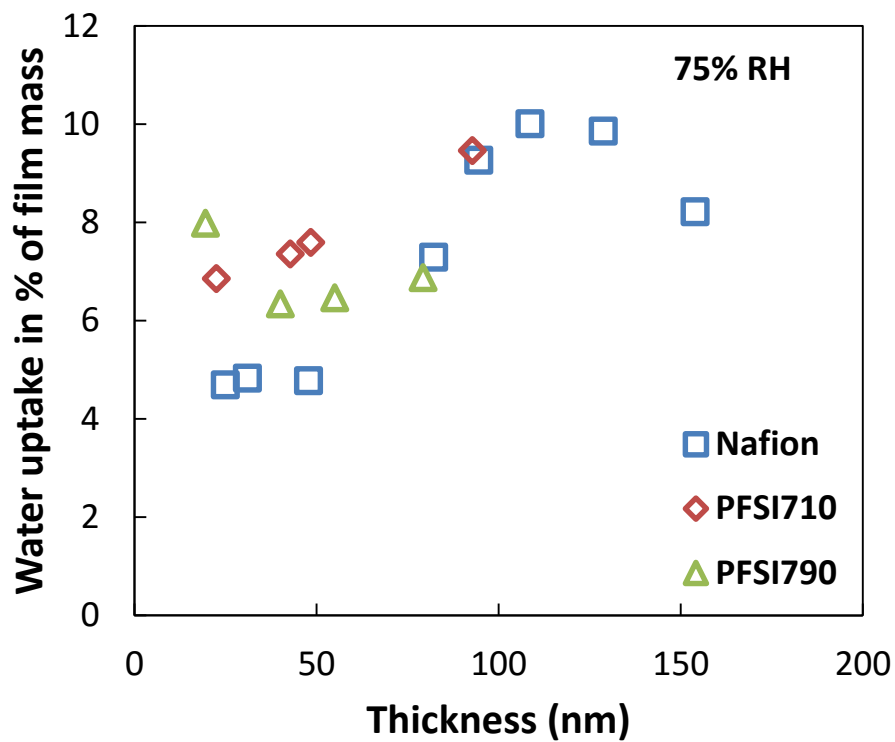


Figure A4: Thickness-dependent mass water uptake at 75% RH for thin films on Au.